ผลของการปรับปรุงสภาพผิวของท่อคาร์บอนนาโนผนังหลายชั้นต่อสัมประสิทธิ์การนำความร้อนของอันเดอร์ฟิลล์สำหรับบรรจุภัณฑ์ไมโครอิเล็กทรอนิกส์

นางสาวอุไรวรรณ พงสา

วิทยานิพนธ์นี้เป็นส่วนหนึ่งของการศึกษาตามหลักสูตรปริญญาวิศวกรรมศาสตรดุษฎีบัณฑิต
สาขาวิชาวิศวกรรมเคมี ภาควิชาวิศวกรรมเคมี
คณะวิศวกรรมศาสตร์ จุฬาลงกรณ์มหาวิทยาลัย
ปีการศึกษา 2555

EFFECT OF SURFACE MODIFICATION OF MULTI-WALLED CARBON NANOTUBES ON THERMAL CONDUCTIVITY OF UNDERFILL FOR MICROELECTRONIC PACKAGING

Miss Uraiwan Pongsa

A Dissertation Submitted in Partial Fulfillment of the Requirements
for the Degree of Doctor of Engineering Program in Chemical Engineering
Department of Chemical Engineering
Faculty of Engineering
Chulalongkorn University
Academic Year 2012

Thesis Title	EFFECT OF SURFACE MODIFICATION OF MULTI-WALLED CARBON NANOTUBES ON THERMAL CONDUCTIVITY OF UNDERFILL FOR MICROELECTRONIC PACKAGING
By	Miss Uraiwan Pongsa
Field of Study	Chemical Engineering
Thesis Advisor	Assistant Professor Anongnat Somwangthanaroj, Ph.D.

Accepted by the Faculty of Engineering, Chulalongkorn University in Partial Fulfillment of the Requirements for the Doctoral Degree

....Dean of the Faculty of Engineering
(Associate Professor Boonsom Lerdhirunwong, Dr.Ing.)

THESIS COMMITTEE

....Chairman
(Professor Piyasan Preserthdam, Dr.Ing.)

....Thesis Advisor
(Assistant Professor Anongnat Somwangthanaroj, Ph.D.)

....Examiner
(Associate Professor M.L. Supakanok Thongyai, Ph.D.)

....Examiner
(Associate Professor Somchai Ratanathammaphan, D.Eng.)

....Examiner
(Assistant Professor Soorathep Kheawhom, Ph.D.)

....External Examiner
(Assistant Professor Sirirat Wacharawichanant, D.Eng.)

อุไรวรรณ พงสา: ผลของการปรับปรุงสภาพผิวของท่อคาร์บอนนาโนผนังหลายชั้นต่อสัมประสิทธิ์การนำความร้อนของอันเดอร์ฟิลล์สำหรับบรรจุภัณฑ์ไมโครอิเล็กทรอนิกส์. (EFFECT OF SURFACE MODIFICATION OF MULTI-WALLED CARBON NANOTUBES ON THERMAL CONDUCTIVITY OF UNDERFILL FOR MICROELECTRONIC PACKAGING) อ. ที่ปรึกษาวิทยานิพนธ์หลัก: ผศ.ดร.อนงค์นาฏ สมหวังธนโรจน์, 126 หน้า.

ในงานวิจัยนี้ท่อคาร์บอนนาโนผนังหลายชั้นถูกดัดแปลงหมู่ฟังก์ชันด้วยกรดเบนซีน-1,3,5-ไตรคาร์บอกซิลิก และกรด 3,5-อะมิโนเบนโซอิก โดยปฏิกิริยาฟรีเดล-คราฟท์เอซิลเลชัน ทำให้เกิดความเสียหายต่อโครงสร้างน้อยมาก ซึ่งยืนยันผลด้วย FT-IR, XPS และ FT-Raman หมู่ฟังก์ชันบนผิวของท่อคาร์บอนนาโนผนังหลายชั้นสามารถเร่งปฏิกิริยาการบ่มของอิพ็อกซีคอมโพสิตได้ ทำให้อุณหภูมิการบ่ม พลังงานความร้อนของปฏิกิริยา และพลังงานก่อกัมมันต์ลดลง นอกจากนี้ความหนาแน่นเชื่อมขวางที่เพิ่มขึ้นและสัดส่วนปริมาตรอิสระที่ลดลง ส่งผลให้อุณหภูมิเปลี่ยนสภาพแก้วเพิ่มขึ้นและสัมประสิทธิ์การขยายตัวทางความร้อนลดลง การเพิ่มขึ้นของสัมประสิทธิ์การนำความร้อนพบในระบบที่เติมท่อคาร์บอนนาโนผนังหลายชั้นที่ดัดแปลงหมู่ฟังก์ชัน เนื่องจากการกระจายตัวดีและค่าความต้านทานความร้อนระหว่างผิวสัมผัสของท่อคาร์บอนนาโนและพอลิเมอร์เมทริกซ์ที่ลดลง ทั้งนี้พบว่า แบบจำลอง แมกซ์เวลล์-การ์เนท อีเอ็มเอ เป็นแบบจำลองที่เหมาะสมสำหรับการทำนายค่าสัมประสิทธิ์การนำความร้อนเชิงประสิทธิผลของอิพ็อกซีคอมโพสิตที่เติมท่อคาร์บอนนาโนผนังหลายชั้นที่ปริมาณต่ำ นอกจากนี้อิพ็อกซีคอมโพสิตที่เติมสารตัวเติมลูกผสมของท่อคาร์บอนนาโนผนังหลายชั้นและซิลิคอนไนไตรด์ที่มีขนาดเล็กกว่าระดับไมครอนแสดงค่าสัมประสิทธิ์การนำความร้อนที่สูงกว่าระบบที่เติมสารตัวเติมเดี่ยว เพราะทำให้เกิดการเรียงตัวของสารตัวเติมอย่างต่อเนื่องและเส้นทางการถ่ายเทความร้อนที่สมบูรณ์

ภาควิชา วิศวกรรมเคมี ลายมือชื่อนิสิต

สาขาวิชา วิศวกรรมเคมี ลายมือชื่อ อ.ที่ปรึกษาวิทยานิพนธ์หลัก

ปีการศึกษา 2555

5171861121: MAJOR CHEMICAL ENGINEERING
KEYWORDS: CARBON NANOTUBES / EPOXY COMPOSITES / FRIEDEL-CRAFTS ACYLATION / X-RAY PHOTOELECTRON SPECTROSCOPY / SURFACE AND INTERFACE

URAIWAN PONGSA: EFFECT OF SURFACE MODIFICATION OF MULTI-WALLED CARBON NANOTUBES ON THERMAL CONDUCTIVITY OF UNDERFILL FOR MICROELECTRONIC PACKAGING. ADVISOR: ASST. PROF. ANONGNAT SOMWANGTHANAROJ, Ph.D., 126 pp.

In this research, multiwalled carbon nanotubes (MWCNTs) were directly functionalized with benzene-1,3,5-tricarboxylic acid (BTC) and 3,5-diaminobenzoic acid (DAB) via a Friedel-Crafts acylation with less structural damage as confirm by FT-IR, XPS and FT-Raman analysis. The functional groups on MWCNT surfaces can accelerate the curing reaction of epoxy composites remarkable inducing rather low exothermic peak temperature (T_p), exothermic heat of reaction (ΔH) and activation energy (E_a). Additionally, the crosslink density (λ) increased and free volume fraction (f_g) decreased with the addition of functionalized MWCNTs, resulting in dramatic increase of glass transition temperatures (T_g) and decrease of coefficient of thermal expansion (CTE). The thermal conductivity enhancement can be observed with functionalized MWCNT systems probably due to good dispersion and decreased interfacial thermal resistance between MWCNT and polymer matrix. Moreover, the modified Maxwell-Garnett typed EMA model is appropriate for predicting effective thermal conductivity of epoxy composites filled with low concentration of MWCNTs. Epoxy composites incorporated with hybrid fillers which consisted of MWCNTs and submicron-sized silicon nitride (Si_3N_4) exhibit higher thermal conductivity than those with single filler, thereby forming high packing density and perfectly heat conductive pathways.

Department : Chemical Engineering Student's Signature ....

Field of Study : Chemical Engineering Advisor's Signature ....

Academic Year : 2012

ACKNOWLEDGEMENTS

I am sincerely grateful to my advisor, Asst. Prof. Dr. Anongnat Somwangthanaroj, for her invaluable guidance and valuable suggestions including constant encourage throughout this study. Thanks are extended to Prof. Dr. C. P. Wong from School of Materials Science and Engineering, Georgia Institute of Technology Materials Science and Engineering, USA for the valuable advices during my short term research program in USA.

I am also grateful to my committee members, who provided constructive and scientific advices for the completion of this thesis. This includes, Prof. Dr. Piyasan Preserthdam, Chairman, Assoc. Prof. Dr. M.L. Supakanok Thongyai and Asst. Prof. Dr. Soorathep Kheawhom from Department of Chemical Engineering, Faculty of Engineering, Chulalongkorn University, Assoc. Prof. Dr. Somchai Ratanathammaphan from Department of Electrical Engineering, Faculty of Engineering, Chulalongkorn University, and Asst. Prof. Dr. Sirirat Wacharawichanant from Department of Chemical Engineering, Faculty of Engineering and Industrial Technology, Silpakorn University.

Sincerely thanks for supporting the education fund, scholarship, materials, analytical instruments and kindly assistance from Mektec Manufacturing Corporation (Thailand) Ltd.

I also appreciate my best friends for always being there through good and bad times. I am very thankful for every inspiration that they have made throughout my difficult years. Thank are also extended to every polymer engineering research laboratory member for every constructive discussion they contributed and all their help.

Finally, my deepest regard to my beloved family and parents, who have always been the source of my support and encouragement. There is never a single day without them standing by me. It is why I can journey this far. I am lifetime beholden.

CONTENTS

PAGE

PAGE

PAGE

PAGE

LIST OF TABLES

TABLE **PAGE**

TABLE **PAGE**

LIST OF FIGURES

FIGURE **PAGE**

FIGURE **PAGE**

FIGURE **PAGE**

FIGURE **PAGE**

LIST OF ABBREVIATIONS

4-ABAc	4-aminobenzoic acid
Al_2O_3	Alumina
AlN	Aluminum nitride
APTES	3-aminopropyltriethoxysilane
BeO	Beryllia
BN	Boron nitride
BTC	Benzene-1,3,5-tricarboxylic acid
CNF	Carbon nanofiber
CNT	Carbon nanotube
CoIIAcAc	Cobalt (II) acetylacetonate
C_p	Specific heat capacity
CTE	Coefficient thermal expansion
CVD	Chemical vapor deposition
DAB	3,5-diaminobenzoic acid
DGEBA	Diglycidyl ether of bisphenol A
DGEBF	Diglycidyl ether of bisphenol A
DMA	Dynamic mechanical analysis
DSC	Differential scanning calorimetry
E'	Storage modulus
E"	Loss modulus
E_a	Activation energy
EEW	Epoxy equivalent weight
ESCA	Electron spectroscopy for chemical analysis
EtO-MWCNTs	MWCNTs functionalized with 4-ethoxybenzoic acid
f	Frequency
f_r	Reference frequency at 1 Hz
f_g	Free volume fraction
FT-IR	Fourier transform infrared spectroscopy
FT-Raman	Fourier transform raman spectroscopy

FESEM	Field emission scanning electron microscopy
HiPCo	High pressure conversion of carbon monoxide
K	Thermal conductivity
MHHPA	Hexahydro-4-methylphthalic anhydride
MW	Molecular weight
MWCNTs	Multi-walled carbon nanotubes
p	aspect ratio
P_2O_5	Phosphorus pentoxide
PET	Polyethylene terephthalate
PPA	Polyphosphoric acid
SEM	Scanning electron microscopy
Si_3N_4	Silicon nitride
SiC	Silicon carbide
SiO_2	Silicon dioxide
SWCNTs	Single-walled carbon nanotubes
T_d	Degradation temperature
T_g	Glass transition temperature
T_{gr}	Glass transition temperature at reference frequency
T_p	Exothermic peak temperature
TGA	Thermogravimetric analysis
TG/DTA	Thermogravimetric/differential thermal analysis
TMA	Thermal mechanical analysis
U-MWCNTs	Unmodified multi-walled carbon nanotubes
WLF	Williams-Landell-Ferry
XPS	X-ray photoelectron spectroscopy
α	Thermal diffusivity
β	Heating rate
λ	Crosslink density
ρ	Density

CHAPTER I
INTRODUCTION

1.1 Overview

In past few years smart devices with ultrathin, light weight and multifunction have become very popular. The increasing interest in these devices has heightened the need for advanced microelectronic packaging appropriate to use in electronics. As continuous development in the miniaturization, the heat dissipation is still a critical problem in packaging, limiting the reliability and high performance. Therefore, the polymer-based composite with high thermal conductivity has been received more attention, especially high thermally conductive underfill. Commercially, underfill is epoxy-based composite which is used to fill into the gap between silicon chip and substrate in microelectronic packaging. Underfill plays a key role to adsorb and to dissipate thermal stresses occurred in the devices, thereby enhancing solder bump fatigue life [1-4].

Traditionally, the addition of inorganic particles with intrinsically high thermal conductivity into a conventional underfill with efficient dispersion has been attracted more attention as the approach to increase the heat dissipation and the thermal conductivity [5-7]. Commonly used inorganic fillers include silicon carbide (SiC), alumina (Al_2O_3), aluminum nitride (AlN), boron nitride (BN) and so forth [5, 8, 9]. The fillers, whose intrinsic thermal conductivity is higher than other fillers, are more effective for increasing thermal conductivity of underfill [10, 11]. Additionally, a shape of filler also affects the thermal conductivity of underfill in which the non-spherical particles can provide filler-filler and filler-matrix interaction better than spherical particles [12, 13]. The fillers with high aspect ratio easily form random bridges or conductive networks that facilitate the heat transfer through polymer matrix by phonon transfer. The formation of effective heat conductive pathways is promoted by an increase of thermally conductive filler loading, commonly higher than 30 vol%, thereby enhancing heat dissipation ability [14, 15]. However, the introduction of high filler concentration into polymer matrix results in an increase of viscosity and limitation of processability.

One solution to this problem might be using the filler with large aspect ratio at lower content to maximize the randomly heat conductive networks in the composites. Multi-walled carbon nanotubes (MWCNTs) are one of the most attractive filler candidates due to the exceptional characteristic of MWCNTs including nanostructure, high aspect ratio and intensively outstanding thermo-mechanical and thermal properties. MWCNTs exhibit extremely powerful performance with very low weight compared with various engineering materials, for example, MWCNTs are many times stronger than steel, though three to five times lighter [16]. Therefore, the incorporation of MWCNTs into the polymer matrix has been proposed for high performance and light-weight composites. Furthermore, MWCNTs are often used in the thermal management applications. It is due to the fact that MWCNTs show extremely high thermal conductivity in which the highest measured thermal conductivity of MWCNTs is 3000 W/mK [17]. However, it is known that the advantage of MWCNTs certainly depends on the degree of dispersion. MWCNTs easily form large agglomerates and are hardly dispersed in polymer matrix due to their high surface area and intrinsic van der Waals force. Besides, weak interfacial interaction between MWCNT and polymer matrix results in a lack of load transfer and heat transfer in polymer composite. These behaviors hinder actual potential of using MWCNTs to obtain targeted properties. Accordingly, an approach to achieve good dispersion and strong interfacial interaction of MWCNTs is a challenge.

The surface modification has widely been considered to overcome the limitation in MWCNT manipulation. MWCNTs were often treated by the harsh chemical oxidation in strong acids like nitric acid and sulfuric acid and/or their mixtures at elevated temperatures [18, 19]. The carboxylic and oxygen-containing groups could be generated on their surfaces that facilitated further functionalization or fabrication [20-22]. Although, better dispersion and interfacial interaction can be achieved via this method, the dramatic structural damages on the surface of MWCNTs can easily occur. Consequently, much attention has been focused on the alternative functionalization methods without or less structural damage. Among various methods of surface modification, it was found that a direct Friedel-Crafts acylation, the functionalization reaction, is convenient and effective for the purification and the functionalization of the reactive functional groups onto the surface of MWCNTs in a one-pot process with trace amount of defects [23-25].

Many recent studies have focused on the addition of hybrid filler systems into the polymer matrix. Polymer composites containing mixed thermally conductive inorganic particles such as BN [26], AlN [27] and SiC [28, 29] have been conducted. The hybrid fillers consisting of MWCNTs and thermally conductive particles have been considered as well. Due to the fact that partial replacement of inorganic filler into the space formed in MWCNT-to-MWCNT networks can be obtained more heat conductive pathways with high packing density that facilitate phonon transfer leading to high thermal conductivity. Among commonly used inorganic particles, silicon nitride (Si_3N_4) is one of the attractive inorganic fillers because of its high thermal conductivity as well as low CTE and more commercially available than BN [30-33]. However, there has not been the study of the effects of Si_3N_4 particles mixed with MWCNTs as hybrid fillers on the thermal conductivity and dynamic mechanical properties yet. Additionally, particle size of fillers is one of the most important factors for the enhancement of thermal conductivity. The micron-sized fillers effectively achieve the expected thermal conductivity of composites, but the settling of fillers in polymer matrix is often observed [34]. Also, the micron-sized particles are not able to flow in narrow gaps. In case of nano-sized fillers, the thermal conductivity of composites exceptionally increases with low filler loading. Due to high surface area of nano-sized particles, the strong agglomeration occurred and thus the surface modification and effective mixing method are required to improve the dispersion, thereby increasing the production costs. Besides, the viscosity of composites intensely increases that hinders the processability. To avoid agglomeration of filler and to obtain low viscous epoxy composite for ease in industrial processing, the submicron-sized Si_3N_4 is considered as ideal filler to generate the hybrid filler with perfect thermal conductive networks.

Accordingly, the crucial objective of this work is to improve the thermal conductivity of epoxy resin for using in microelectronic packaging, which requires insulation properties. Consequently, this study was designed to evaluate the effect of surface functionalization with various reactive functionalizing reactants via Friedel-Crafts acylation in a mild medium on the properties of MWCNTs. The dynamic mechanical and thermal properties of MWCNT/epoxy composites were investigated as well. Thermal conductivity of MWCNT/epoxy composites was compared with the theoretical values predicted by using various theoretical and empirical models. In addition, the properties of epoxy composites incorporated with hybrid fillers between MWCNTs and submicron-sized Si_3N_4 were also explored.

1.2 Objectives of research

1. To evaluate the effect of surface functionalization of MWCNTs via Friedel-Crafts acylation on the surface properties of MWCNTs and the properties of epoxy composites

2. To investigate the effect of MWCNT concentration and hybrid fillers on thermal conductivity, mechanical and thermal properties of epoxy composites

1.3 Scopes of research

1. Functionalization and characterization of MWCNTs with reactive reactants which are benzene-1,3,5-tricarboxylic acid (BTC) and 3,5-diaminobenzoic acid (DAB) via Friedel-Crafts acylation.

2. Preparation of epoxy composites filled with unmodified and functionalized MWCNTs varied in the range of 0.3% to 1.0% by volume.

3. Preparation of epoxy composites filled with hybrid fillers of 1.0vol% MWCNTs and submicron-sized Si_3N_4 particles at 2.5%, 5.0% and 7.5% by volume.

4. Investigation of the morphology, thermal conductivity, mechanical and thermal properties of epoxy composites.

5. Predication of thermal conductivity of epoxy composites by using theoretical and empirical models.

CHAPTER II

THEORY

This chapter gives a brief overview of underfilling technology, focusing on the flip-chip packaging, the required properties of underfill materials and the development of underfill formulation. The principle of carbon nanotubes and surface modification including Friedel-Crafts acylation are also described in this chapter.

2.1 Underfilling technology

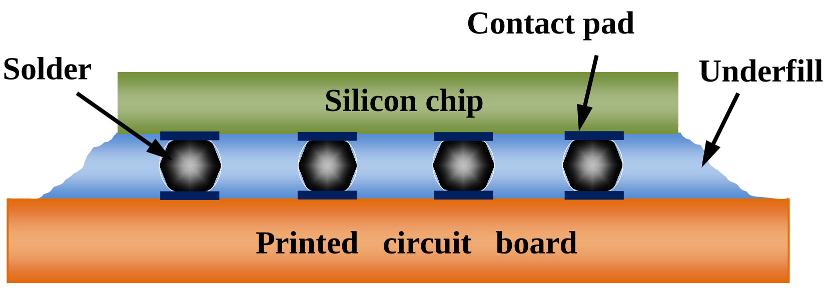

Figure 2.1 Scheme of flip-chip packaging [35]

Flip-chip is the first level integrated circuit packaging approach in which the active side of the silicon chip is faced down and connected to the substrate. The active side of the chip is bumped with solder balls that can be molten and wetted on the metal pad of the substrate, and form the electrical and mechanical connections between the silicon chip and the substrate [36]. A general scheme of the flip-chip packaging is shown in Figure 2.1. Although the organic substrate is favored in terms of its low dielectric constant and low cost, the high CTE mismatch between the silicon chip and the organic substrate produces the cracking caused by excess thermal stress inside the packaging resulting in decreasing its reliability and performance. Therefore, a liquid encapsulant called underfill, usually based on uncured epoxy resin monomer heavily filled with fused silica (SiO_2), is filled the gap between chip and substrate to assure that the solder connection does not crack or open during the thermal cycling [37]. According to the different processes, underfilling can be classified into capillary underfill, molded underfill, no-flow underfill, and wafer level underfill, which are listed in Table 2.1. The conventional capillary underfill and no-flow underfill are considered in this study.

Table 2.1 Classification of underfill process [38]

Process	**Dispense Stage**	**Application Location**	**Fluxing ability**	**Material Form**
Capillary underfill	After chip assembly and reflow	Between chip and substrate	No	Liquid
Molded underfill	After chip assembly and reflow	Between chip and substrate, overmolding the chip	No	Solid
No-flow underfill	Before chip assembly and reflow	On the substrate	Yes	Liquid
Wafer level underfill	After IC fabrication and before wafer dicing	On the wafer	Yes	Semi-solid

In the conventional capillary underfill, also called conventional underfill for short, as shown in Figure 2.2(a), the chip is placed on the substrate and the following processes are alignment, flux dispersing, solder bump reflow in which the solder bumps are joined between chip and substrate, flux cleaning, underfilling and curing, respectively [36, 39]. The conventional underfill is drawn into the gap between chip and substrate by the capillary force, which is usually slow and possibly causes the void formation resulting in the incomplete capillary flow. The curing of the underfill takes long time that consumed manufacturing time. In addition, decreasing bump pitch and chip height, and increasing bump density ultimately push the limits of conventional underfill materials.

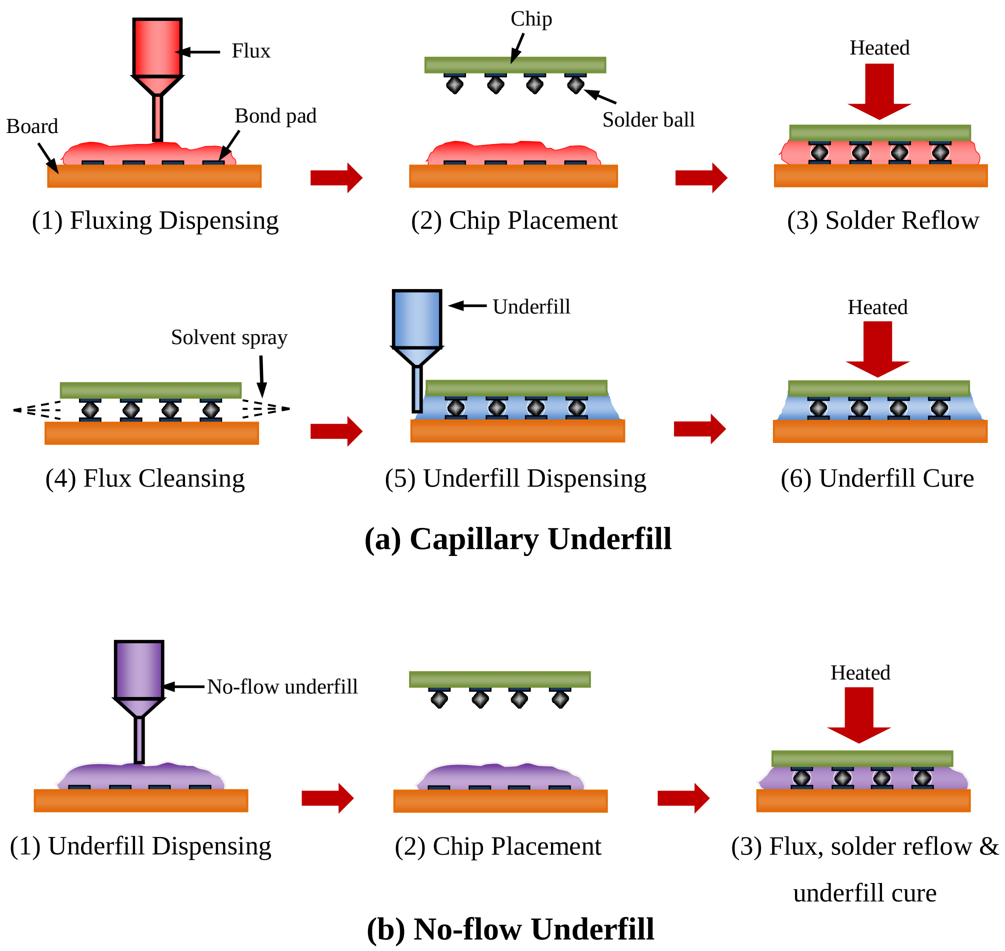

Figure 2.2 Scheme of (a) conventional capillary underfill and (b) no-flow underfill processes [40]

The no-flow underfill was invented by Wong et al. in 1996 to replace the conventional underfill and to reduce the cost because the no-flow underfill has fewer processing steps than the conventional underfill [41-44]. The scheme of no-flow underfill process is illustrated in Figure 2.2(b). The underfill material is dispensed onto the substrate followed by placing the chip on the substrate. After that the whole assembly is subjected to solder reflow and the underfill is cured in one step. Minimal curing reaction before the solder bump reflow and rapid curing reaction later are the crucial requirements of the materials for the no-flow underfill process that must match the reflow profile of the solder bump. The temperature profile of no-flow underfill process is demonstrated in Figure 2.3. The no-flow underfill process not only eliminates the limits on the viscosity of underfill material and the package size, but also improves the production efficiency.

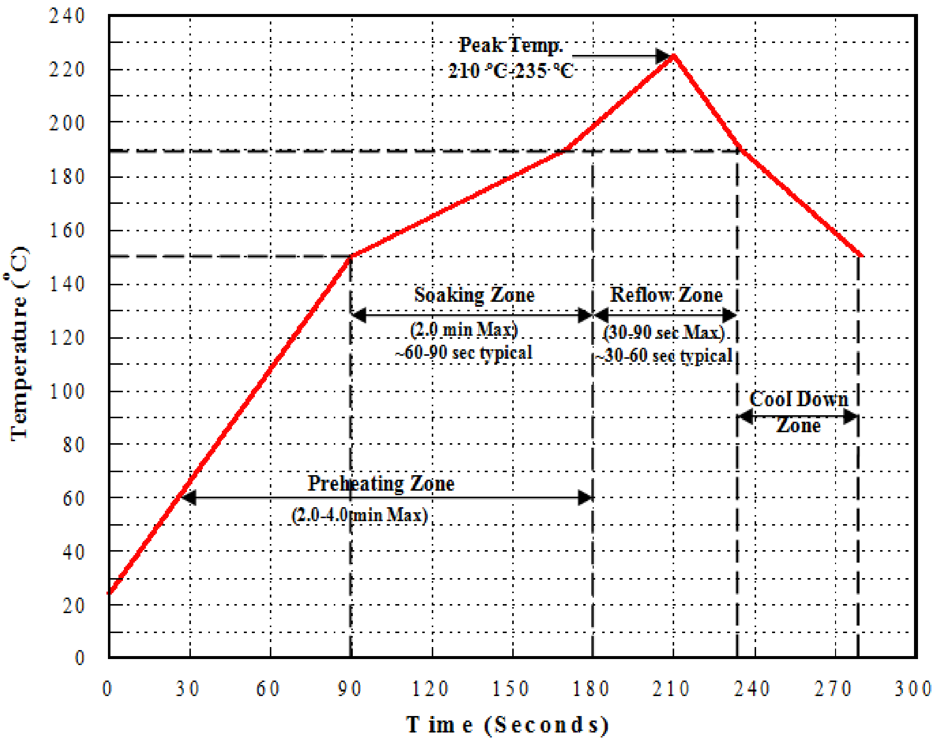

Figure 2.3 Temperature profile of no-flow underfill process[40]

2.2 Underfill materials

In addition to the advancement of underfill processes, underfill materials have been developed to be appropriate for the invented processes. Most underfill materials are based on epoxy resins [36]. The general underfill formula is composed of an epoxy resin monomer or epoxy mixture, a curing agent, a catalyst, SiO_2 filler, and other necessary additives (such as fluxing agent, toughening agent, adhesion promoter and dispersant agent) depending on the specific application [38]. The composition of underfill material is described in more detail below. Although the properties of underfill materials vary with the different underfill processes, the general requirement of the underfill material for flip-chip packaging can be summarized in Table 2.2.

Table 2.2 Desired properties of underfill materials for flip-chip packaging [36]

Property	Value
Coefficient of thermal conductivity (CTE)	22-27 ppm/°C
Glass transition temperature (T_g)	> 125 °C
Curing time	< 30 min
Working life (viscosity double @ 25°C)	> 16 hrs
Viscosity (@ 25°C)	<20 kcps
Modulus	8-10 GPa
Fracture toughness	> 1.3 MPa/m^2
Volume resistance (@ 25°C)	> 10^{13} ohm/cm
Dielectric constant (@ 25°C)	< 4.0
Filler content	< 70%

2.2.1 Epoxy resins

The thermosetting polymer containing the epoxy group or oxirane, a three-member ring consisting of an oxygen atom and two carbon atoms, can be called as epoxy resin [45]. The commonly used epoxy resin monomers can be categorized into three main groups: diglycidyl ether type, cycloaliphatic type and epoxy novolac type [46]. The selection of base epoxy resins plays a key role to succeed the underfill technology since many desired material properties are mainly determined by the base epoxy resins [38]. With the different polymerization degree and molecular weight, the epoxy before curing can be low viscosity liquid, high viscosity liquid, semi-solid and solid. The types of epoxy resins are shown in Table 2.3.

Table 2.3 Epoxy resin types [46]

Epoxy resin type	**Examples: Resin/Supplier**	**Characteristics**	**EEW[a]**
Diglycidyl ether of bisphenol A (DGEBA)	EPON 828/Resolution DER 331/Dow Chemical Co.	General-purpose use	185-192
Diglycidyl ether of bisphenol F (DGEBF)	EPON 826/Resolution	High flexibility, low viscosity	166-177
Epoxy novolac resin	DER 438/Dow Chemical Co. EPON 164/Resolution	High heat and chemical resistance	170-230
Cycloaliphatic epoxy resin	ERL 4221/Aldrich Chemical Co.	Good electrical characteristics and chemical resistance, low viscosity	131-143

[a]Epoxy equivalent weight (EEW) is the weight of resin per epoxy group.

2.2.2 Curing agents

A curing agent, also known as hardener, is an organic compound used to promote the curing reaction or the cross-linking reaction by reacting with the available epoxy or hydroxyl groups of epoxy resin monomer [45]. Amines and anhydrides are the common curing agents which have been intensively used in electronic applications. For underfilling technology, the decision among curing agents should be considered from the viscosity and flowability, curing mechanism, gelation behavior, wetting ability to the metal before curing, as well as the chemical structure and material properties after curing [38]. The advantages and disadvantages of distinct types of curing agents are detailed in Table 2.4.

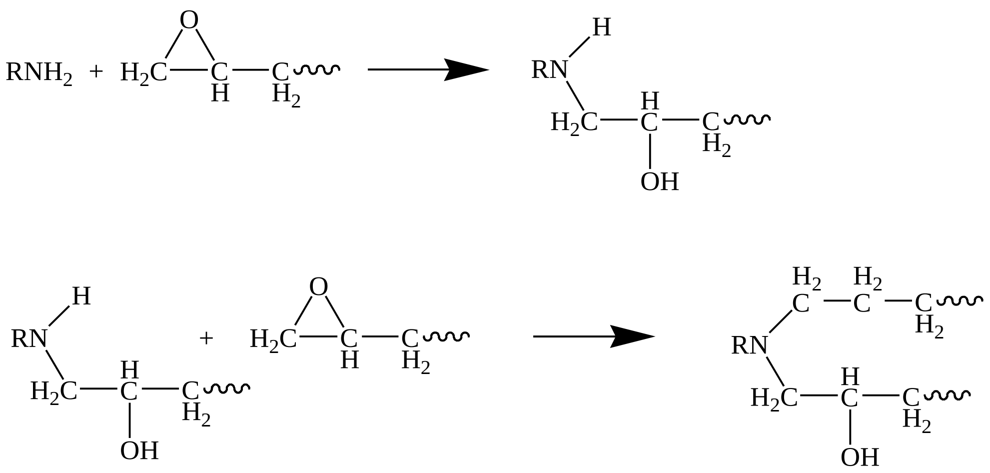

Figure 2.4 Mechanism of epoxy cured with amine curing agent [45]

Epoxy resins may be cured with the variety of curing agents that have a reactive hydrogen atom or hydroxyl group. Generally, the reactive hydrogen of curing agent can react with the epoxy groups of epoxy resins and initiates the polymerization process. For example, each primary amine curing agent has two reactive hydrogens that can react with two epoxy groups. The mechanism of amine curing agent as illustrated in Figure 2.4 starts with the reactive hydrogen of primary amines rapidly attaches to the oxygen atom to open the epoxy groups and to form a secondary amine. The resulting secondary amine further reacts with the other epoxy groups producing a tertiary amine and generating more hydroxyl groups that can further react and crosslink with other epoxy groups.

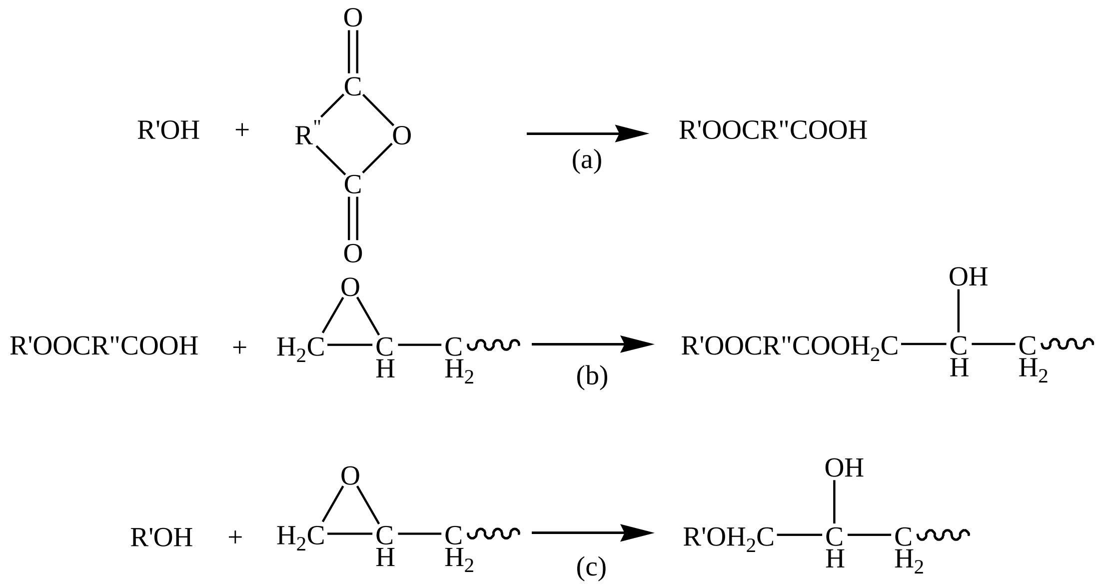

Figure 2.5 Mechanism of epoxy cured with anhydride curing agent [38]

Furthermore, anhydride curing agents are commonly used to cure epoxy resins, especially liquid anhydrides that have low viscosity and are easy to mix with epoxy resins. Nevertheless, the reactivity of some anhydrides with epoxies is low. Tertiary amines, metallic salts and imidazoles are often used as accelerator to accelerate gelation time and cure. The principle curing reaction is shown in Figure 2.5. The anhydride possibly reacts with the hydroxyl group of epoxy resin to produce monoester and a free carboxyl group (COOH) as illustrated in Figure 2.5(a). Then, free carboxyl group reacts with the epoxy group to form a second ester linkage and a free hydroxyl group as shown in Figure 2.5(b) that can react with other epoxy groups. Also, a free hydroxyl group may directly attach the epoxy group as displayed in Figure 2.5(c).

2.2.3 Catalysts

Catalyst is an initiator or a promoter of epoxy curing reaction by initially opening the epoxy ring and causing homopolymerization of the resins [38, 45, 46]. The types and amounts of catalyst used with the epoxy resins are determined to provide the optimal properties under required processing condition. Generally, only several parts per hundred of catalyst is used with the epoxy resins. The excess amounts of catalyst can result in the poor physical properties and degraded resins. There are at least four categories of catalysts that have been used in electronic applications including imidazoles and their derivatives, quaternary phosphonium compounds, metal acetylacetonates and some photoliable onium salts.

In addition to epoxy resins and curing agents, underfill materials are formulated with various additives to enhance or to modify their properties. For example, diluents with low viscosity are used to reduce the viscosity or to improve the solubility of epoxy resins. Diluents may be either reactive or non-reactive. Elastomeric polymer is possibly added to enhance toughness and flexibility. The great important additive in underfill formulation is the filler. The fillers, such as metal, metal oxide and inorganic particles, are incorporated with the polymers to improve their basic properties. The use of metal filler can enhance both thermal and electrical properties of polymers but it is not suitable for underfill materials which electrical insulation is required. Therefore, the metal oxide and inorganic particles are the candidates.

Table 2.4 Typical epoxy curing agents [38]

Curing Agent	Application	Advantage	Disadvantage
Aliphatic amines	Room temperature or low-temperature cure	- Low viscosity - Low formulation cost - Moderate chemical resistance	- Critical mix ratios - Strong skin irritant - High vapor pressure - Short working life, high exothermic reaction - Rigid, poor peel and impact properties
Aromatic amines	Heat cure	- Moderate heat and chemical resistance	- Solid at room temperature - Rigid - Long elevated-temperature cures
Polyamides	Room temperature or low-temperature cure	- Low toxicity - Good bond strength and flexibility - Moderately high peel and impact strength	- High formulation cost - Long cure times at room temperature - High viscosity - Low heat and chemical resistance
Anhydrides	Heat cure	- Good heat and chemical resistance	- Long elevated-temperature cure - Critical mix ratio - Rigid

2.2.4 Inorganic fillers

Underfill materials are applied in flip-chip packages to adhere between the silicon chip and the substrate and to protect the solder-ball interconnections by minimizing the thermal stress and strain caused by mismatches in CTE of devices. As component density increases**,** the operating at high speeds and consuming high power of devices, thermal and stress dissipation are becoming important. Underfill materials play a rule in conducting heat from the devices; however, underfill materials based on epoxy resin have low thermal conductivity and high CTE. Accordingly, the inorganic fillers as demonstrated in Table 2.5 that are electrical insulation and have low CTE are widely used in underfill applications.

Table 2.5 Thermal conductive materials commonly used in electronic packages [38]

Material	Symbol	Thermal conductivity (W/mK)
Alumina	Al_2O_3	18-40
Aluminum nitride	AlN	170-260
Beryllia	BeO	250
Boron nitride	BN	130-260
Diamond	Crystalline	1500-2000
Gallium arsenide	GaAs	43-50
Indium phosphide	InP	68
Quartz	Crystalline SiO_2	1.4
Silicon carbide	SiC	270
Silicon dioxide	SiO_2	1.5-7
Silicon nitride	Si_3N_4	170

*Values vary depending on the purity of the sample, testing condition and testing method.

Nevertheless, inorganic fillers are used to achieve the thermal transport properties of underfill materials at very high filler content resulting in increasing their viscosity abruptly. Accordingly, finding of new ideal materials to modify the thermal transport properties of underfill materials is the challenge. Recently, the carbon-based materials, especially MWCNTs and SWCNTs that are mentioned in the next section, have been paid more attention to use in electronic applications due to the outstanding thermal, electrical and mechanical properties. Thus, MWCNTs and SWCNTs are the filler candidates in this work.

2.3 Carbon nanotubes (CNTs)

Carbon nanotubes (CNTs) were first discovered by Iijima in 1991while studying the material deposited on the cathode during the arc evaporation synthesis of fullerene. Since the performing of a large-scale synthesis method by Ebbesen and Ajaian in 1992, there are many investigations and attempts that have been made to understand their chemical structures in order to improve the synthesis techniques and understand the relationship between structure and properties. The brief knowledge of CNTs is described in this section.

2.3.1 Fundamentals of carbon nanotubes

Carbon nanotubes are fullerene-based structures that can be visualized as a sheet of graphite rolled into a tube. Ideally all carbon atoms in the nanotubes are covalently bonded and form repeated close-packed hexagonal structures in each layer or shell where each carbon atom is bonded to three neighboring carbon atoms through sp^2 hybridization . Commonly, there are two main forms of CNTs:

Single-walled carbon nanotubes (SWCNTs) are close to an ideal fullerene fiber and consist of a single-layer cylinder extending from end to end with a narrow distribution in diameter range (1 to 2 nm).

Multi-walled carbon nanotubes (MWCNTs) consist of concentric cylinders placed around a common central hollow area with a constant separation between the layers close to the graphite interlayer spacing (0.34 nm). Each individual cylinder can be characterized by a different helicity and has a diameter ranging from 2 to 25 nm and a length of several microns.

Table 2.6 Physical properties of different carbon materials [47]

Property	**Carbon material**				
	Graphite	**Diamond**	**Fullerene**	**SWCNT**	**MWCNT**
Specific gravity (g/cm^3)	1.9-2.3	3.5	1.7	0.8	1.8
Electrical conductivity (S/cm)	4000^p, 3.3^c	10^{-2}-10^{-15}	10^{-5}	10^2-10^6	10^3-10^5
Electron mobility (cm^2/Vs)	2.0×10^4	1800	0.5-6	$\sim 10^5$	10^4-10^5
Thermal conductivity (W/mK)	298^p, 2.2^c	900-2320	0.4	6000	3000
Coefficient of thermal expansion (ppm/K)	-1^p, 0.29^c	1-3	0.62	n/a	n/a
Thermal stability in air (°C)	450-650	<600	<600	<600	<600

p: in-plane; c: c-axis.

SWCNTs tend to be stronger and more flexible than MWCNTs. Sliding of individual cylinders inside one another is one reason that MWCNTs are weaker. SWCNTs also possess better electrical conductivity and more transparent. However, their production and purification process are complicate thus SWCNTs are more expensive. Currently, MWCNTs are more widely used in composite materials than SWCNTs for these reasons. The properties of CNTs depend on chirality (how the graphite sheet is rolled), the diameter and the length of the tube and the morphology. The principle properties of CNTs are shown in Table 2.6.

2.3.2 Synthesis of carbon nanotubes

Since CNTs were first discovered, they have been intensively investigated in wide range of applications. In the early research, CNTs were produced in small quantity, difficult to purify and to manipulate and expensive. Thus, researchers have tried to develop the synthesis method to produce CNTs in the large scale and high purity. The widely used methods to synthesis CNTs are:

2.3.2.1 Arc discharge

The arc discharge method is probably one of the simplest ways to produce carbon nanotubes. The electric arc discharge is produced between two graphite electrodes placed end to end under an inert gas atmosphere, generally He or Ar. A direct current (~50 to 100 amps) driven by a low-voltage (~12 to 25 V) generates a high temperature discharge or plasma between the two electrodes. The discharge vaporizes the anode rod and forms carbon nanotubes deposited on the cathode rod. This method is usually used to produce MWCNTs, but if the anode is doped with a metal catalyst, such as Fe, Co, Ni, or Mo, the arc discharge can produce SWCNTs. Producing carbon nanotubes in high yield depends on the uniformity of the plasma arc, the current density, inert gas pressure and the cooling temperature of the deposit form on the graphite electrode.

2.3.2.2 Laser ablation

In the laser ablation process, a pulsed laser vaporizes a graphite target in a high-temperature reactor while an inert gas is bled into the chamber. Carbon nanotubes are produced and then deposited onto the collector surface, the water-cooled metallic. The laser ablation method has been proven to be the efficient technique for the production of high purity carbon nanotubes.

2.3.2.3 Chemical vapor deposition (CVD)

The CVD process encompasses a wide range of synthesis techniques, from the gram-quantity bulk formation of nanotube material to the formation of individual aligned SWCNTs on SiO_2 substrates for use in electronics. CVD can also produce aligned vertical MWCNTs for use as high-performance field emitters. Additionally, CVD in its various forms produces SWCNT material of higher atomic quality and higher percent yield than the other methods currently available and, as such, represents a significant advance in SWCNT production. The majority of SWCNT production methods developed lately have been direct descendents of basic CVD. Simply put, gaseous carbon feedstock is flowed over transition metal nanoparticles at medium to high temperature (550 to 1200˚C) and reacts with the nanoparticles to produce SWCNTs. With CVD, SWCNTs anywhere from 0.4 to 5 nm can be readily produced, and depending on the conditions, feedstock, and catalyst, the yield can exceed 99% (weight percent of final material) and the final product can be completely free of amorphous carbon.

2.3.2.4 High pressure conversion of carbon monoxide (HiPCo)

One of the recent methods for producing SWCNTs is the HiPCo process. Though related to CVD synthesis, HiPCo deserves a separate mention, since in recent years it has become a source of high-quality, narrow-diameter distribution SWCNTs around the world. The metal catalyst is formed in situ when Fe(CO) or Ni(CO) is injected into the reactor along with a stream of carbon monoxide (CO) gas at 900 to 1100˚C and at a pressure of 30 to 50 atm. The reaction to make SWCNTs is the disproportion of CO by nanometer-size metal catalyst particles. Yields of SWCNT material are claimed to be up to 97% atomic purity. The SWCNTs made by this process have diameters between 0.7 and 1.1 nm. By tuning the pressure in the reactor and the catalyst composition, it is possible to tune the diameter range of the nanotubes produced.

2.3.3 Surface modification of carbon nanotubes

Although CNTs have many advantages for electronic applications, the difficult to manipulate is a crucial problem. Due to the insolubility and non-reactive surface of CNTs, the properties of CNT/polymer composites are lower than those from the theoretical prediction. To overcome this problem, the surface modification by functionalizing the surface of CNTs is applied to enhance the interaction between CNT and polymer matrix. The approaches to modify surface of CNT are given as follows:

2.3.3.1 Acid treatment

Acid treatment, also called acid oxidation, is an essential process to purify CNTs by removing the impurity compounds on the CNT surface such as metal catalysts, carbon fragments and amorphous carbon particles. During acid oxidation, the carbon-carbon bonded network of the graphitic layers is broken allowing the decoration of CNT surface with oxygen-containing groups including carboxyl, phenolic and lactone groups. Generally, the strong acids, like nitric acid, sulfuric acid and their mixture, are used as medium for this process at elevated temperature. The functional groups attached on surface of CNTs have been extensively exploited for further chemical functionalization. The attachment of silane coupling agent on modified CNT surface by acid treatment is illustrated Figure 2.6.

2.3.3.2 Friedel-Crafts acylation

Friedel-Crafts reactions were discovered in 1877 by Charles Friedel and James Crafts. There are two main types of Friedel-Crafts reactions including alkylation and acylation. This type is a part of electrophilic aromatic substitution reactions that feature an electrophile replacing a hydrogen atom in an aromatic compound and can form a new carbon-carbon bond if done with an electrophilic carbon species.

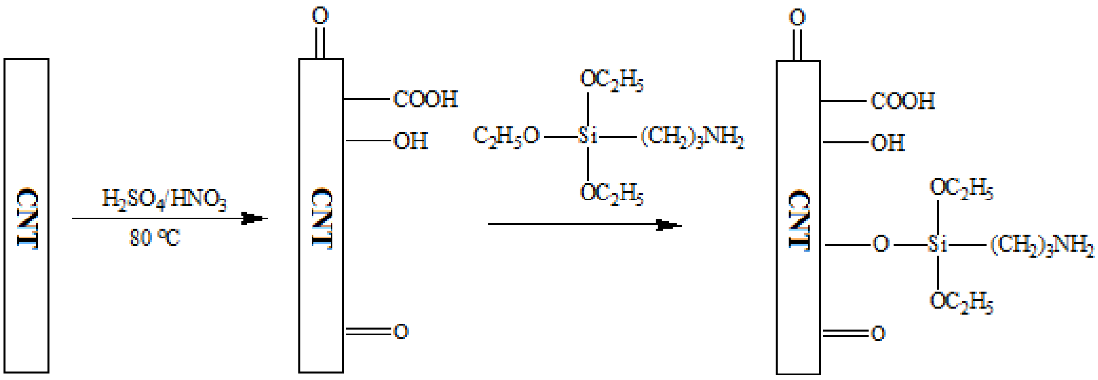

Figure 2.6 Attachment of silane coupling agent on modified CNT surface by acid treatment [48]

Friedel–Crafts acylation is the acylation of aromatic rings with an acyl chloride using a strong Lewis acid catalyst. Friedel–Crafts acylation is also possible with acid anhydrides. Reaction conditions are similar to the Friedel–Crafts alkylation mentioned above. This reaction has several advantages over the alkylation reaction. Due to the electron-withdrawing effect of the carbonyl group, the ketone product is always less reactive than the original molecule, so multiple acylations do not occur. Also, there are no carbocation rearrangements, as the carbonium ion is stabilized by a resonance structure in which the positive charge is on the oxygen. The scheme of Friedel-Crafts acylation is illustrated in Figure 2.7.

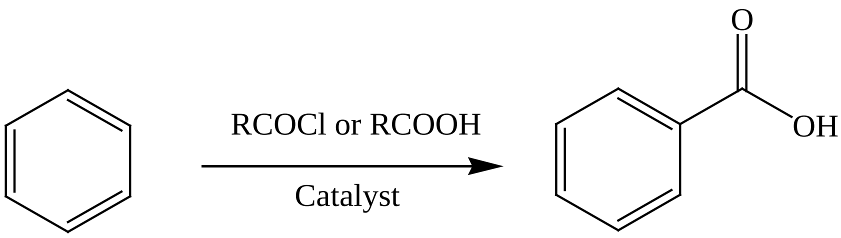

Figure 2.7 Scheme of Friedel-Crafts acylation

CHAPTER III
LITERATURE REVIEWS

Effective underfill materials should not only have a suitable CTE to IC devices and a low dielectric constant to reduce the device propagation delay, but also possess a high thermal conductivity to dissipate heat from electronic packaging. Underfill materials are commonly based on epoxy resins which have poor thermal properties resulting in poor reliability and performance of packaging. Therefore, the improvement of thermal conductivity of underfill materials has been extensively considered that some literatures are reviewed in this chapter.

3.1 Underfill materials incorporated with thermal conductive fillers

Commonly, silica has been added into epoxy resins to reduce CTE of underfill materials; however, silica has poor thermal conductivity thus the high thermal conductive particles are the potential candidates. According to the early researches, the ceramic particles like SiC [5], BN [9] and AlN [8, 12] were added into epoxy resins to modify the global properties of underfill materials. It was found that thermal conductivity of epoxy composites increased almost linearly with increasing filler content [2, 3]. The formation of heat conductive networks was promoted by increasing filler concentration responding to heat conduction passing through the composites. Considering at same loading, the fillers with higher intrinsic thermal conductivity provide the higher thermal conductivity of epoxy composites [1, 4]. Also, the influence of filler's geometry was studied. The fillers with high aspect ratio easily provided the networks between them, known as conductive paths, resulting in better contact between the filler and polymer matrix which is possible to reduce thermal contact resistance, thereby increasing thermal conductivity of composites [13]. There are several literatures that explored the effect of hybrid fillers on the properties of composites. It was clear that the filler systems containing the different shapes, that gave high packing density, were effective to promote the heat conductive pathways[9, 12]. However, the high thermal conductivity achieved at very high filler loading, resulting in the high viscosity, limits underfill applications.

3.2 CNT/polymer composites

Carbon nanotubes (CNTs) are the carbon-based fillers that have the outstanding properties rather than other carbon materials. Due to excellent thermal and mechanical properties, low density and high aspect ratio, CNTs have been comprehensively employed as ideal reinforcing additives in various thermoplastics and thermosetting matrices [47,49, 50]. Some literatures revealed that mechanical properties of composites were achieved by incorporation of CNTs into polymer matrix because the aspect ratio of CNTs is adequately large to maximize the load transfer between the CNTs and the matrix [51-54]. Moreover, CNTs were expected to be effective fillers to rectify the thermal properties of polymers owing to the high thermal conductivity and good thermal stability. Thus, many efforts have been devoted to employing CNTs as thermal conductive filler in polymer composites. For CNT/polymer composites, the thermal conductivity depends on several factors including the content, aspect ratio, dispersion of CNTs and their interfacial interactions with polymer matrix. It was found that thermal conductivity of composite was improved with increasing CNT loading. Unfortunately, the composite undergoes an insulator-to-conductor transition when CNT loading was gradually increased [53, 55]. Rising to the critical filler content as the percolation threshold, the electrical conductivity of the composite sharply jumps up several orders of magnitude due to the formation of continuous electron paths or conductive networks. To minimize aforementioned problem, the few amounts of CNTs were incorporated into polymers for insulating materials. Generally, CNTs are held together in bundles or entanglements by Van der Waals force because of the small diameter in nanoscale with high aspect ratio (>1000) and extremely large surface area of CNTs. The nature of CNT dispersion is different from other fillers, such as spherical particles and carbon fibers that the homogeneous distribution of individual particles in polymer matrix can be done easily. Meanwhile, CNTs are very insoluble in most solvents and also aggregate when they are filled into polymer matrix. Accordingly, the properties of composites reinforced with CNTs are also lower than those with theoretical predictions related to individual CNTs. The methods on how to divide individual CNT from CNT bundles and to disperse them in polymer matrix are the challenge.

To take advantage of their properties as predicted, achieving homogeneous dispersion and good interfacial interaction between CNTs and polymer matrix is a crucial issue on incorporation of CNTs and polymer matrix. The several literatures have reported on the dispersion techniques of CNTs in polymer matrix [47, 56]. CNTs must be efficiently dispersed as an individual tube into the polymer matrix. Ultrasonication is one of the most effective physical approaches to disperse CNTs [47]. The principle of this method is applying the ultrasound energy to agitate particles in a solution and to promote the peeling off of individual particles located at the exterior of bundles or agglomerates. CNTs are effectively dispersed in low viscous liquids; however, most polymers are either in a solid or viscous liquid form. The solvents or the diluents are required to dissolve and to reduce the viscosity of polymers. Furthermore, the processing conditions of ultrasonication affect the quality of CNTs. If the treatment is too long and/or too aggressive, the CNT structures can be easily damaged and converted into carbon fibers or carbonaceous in serious cases resulting in the lower thermal and mechanical properties. Unfortunately, ultrasonication is ineffective to provide strong interfacial interaction between CNTs and polymer matrix. Therefore, other effective methods have been studied for CNTs incorporated into polymer matrix.

3.3 Surface modification of CNTs

Due to the inert surface of CNTs, and the large difference in surface energies of CNTs and the polymer matrix, physical interaction between components may not be adequate to execute maximum enhanced properties of composites. Thus, chemical treatment approaches have become popular and an alternative approach for CNT surface modification is chemical oxidation. In typical chemical oxidation, CNTs are treated in high concentration acids, such as nitric acid and sulfuric acid and/or their mixtures, at elevated temperatures. After acid treatment, metal impurities and amorphous carbon were removed [50, 57]. Also, the carboxylic groups and oxygen-containing groups were observed on CNT surface [58]. These functional groups facilitate further reactions such as silanization and polymer grafting [59-61]. The surface modification of CNTs by acid treatment is demonstrated in Figure 3.1. Some investigations indicated that dispersibility and solubility of modified CNTs were improved, resulting in better global properties of composites [19, 50, 62]. However, many cases often show damage to CNT structures owing to the harsh reaction conditions. Significant damage to the CNT framework is unavoidable, such as sidewall opening, breaking, and turning into amorphous carbon [18]. Consequently, developing an efficient chemical modification method without or with little damage to CNT surface is very important for the development of the CNT utility.

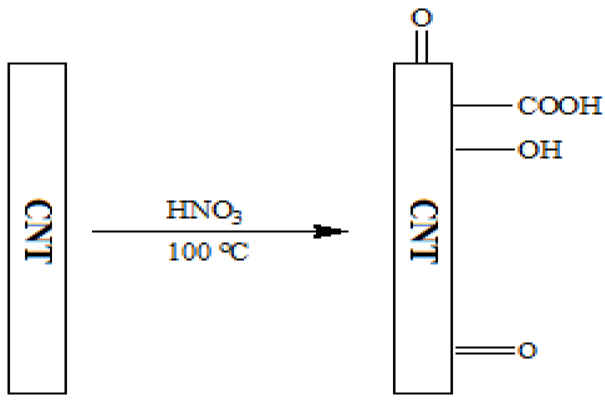

Figure 3.1 Surface modification of CNTs by acid treatment [19]

Recently, carbon nanofibers were successfully grafted with monomer by using an electrophilic substitution reaction, also called Friedel-Crtafts acylation. Polyphosphoric acid (PPA)/phosphorus pentoxide (P_2O_5) were used as medium reaction [63]. It is envisioned that the presence of versatile carbonyl groups on the surface of carbon nanofibers will allow further development of CNT-based materials. In this method, PPA not only serves as Friedel-Crafts catalyst, but also plays two forceful roles in the functionalization of CNF surface. Its moderate acidity promotes debundling of CNFs that implies to promote homogeneous distribution, and its high viscosity helps to impede CNF reaggregation after their dispersion. Moreover, several studies reported that the various 4-substituted benzoic acids could be introduced on MWCNT surface via Friedel–Crafts acylation as shown in Figure 3.2 [24, 64]. It revealed that the solubility and thermal stability of functionalized MWCNTs were greatly influenced by the nature of surface groups. The results envision that they potentially provide basic knowledge on the selection of surface groups for specific applications and are very useful for the composite preparation. For example, MWCNTs functionalized with 4-ethoxybenzoic acid (EtO-MWCNTs) could be homogeneously dispersed in ethylene glycol and in situ polymerized with terephthalic acid to prepare EtO-MWNT/PET nanocomposites [64].

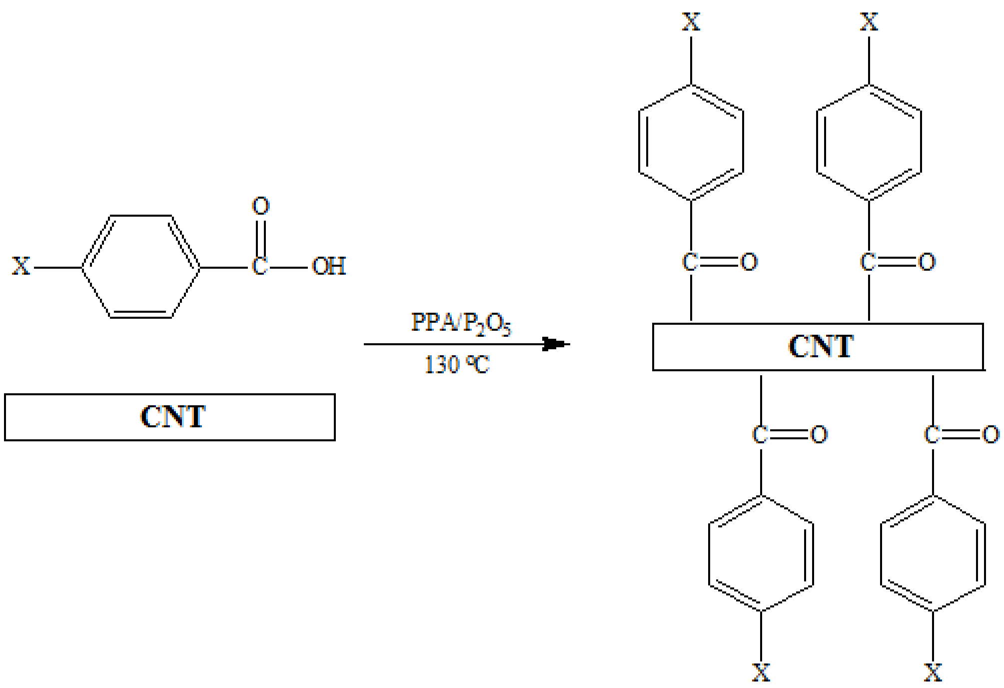

X = NH_2, OH, OCH_2CH_3, OCH_3, H, F, Cl, Br, I, NO_2

Figure 3.2 Functionalization of MWCNTs with 4-substituted benzoic acids in PPA/P_2O_5 at 130 $^{\circ}$C [24]

From these developments, Han et al. have attempted to purify and to functionalize SWCNTs in one-pot process using a mild PPA/P_2O_5 medium because the purification and surface modification of SWCNTs are equally important for the further development and utility [23]. From the FTIR results, the spectra of all purified SWCNTs have few or no change compared with the spectrum of as-received SWCNTs. It could be confirmed that PPA does not oxidize SWCNTs to create more carboxylic acid (COOH) groups on the side walls of them during the purification unlike the purification by using acid oxidation. This result also implies that a mild PPA is indeed an excellent medium to purify SWCNTs without or little damage to the SWCNT surface. Also, the functionalization of SWCNTs with 4-aminobenzoic acid (4-ABAc) was conducted in the same purification medium that the characteristic peak of the carbonyl group was observed at 1656 cm^{-1} in FTIR spectrum. Consequently, the purification and functionalization of SWCNTs could be performed in a one-pot manufacturing process that allows further development to generate interesting CNT-based materials. Recently, Yang et al. studied the grafting of benzenetricarboxylic acid (BTC) onto MWCNTs via Friedel-Crafts reaction [49]. The dispersion and thermal properties of BTC-MWCNT/epoxy composites were investigated comparing with pristine-MWCNTs and oxidized MWCNTs. From Raman spectra, I_D/I_G ratio of BTC-MWCNTs was smaller than others in which it revealed that BTC-MWCNTs provided better structure than those of pristine-MWCNTs and oxidized MWCNTs. Thermal conductivity of BTC-MWCNT/epoxy composites increased more than 315% by adding 1 vol% of BTC-MWCNTs. Knowledge of surface modification via Friedel-Crafts acylation have led to the hope that CNTs grafted with functional groups, that can be reacted with epoxy groups, via this method will improve the global properties of underfill materials.

CHAPTER IV
EXPERIMENTAL

4.1 Materials

Diglycidyl ether of bisphenol A (DER331, MW 372) from Dow Chemical Company, hexahydro-4-methylphthalic anhydride (MHHPA, 96%) and cobalt (II) acetylacetonate (CoIIAcAc) from Sigma-Aldrich Co. were used as polymer matrix, curing agent and catalyst, respectively. The purified multi-walled carbon nanotubes (MWCNTs) produced by a chemical vapor deposition (CVD) process from Chengdu Organic Chemicals Company (Chinese Academy of Sciences) and submicron-sized silicon nitride (Si_3N_4, 1 μm) from Sigma-Aldrich Co were used as fillers. Polyphosphoric acid (PPA, 83% assay) and phosphorus pentoxide (P_2O_5) from Sigma-Aldrich Co. were used as a reaction medium for the functionalization in which benzene-1,3,5-tricarboxylic acid (BTC) and 3,5-diaminobenzoic acid (DAB) from Sigma-Aldrich Co. were used as functionalizing reactants. The chemical structures and properties of materials are shown as follows.

Table 4.1 Properties of as-received MWCNTs

Properties	**Value**
CNT content	>90%
Outer Diameter	<8 nm
Inner Diameter	2-5 nm
Length	10 μm
Special Surface Area	500 m^2g^{-1}
True density	~2.1 gcm^{-3}
Electrical Conductivity	>100 scm^{-1}

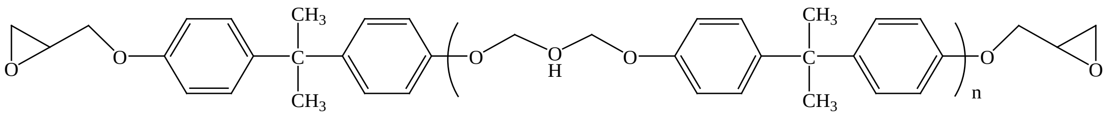

Figure 4.1 Structure of epoxy monomer

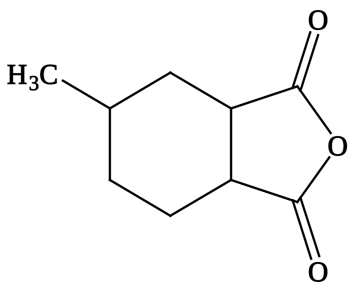

Figure 4.2 Structure of hexahydro-4-methylphthalic anhydride (MHHPA)

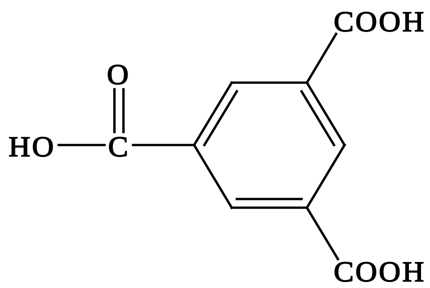

Figure 4.3 Structure of benzene-1,3,5-tricarboxylic acid (BTC)

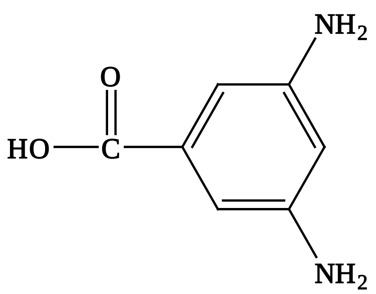

Figure 4.4 Structure of 3,5-diaminobenzoic acid (DAB)

Table 4.2 Properties of Si_3N_4

Properties	**Value**
Diameter	<1 μm
Molecular Weight	140.28 $gmol^{-1}$
Density	3.44 gml^{-1}
Coefficient of Thermal Expansion	4.4 ppm°C^{-1}
Thermal Conductivity	>150 $Wm^{-1}K^{-1}$

4.2 Preparation of functionalized MWCNTs

In this work, MWCNTs were covalently functionalized with functionalizing reactants via electrophilic substitution reaction which was called a direct Friedel-Crafts acylation in a mild PPA/P_2O_5 medium. Due to its moderate acidic, PPA not only promoted the oxidation of metallic impurities and carbonaceous fragments on the surface of MWCNTs, but also effectively catalyzed the Friedel-Crafts reaction. Besides, the viscous characteristic of PPA could impede the reaggregation of MWCNTs. P_2O_5 was used as a dehydrating agent to promote the functionalization. The scheme of functionalizing reaction is demonstrated in Figure 4.5 and the experimental details are described as follows.

The specific weight of functionalizing reactant**,** as-received MWCNTs, PPA and P_2O_5 were placed in a 100 ml round-bottom flask equipped with a mechanical stirrer, nitrogen inlet and outlet. This mixture was stirred at 130 °C for 72 hr under dry nitrogen purge. Distilled water was added to the mixture after cooling down to room temperature. The obtained MWCNTs separated by centrifuge were stirred in acetone for 1 day to remove unreacted chemicals. The MWCNT solution was then separated by centrifuge. The above-mentioned purification steps were repeated for 2–3 times. After that, the MWCNTs were washed with distilled water and separated by centrifuge. Then, the collected powder was freeze dried for 3 days to remove remaining solvent. In this research, the unmodified MWCNTs are defined as U-

MWCNT where MWCNTs functionalized with BTC and DAB are defined as BTC-MWCNT and DAB-MWCNT, respectively.

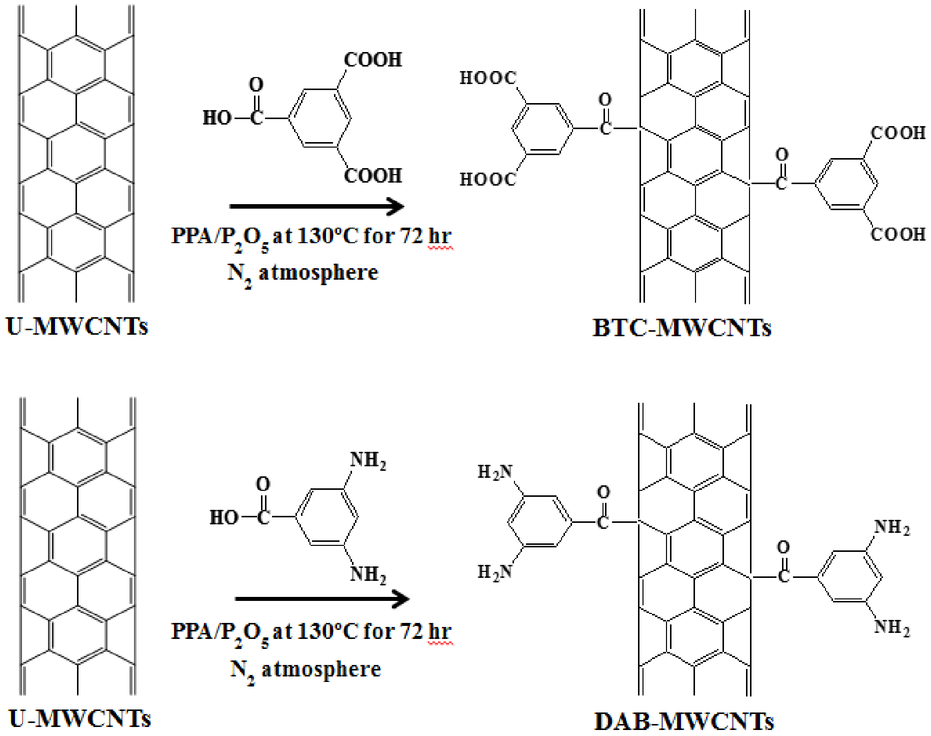

Figure 4.5 Functionalization of MWCNTs via a direct Friedel-Crafts acylation

4.3 Preparation of MWCNT/epoxy composites

Owing to poor dispersion of MWCNTs in epoxy, MWCNTs were firstly sonicated in the curing agent that was also acted as a solvent due to its low viscosity for 1 hr. In case of hybrid filler systems, submicron-sized Si_3N_4 particles were mixed and sonicated in MWCNT mixture. Epoxy was then added and stirred in the mixture. The catalyst was dissolved in the mixture by ultrasonication for 30 min. The mixture was then stirred until homogeneous. The obtained mixture was transferred to aluminum mold and degassed in a vacuum oven. After curing at 230 °C for 1 hr, the sample was slowly cooled down to room temperature. The mold was peeled off and the sample was polished for further analysis. Figure 4.6 demonstrates the procedure of epoxy composite preparation.

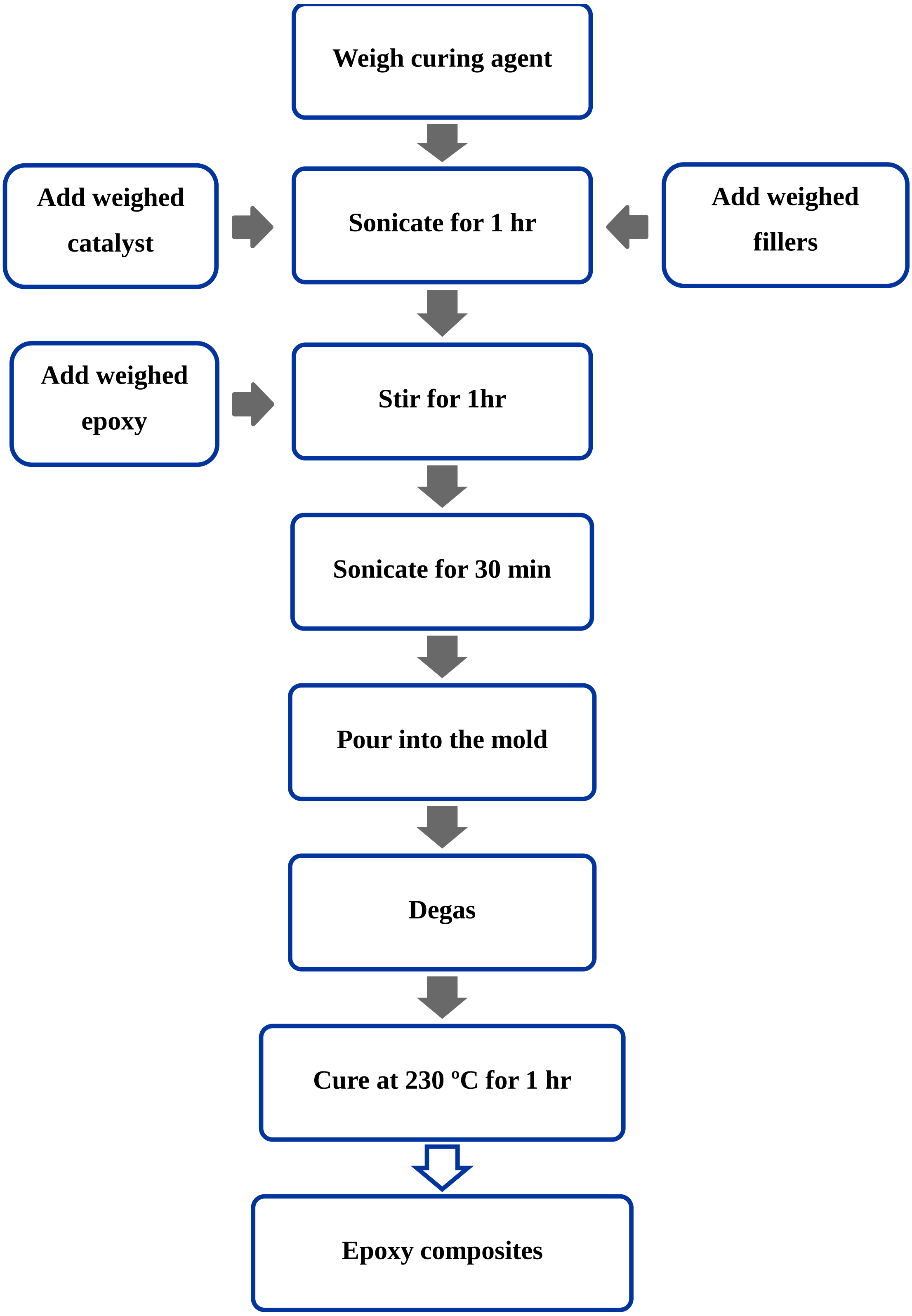

Figure 4.6 Scheme of epoxy composite preparation

4.4 Characterization

4.4.1 Fourier Transform Infrared Spectroscopy

To investigate the functional groups on MWCNT surface before and after the functionalization, FT-IR spectra were conducted by using a Spectrum GX FT-IR spectrometer (Perkin Elmer, USA). The powder sample and KBr powder were ground together. The ground powder was pressed into pellet with a smooth surface. The pellet was loaded into a sample holder and then placed in a chamber. All FT-IR spectra were collected in a range of 4000-650 cm^{-1} with a resolution of 4.0 cm^{-1} under continuous nitrogen flow.

4.4.2 X-ray Photoelectron Spectroscopy

Surface chemistry of unmodified and functionalized MWCNTs was evaluated by using XPS. XPS analysis was performed by using an AMICUS photoelectron spectrometer equipped with a Mg K_α X-ray as a primary excitation and a KRATOS VISION2 software. The XPS curve fitting of C1s, O1s and N1s was accomplished by Origin 8.1.

4.4.3 Fourier Transform Raman Spectroscopy

The effect of functionalization on the structural quality of MWCNTs was examined by using a Spectrum GX FT-Raman spectrometer (PerkinElmer, USA). FT-Raman analysis was performed over a range of 0-1000 cm^{-1} with a laser in the near infrared-usually at 1064 nm.

4.4.4 Thermogravimetric/Differential Thermal Analysis

The thermal stability of MWCNTs before and after the functionalization was evaluated by using a Diamond TG/DTA instrument (PerkinElmer, USA). Samples were loaded in ceramic pans and then heated to 800 °C at 10 °C/min under nitrogen atmosphere at 100 ml/min flow rate.

4.4.5 Dispersion Analysis

The dispersion stability of MWCNTs at different time intervals was investigated. MWCNTs were dispersed in ethanol with 0.4 mg/ml via ultrasonication for 30 min and dispersibility was then observed at different time intervals.

4.4.6 Scanning Electron Microscopy

Morphology of the fracture surface of epoxy composites was observed by using a Hitachi S-3400 scanning electron microscope (SEM) to study the dispersion of fillers in the polymer matrix. All samples were quenched in liquid nitrogen and fractured to obtain the cross-sections. The samples were then sputter coated with gold before the SEM observation.

4.4.7 Differential Scanning Calorimetry

The curing behavior of epoxy composites filled with unmodified and functionalized MWCNTs was examined by differential scanning calorimetry (TA Instrument, model 2910 DSC, USA). The non-isothermal scanning experiments were performed at different heating rates of 3, 5, 10 and 20 ºC min^{-1}. A full temperature scan was performed between 30 ºC and 350 ºC under nitrogen atmosphere at a flow rate of 50 ml min^{-1}.

4.4.8 Density Analysis

The density of epoxy composites was measured by water displacement which can be given by

$$\rho = \frac{W_{dry}}{W_{dry} - W_{wet}} \rho_{water}(T) \qquad (1)$$

where ρ is the density of epoxy composite; W_{dry} and W_{wet} are the weight of sample in air and water, respectively; and $\rho_{water}(T)$ is the density of water at measured temperature.

The theoretical density of composites was also calculated by using a following equation

$$\rho=\rho_m(1-\sum_{i=1}^{n} V_i)+\sum_{i=1}^{n} \rho_i V_i \qquad (2)$$

where ρ_m, and ρ_i are the density of polymer matrix and filler, respectively; and V_i is the volume fraction of filler.

4.4.9 Dynamic Mechanical Analysis

The dynamic mechanical properties of epoxy composites were investigated by using a Pyris Diamond DMA instrument (Perkin-Elmer, USA). The bending mode was performed at various frequencies of 1, 2, 5, 10, 20 and 50 Hz for all of samples. The samples were heated from room temperature to 200 °C at a heating rate of 5 °C/min under N2 atmosphere.

4.4.10 Thermomechanical Analysis

The coefficient of thermal expansion (CTE) of all samples was determined by using a Pyris Diamond TMA instrument (Perkin-Elmer, USA). The expansion probe was performed with 3 mN of static force. The temperature was scanned from room temperature to 250 °C at a heating rate of 5 °C/min under N_2 atmosphere.

4.4.11 Thermal Conductivity Analysis

The laser-flash thermal conductivity measurement was performed in this work. The measurement of thermal diffusivity was conducted by using a LFA 1000 Laser flash (NETZSCH, Germany). The sample surface was irradiated with very short laser pulse and temperature rise was measured on the opposite side of the sample, leading to calculating the thermal diffusivity. Specific heat capacity was measured by using a Pyris Diamond DSC instrument (Perkin Elmer, USA). Also, the bulk density of the specimen was measured by water displacement.

CHAPTER V
RESULTS AND DISCUSSION

The primary goal of this work was to enhance thermal conductivity of underfill materials by using MWCNTs as fillers. MWCNTs were directly functionalized with various functionalizing reactants via Friedel-Crafts acylation to enhance the dispersion and interfacial interaction between filler and polymer matrix. The results of functionalization were discussed in this chapter. The properties of epoxy composites filled with unmodified and functionalized MWCNTs were investigated by using various analytical techniques. Additionally, thermal conductivity of composites was evaluated and compared with several theoretical and empirical models as well. Furthermore, the results of hybrid fillers containing MWCNTs and submicron-sized Si_3N_4 particles on the properties of underfill materials were also discussed in detail.

5.1 Functionalization of MWCNTs

To obtain great performance of MWCNTs as reinforcing filler in polymer composites, enhancing dispersion and interfacial interaction between MWCNT and polymer matrix is necessary. In this research, MWCNTs were covalently functionalized with reactive functionalizing reactants, i.e., benzene-1,3,5-tricarboxylic acid (BTC) and 3,5-diaminobenzoic acid (DAB), via a direct Friedel-Crafts acylation, electrophilic substitution reaction, in a mild PPA/P_2O_5 medium under nitrogen atmosphere. After the functionalization, MWCNT surface would be decorated with carboxyl and amino functional groups which were really helpful for further composite fabrication. The results of functionalization and preparation of MWCNT/epoxy composite were investigated via various analytical techniques and discussed as follows.

5.1.1 Surface chemistry of functionalized MWCNTs

Surface chemistry of MWCNTs before and after the functionalization was investigated by using FT-IR as illustrated in Figure 5.1. It was clearly seen that U-MWCNTs show a peak at ~1567 cm^{-1} assigned to aromatic C=C stretch of benzene ring and a small peak at ~1189 cm^{-1} corresponded to C-O stretch of the phenols [65, 66]. It revealed that there were small amounts of oxygen-containing groups established on the surface of U-MWCNTs. After the functionalization, BTC-MWCNTs exhibit peaks at ~1622 and ~1718 cm^{-1} ascribed to C=O stretch and another peak at ~3434 cm^{-1} assigned to O-H stretch of carboxylic group on their surface [67] as depicted in Figure 5.1(b). A characteristic peak at ~1216 cm^{-1} is observed in DAB-MWCNT spectrum as shown in Figure 5.1(c) which is attributed to N-H stretch of primary aromatic amine. Also, the peaks at ~1736 and ~3435 cm^{-1} can be ascribed to C=O stretch of carbonyl group and N-H stretch of amine groups, respectively [68]. These observations indicated that the functionalization was successful to introduce the functionalizing reactants as BTC and DAB onto MWCNT surfaces.

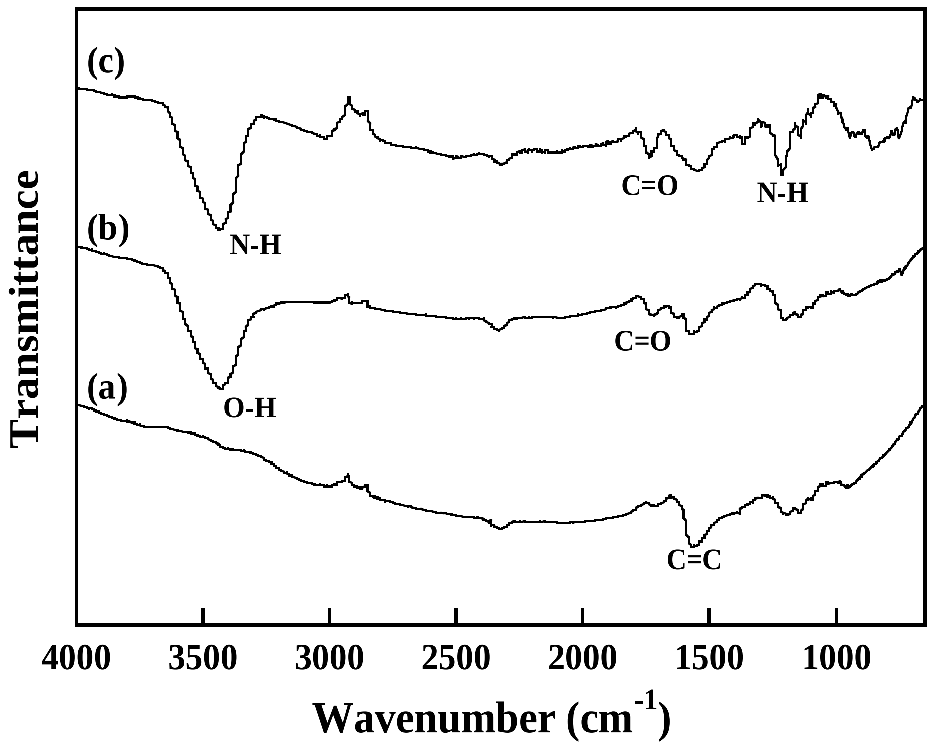

Figure 5.1 FTIR spectra of (a) U-MWCNTs, (b) BTC-MWCNTs and (c) DAB-MWCNTs

Additionally, XPS analysis was conducted to determine the surface elements of MWCNTs before and after the functionalization. The XPS survey spectra of all samples are displayed in Figure 5.2. Peaks of C1s at ~285 eV and O1s at ~534 eV can be attributed to the carbon structures of MWCNTs and oxygen-containing groups on MWCNT surfaces, respectively [69]. As expected, N1s peak was only visible in the spectrum of DAB-MWCNTs at ~400.2 eV (N-C), indicating the existence of amino groups on their surface, whereas other spectra do not show any peak in this range [70, 71]. The magnification of XPS spectra in N 1s region of all samples are shown in Figure 5.3. The surface element composition of unmodified and functionalized MWCNTs based on the ratios of peak areas from XPS analysis are summarized in Table 5.1. Relative concentration of O and N atoms noticeably increased after the functionalization whereas the amounts of C atom significantly decreased. This is due to the fact that the carbon atoms were possibly eliminated and generated the additional defects during the functionalization, where the ring structure was opened and oxygen-containing groups can be added to this defect to stabilize the structure. Thus, O/C ratio of functionalized MWCNTs increased about 2 times, comparing with that of U-MWCNTs. In the case of DAB-MWCNTs, it was evident that N content obviously increased to 5%. The degree of functionalization was also determined based on the normalized elemental composition and the known structure of the functional groups as shown in Table 5.1.

The fitting spectra of C1s and O1s were also performed to obtain more informative bonding structure of MWCNTs before and after the functionalization. C1s peaks were deconvoluted into several Gaussian peaks to identify the type of carbon bonding as depicted in Figure 5.4. The main peak at 284.2 - 284.5 eV represents the sp^2-hybridized graphite-like carbon atoms (C=C). The peak at around 285.2 - 285.5 eV corresponds to the sp^3-hybridized diamond-like carbon atoms (C-C), referring to the defects on the nanotube structure. Various functionalities on MWCNT surface were observed as small peaks at 286.1 - 286.3 eV (C-O), 286.6 eV ($C-NH_2$), 287.4 - 287.6 eV (C=O), and 288.1 eV (COOH) [71]. Also, the peak at 290.8 eV can be assigned to π-π* transition. It was an interesting phenomenon that the relative concentration of C=C fairly decreased while the concentration of C=O, COOH and $C-NH_2$ increased after the functionalization. It is due to the fact that some of C=C structures were possibly interrupted and altered to C-C structures because of the attachment of BTC and DAB moieties during the functionalization. These results are consistent with previous publications [71, 72]. Figure 5.5 gives the deconvolution of O1s spectra which exhibit two peaks assigned to O=C at 351.6 - 351.7 eV and O-C at 533.3 - 533.6 eV [61, 70, 71]. Relative concentration of O=C significant increased for the functionalized samples. It is possibly due to grafting of functional groups onto the MWCNT surface through carboxyl bonding.

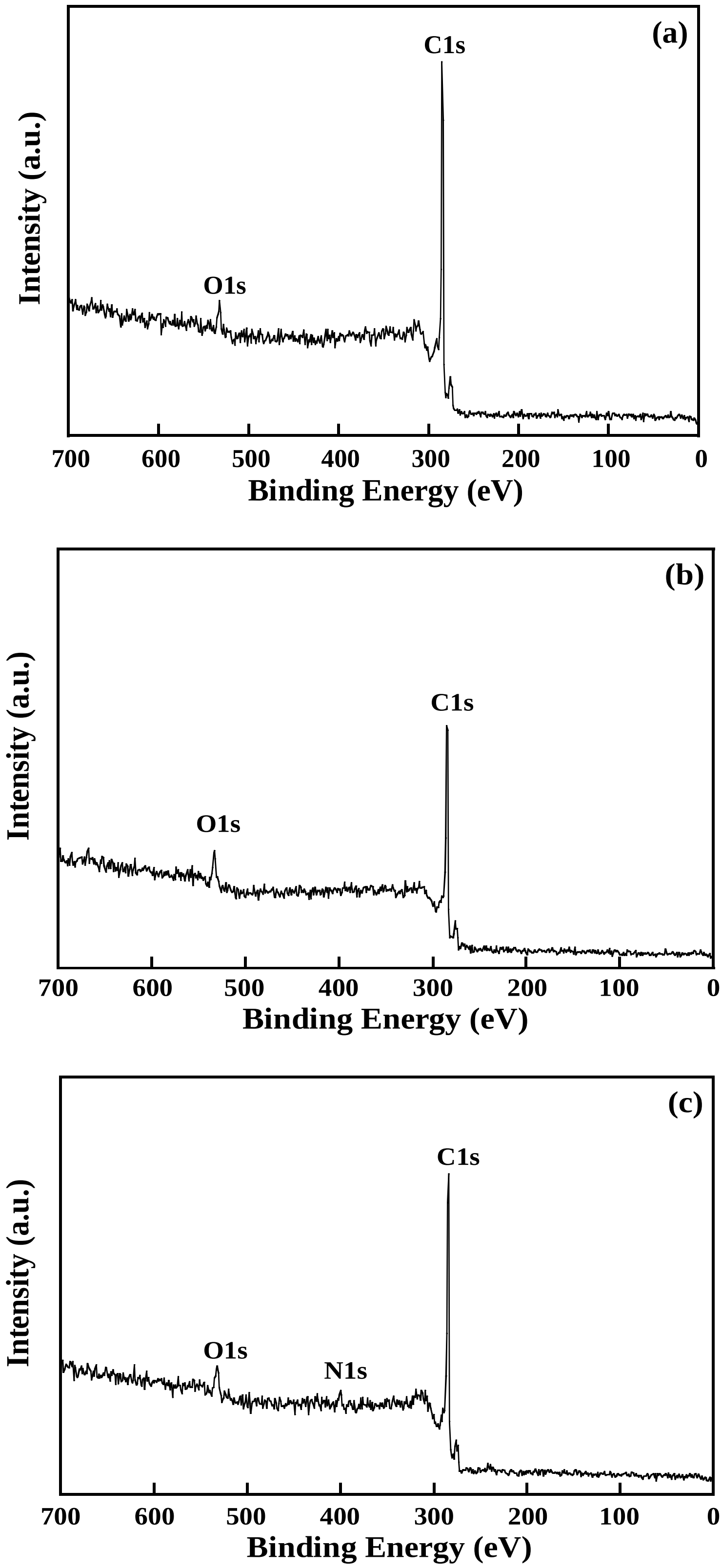

Figure 5.2 XPS survey spectra of (a) U-MWCNTs, (b) BTC-MWCNTs and (c) DAB-MWCNTs

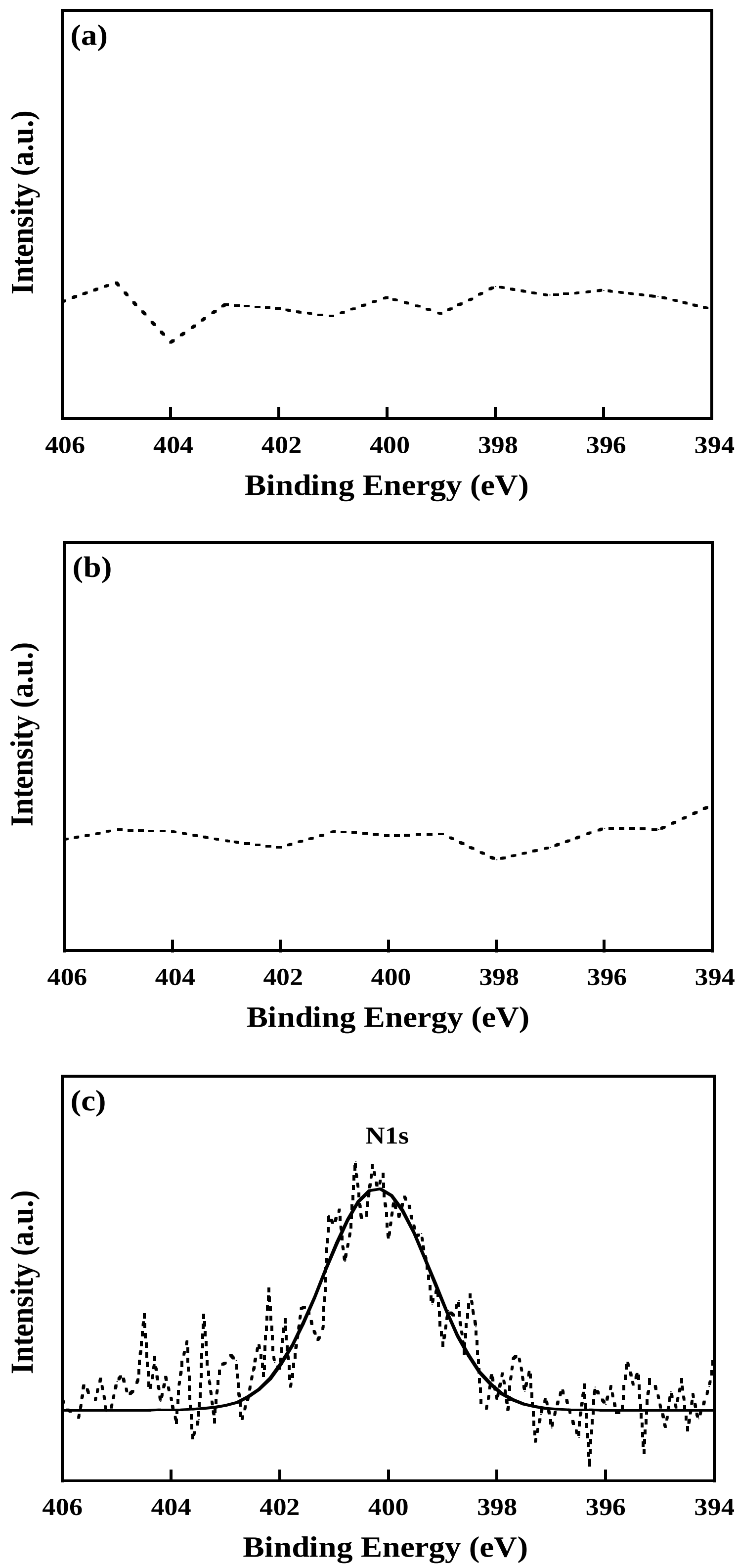

Figure 5.3 High-resolution XPS spectra for N1s region of (a) U-MWCNTs, (b) BTC-MWCNTs and (c) DAB-MWCNTs

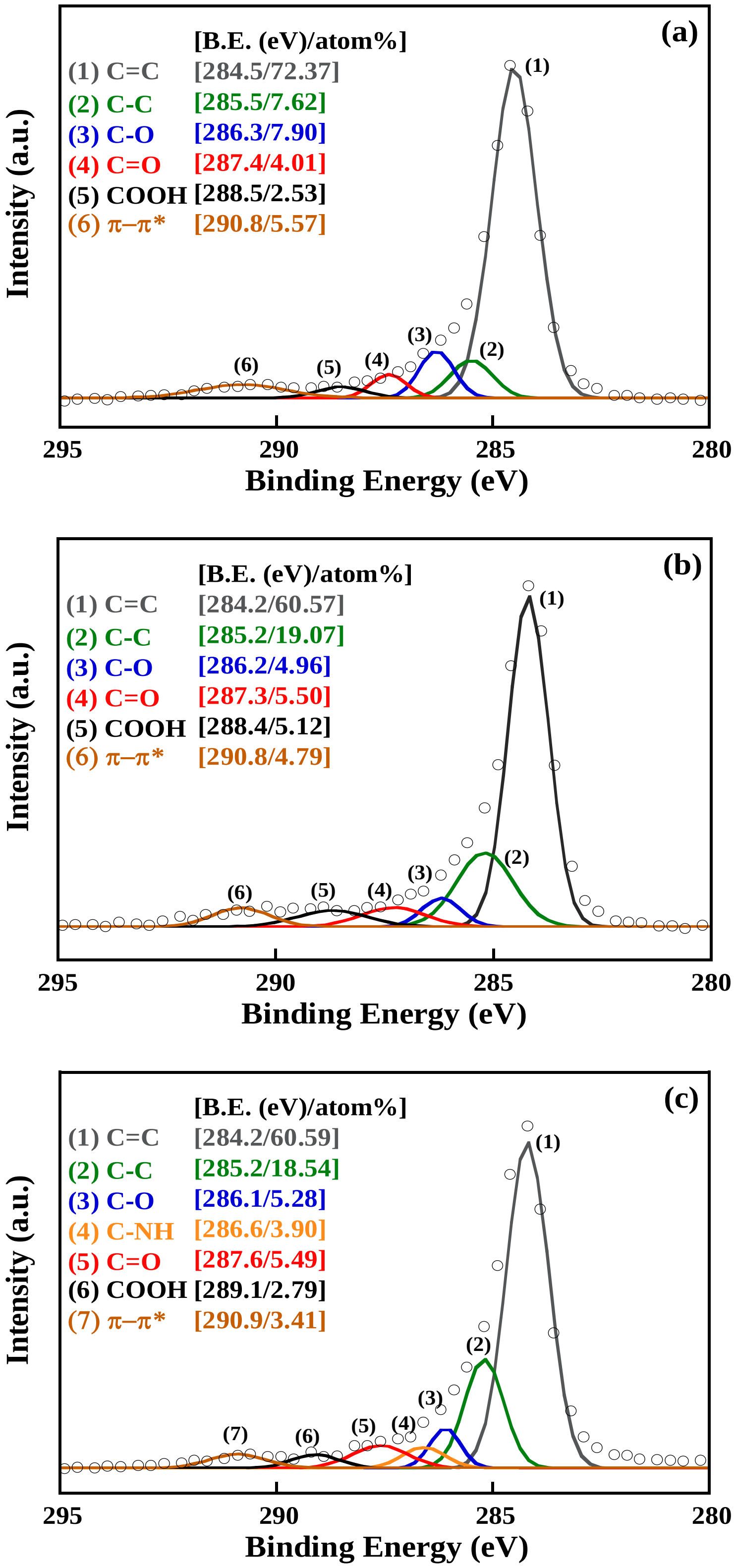

Figure 5.4 High-resolution XPS spectra for C1s region of (a) U-MWCNTs, (b) BTC-MWCNTs and (c) DAB-MWCNTs

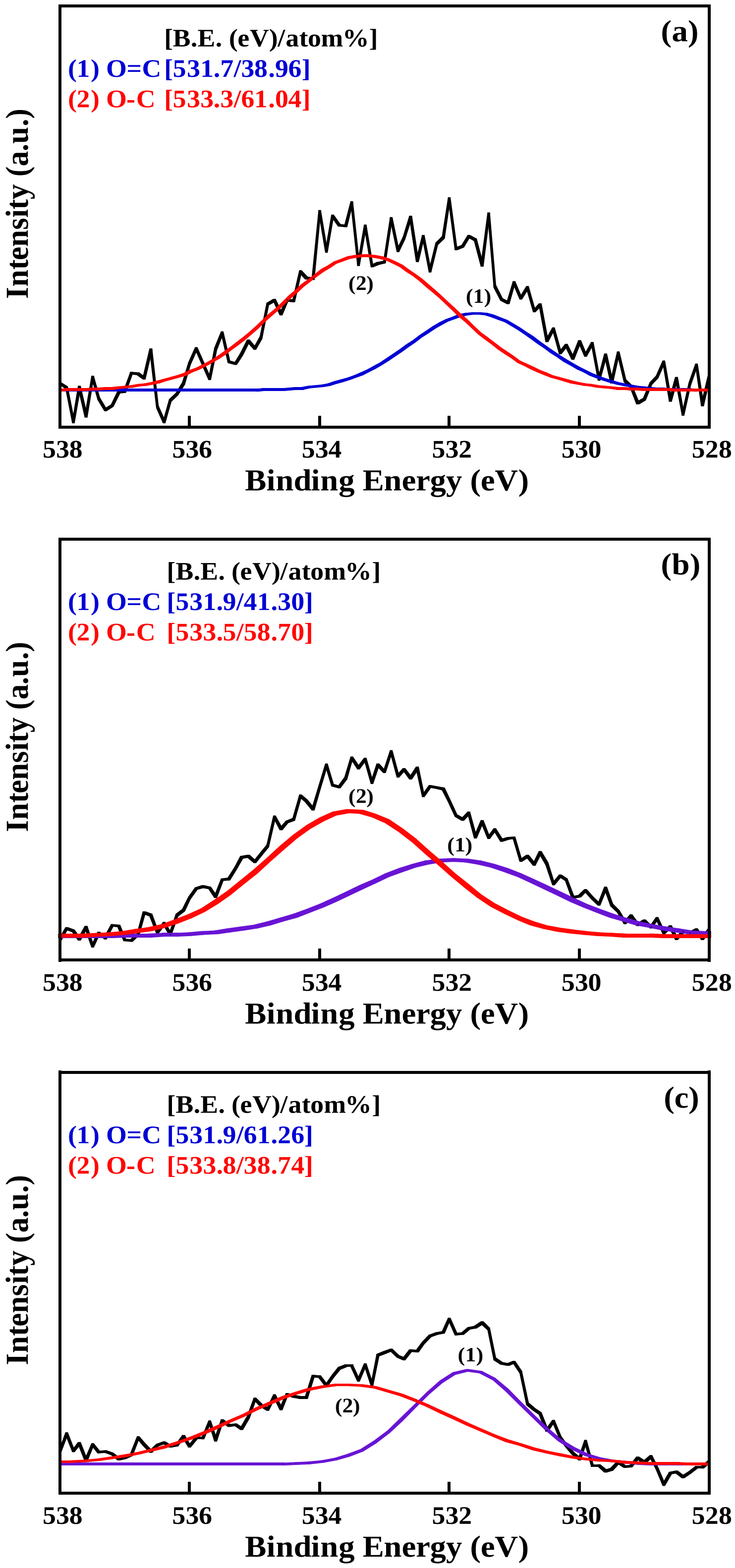

Figure 5.5 High-resolution XPS spectra for O1s region of (a) U-MWCNTs, (b) BTC-MWCNTs and (c) DAB-MWCNTs

Table 5.1 Surface elements of unmodified and functionalized MWCNTs analyzed using XPS

Sample	XPS Atomic (%)			O/C (%)	N/C (%)	% functionalization
	C 1s	O 1s	N 1s			
U-MWCNT	90.20	9.80	-	0.11	-	-
BTC-MWCNT	79.75	20.25	-	0.25	-	3.43
DAB-MWCNT	79.82	15.83	4.35	0.20	0.05	3.37

The effect of functionalization on the structural destruction of MWCNTs was evaluated by using FT-Raman spectroscopy. Figure 5.6 provides FT-Raman spectra for unmodified and functionalized MWCNTs. It is obviously shown that two characteristic bands located at ~1590 cm^{-1} and ~1284 cm^{-1} commonly refers to the in-plane tangential mode (G band) for stretching vibrations of the sp^2-hybridized carbons (C=C) and disorder-induced modes (D band) of sp^3-hybridized carbons or defects (C-C), respectively [23, 73]. The ratio of integral area of D band to G band (I_D/I_G) is often used to investigate the amount of defects in nanotube structure before and after the functionalization [74]. The FT-Raman results are summarized in Table 5.2. It was found that the I_D/I_G ratio of functionalized MWCNTs was higher than that of U-MWCNTs. It revealed that the amount of the sp^3-hybridized carbons or defects on the MWCNT surface increased after the functionalization because some of C=C structures were interrupted possibly due to the grafting of functional groups and converted to C-C structures. However, the I_D/I_G ratio of functionalized MWCNTs via this method was not significantly changed, comparing with the conventional surface treatment. It is due to the fact that MWCNTs were functionalized in the mild medium reaction which could introduce functional groups onto their surface via covalent bonds but it was not too strong to generate many defects on their surface. Therefore, this result is confirmed that functionalized MWCNTs were obtained with less structural damage.

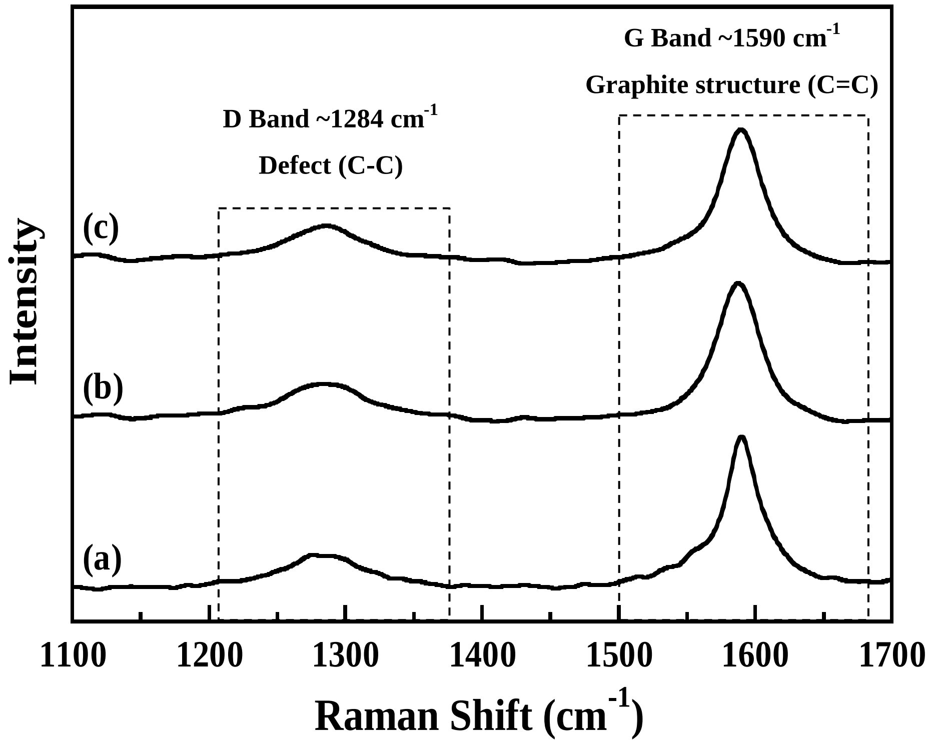

Figure 5.6 FT-Raman spectra of (a) U-MWCNTs, (b) BTC-MWCNTs and (c) DAB-MWCNTs

Table 5.2 FT-Raman results of unmodified and functionalized MWCNTs

Material	Intensity		FWHM	I_D/I_G
	D band	G band		
U-MWCNT	0.204	0.855	32.25	0.449
BTC-MWCNT	0.246	0.932	35.92	0.487
DAB-MWCNT	0.236	0.896	36.93	0.455

5.1.2 Thermal stability of functionalized MWCNTs

TGA analysis was carried out on MWCNTs before and after functionalization in order to evaluate their thermal stability. TGA measurement was conducted from room temperature to 800 ºC in air and nitrogen atmosphere at heating rate of 10 ºCmin^{-1}. Figure 5.7 demonstrates TGA thermograms of various MWCNTs in N_2 atmosphere. It was found that the weight of functionalized MWCNTs decreased in temperature range of 300 ºC to 600 ºC, whereas the weight of U-MWCNTs barely decreased. It is associated with the decomposition of oxygen-containing groups possibly generated during surface treatment and substituted compounds attached on their surface. The disordered and amorphous carbons on the surface of all MWCNTs were obviously decomposed at temperature higher than 600 ºC. However, all of samples obviously exhibit high thermal stability that is consistent with high residual weight at 800 ºC.

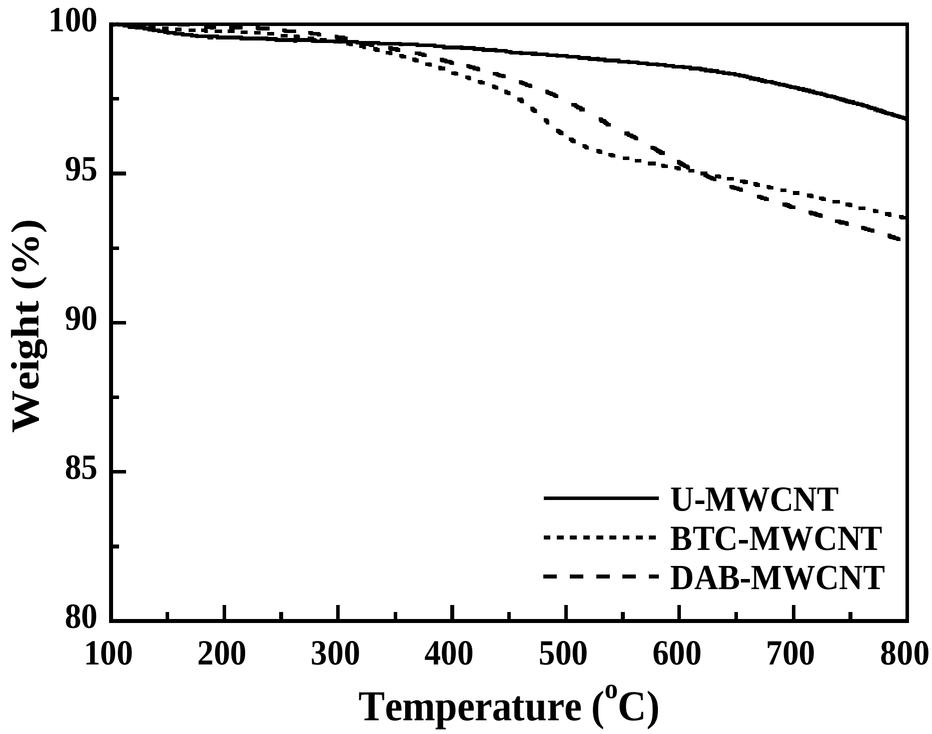

Figure 5.7 TGA curves of the unmodified and functionalized MWCNTs in N_2 atmosphere

Additionally, thermal stability of all samples was also conducted in air atmosphere as shown in Figure 5.8. For TGA curves of BTC-MWCNTs and DAB-MWCNTs, the slight weight loss was observed at temperature under 300 ºC possibly due to disintegration of organic compounds as carboxylic, amino and O-containing groups adsorbed on the MWCNT surface. The amorphous carbons tended to be oxidized at temperature higher than 300 ºC. Also, it can be observed that the graphitic carbons were oxidized at temperature higher than 500 ºC. The weight of U-MWCNTs is fairly stable at low temperature and terribly decreased around 500 ºC whereas the weight of the functionalized MWCNTs significantly decreased around 650 ºC. This result corresponded with the degradation temperature (T_d) obtained at 10% weight loss as shown in Table 5.3. The T_d of functionalized MWCNTs is intensively higher than that of U-MWCNTs. It is notable that thermal stability of MWCNTs substantially enhanced after surface treatment because the disordered and amorphous carbons were probably removed during the functionalization.

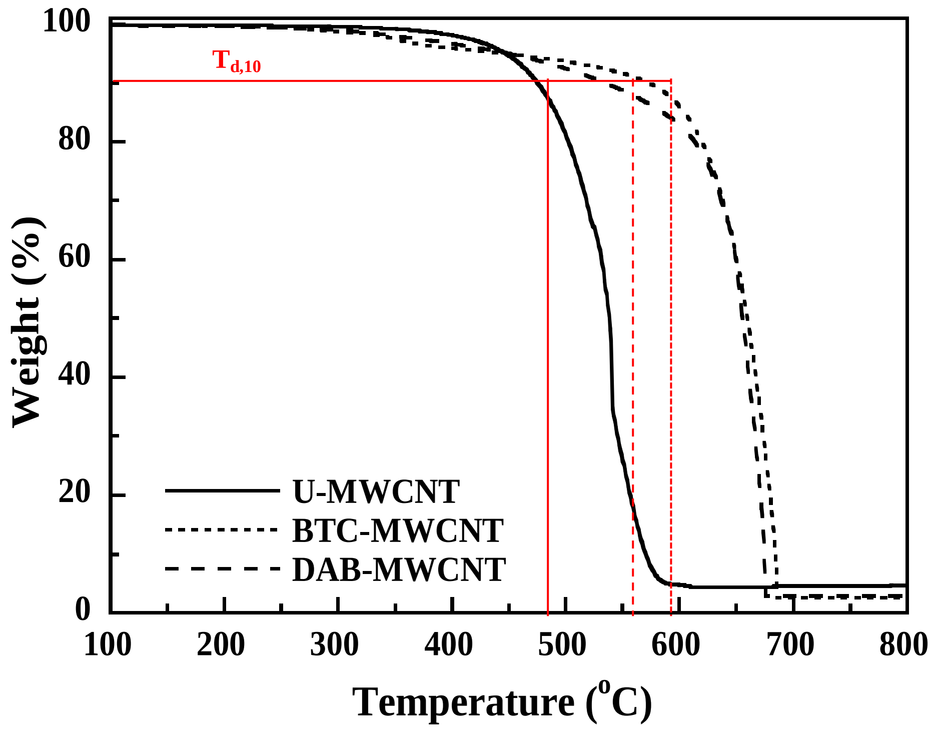

Figure 5.8 TGA curves of the unmodified and functionalized MWCNTs in air atmosphere

Table 5.3 Degradation temperatures at 10% weight loss of unmodified and functionalized MWCNTs in air atmosphere

Material	$T_{d,10}$ (ºC)
U-MWCNT	475
BTC-MWCNT	573
DAB-MWCNT	535

5.1.3 Dispersibility of functionalized MWCNTs

The investigation of the settling behavior of the MWCNTs suspended in a polar solvent is a practical technique due to its simplicity, inexpensive, fast and the qualitative information [19, 25, 62]. The unmodified and functionalized MWCNTs were dispersed in ethanol using ultrasonication and their stability was monitored at different time intervals. The photographs of MWCNT dispersion state taken at different time intervals are illustrated in Figure 5.9. The first photograph was taken right after stopping ultrasonication. All of samples showed good dispersion in ethanol. Nevertheless, U-MWCNTs settled gradually and completely after 18 hrs because of their agglomeration and poor hydrogen-bonding ability. Remarkably, BTC-MWCNTs and DAB-MWCNTs still exhibited good dispersibility. It is noteworthy that the presence of carboxylic and amino groups on the surface of BTC-MWCNT and DAB-MWCNT, respectively, led to the decrease of van der Waals force among them which promotes their separation and dispersion in ethanol. It is due to the fact that the functional groups on the MWCNT surfaces provided polarity and their hydrogen-bonding ability. This enhanced dispersibility has a positive effect on the manipulation of MWCNT/polymer composites.

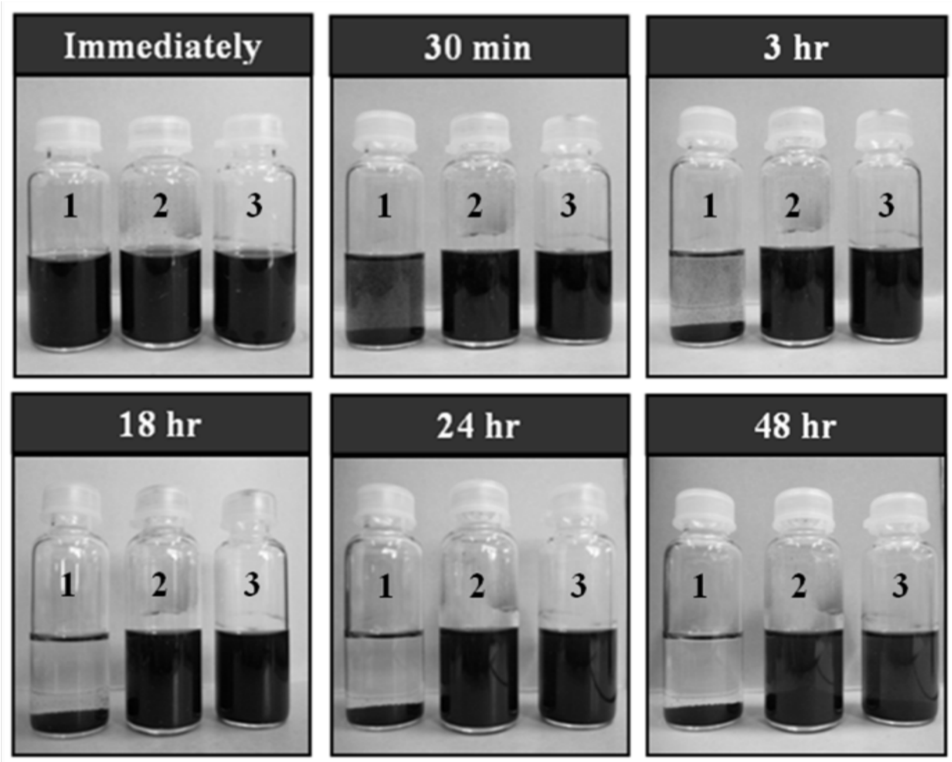

Figure 5.9 Photographs of the dispersion behavior for (1) U-MWCNT, (2) BTC-MWCNT and (3) DAB-MWCNT in ethanol observed at several time intervals

5.2 Variation of chemical structure of functionalized MWCNTs

The effect of chemical structure of functionalized MWCNTs on the properties of epoxy composites was studied in this part. The epoxy composites were fabricated by incorporating unmodified and functionalized MWCNTs at filler content of 0.3 vol%. The scheme of reaction to produce functionalized MWCNT/epoxy composites is demonstrated in Figure 5.10.

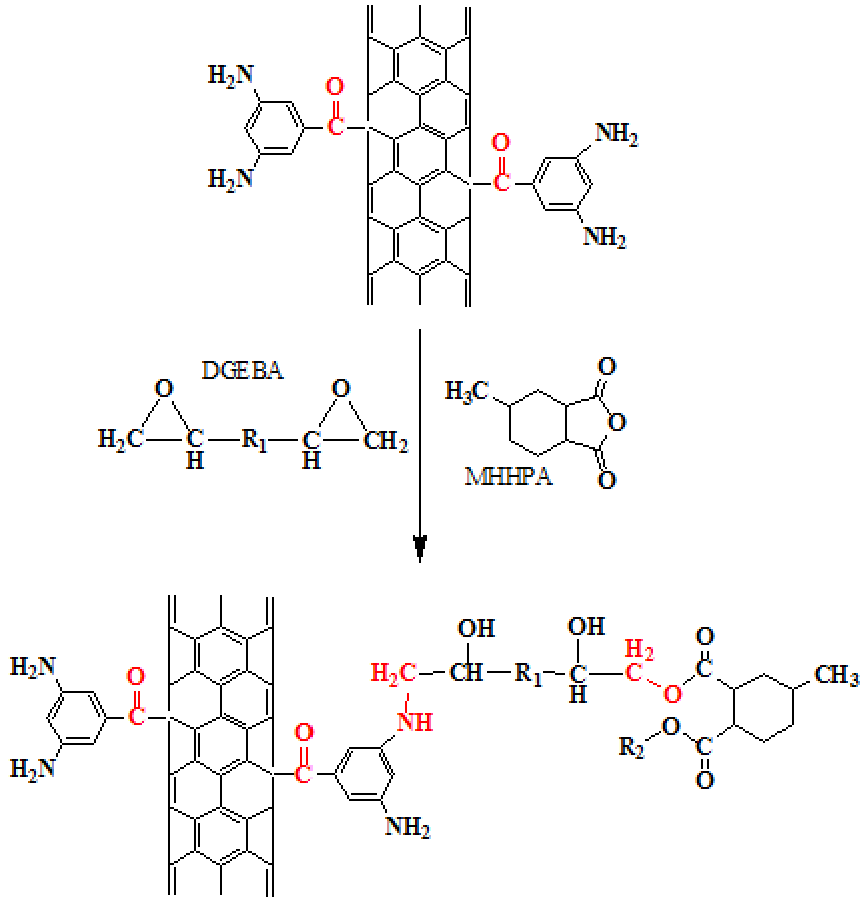

Figure 5.10 Procedure of functionalized MWCNTs/epoxy composite

5.2.1 Curing behavior of MWCNT/epoxy composites

In order to investigate the effect of functionalization of reactive substituted groups onto MWCNTs, the curing behavior of epoxy composites was elucidated via DSC. Figure 5.11 presents curing exotherms of epoxy composites incorporated with unmodified and functionalized MWCNTs at heating rate of 10 ºC min^{-1}.

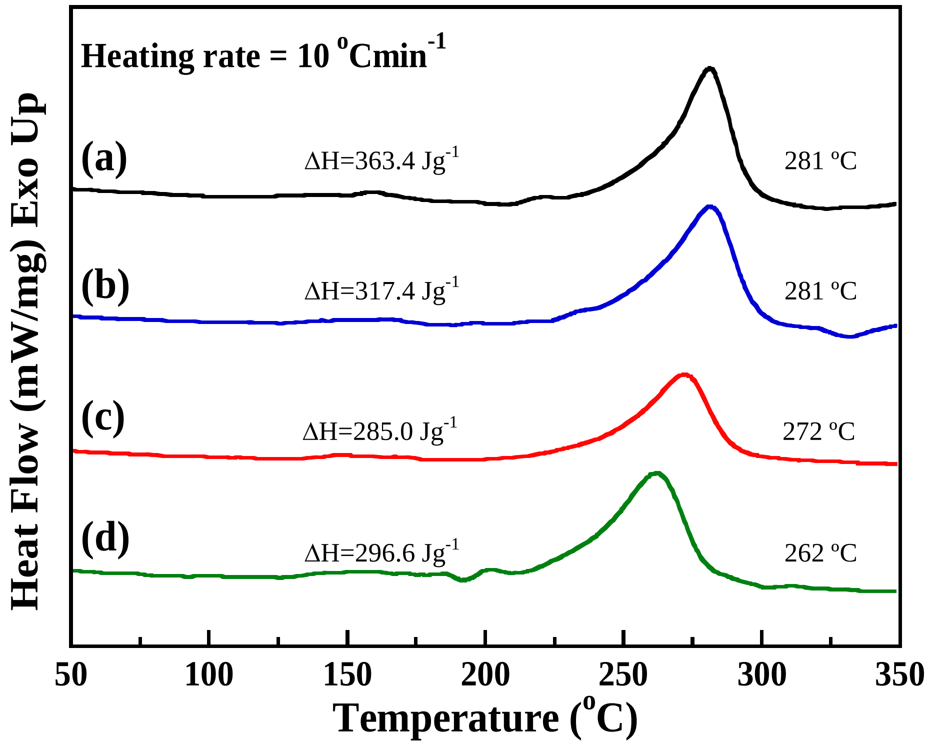

Figure 5.11 DSC thermograms of (a) neat epoxy and epoxy composites filled with (b) U-MWCNTs, (c) BTC-MWCNTs, and (d) DAB-MWCNTs at filler content of 0.3 vol%

As it was clearly seen, the curing profiles of epoxy composites filled with functionalized MWCNTs shifted to lower temperature than that of neat epoxy resin. The exothermic peak temperature (T_p) decreased from 281 ºC to 262 ºC with the presence of MWCNTs in epoxy systems. Interestingly, the incorporation of U-MWCNT into epoxy matrix provided lower T_p than the neat epoxy which may be due to the presence of metallic catalysts and oxygen-containing groups on the surface of the as-received MWCNTs. The metallic catalyst can promote the early state of the curing reaction [75]. Besides, the oxygen-containing groups like hydroxyl and carboxyl groups possibly accelerate the ring opening of epoxy monomer which initiates the curing process [76]. The introduction of functionalized MWCNTs into epoxy matrix was found to remarkably decrease T_p. It is attributed to the carboxyl and amino functional groups on the surface of BTC-MWCNTs and DAB-MWCNTs, respectively, because in nature they are highly reactive towards oxirane rings. The carboxyl and amino groups can open the oxirane ring and generate the network formation. This phenomenon is consistent with the results of Zhou and co-workers who found that both COOH-MWCNTs and silane treatment of COOH-MWCNTs have catalytic effects on the curing process, shortening pre-cure time [77].

Also, the heat of reaction (ΔH) of samples significantly decreased by adding functionalized MWCNTs into polymer matrix. The ΔH value of epoxy composites incorporating with DAB-MWCNTs was quite higher than that of BTC-MWCNTs It is possibly due to higher reactivity of amines on DAB-MWCNT surface, enhancing crosslink networks in polymer composites [46]. The reactive hydrogen of primary amines rapidly attached to the oxygen atom to open the epoxy groups and to form a secondary amine. The resulting secondary amine further reacted with the other epoxy groups producing a tertiary amine and generating more hydroxyl groups that can further react and crosslink with other epoxy groups.

To study curing kinetics of epoxy composites, the Kissinger and Ozawa methods were used to investigate kinetics of MWCNT/epoxy composites by using DSC data at various heating rates [78, 79]. DSC thermograms of 0.3vol% DAB-MWCNTs/epoxy composites at various heating rates are shown in Figure 5.12. It was found that T_p of all samples decreased as heating rate decreased as listed in Table 5.4.

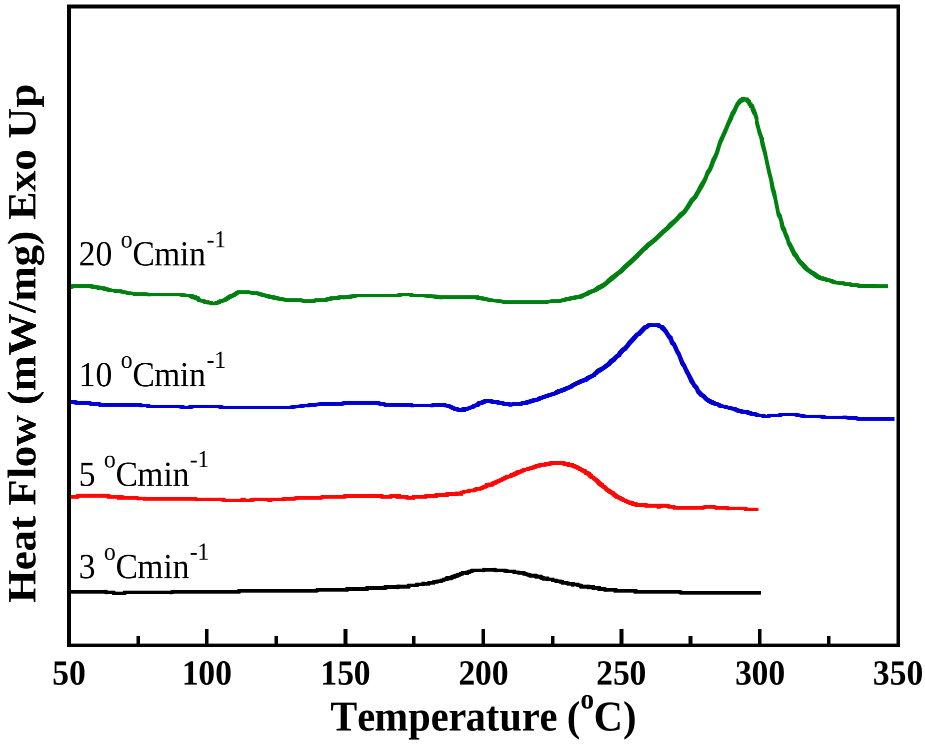

Figure 5.12 DSC thermograms of epoxy composites filled with 0.3vol% DAB-MWCNTs at various heating rates

Table 5.4 Exothermic peak temperatures of epoxy composites at various heating rates

Sample	Heating rate, β (°Cmin^{-1})				
	1	**2**	**5**	**10**	**20**
Neat epoxy	222.55	216.33	206.68	203.49	222.55
U-MWCNT 0.3	248.38	248.38	229.21	226.63	248.38
BTC-MWCNT 0.3	281.15	281.09	272.22	262.34	281.15
DAB-MWCNT 0.3	306.93	304.62	297.32	294.72	306.93

Kissinger method is based on a linear relationship between $\ln(\beta/T_p^2)$ against the inverse of the peak temperature of the exothermic curing reaction ($1/T_p$).The activation energy (E_a) can be obtained as follows:

$$\ln\frac{\beta}{T_p^2} = \ln\left(\frac{Q_p AR}{E_a}\right) - \frac{E_a}{RT_p} \tag{3}$$

where β is a constant heating rate, $f(\alpha)$ is differential conversion function depending on reaction mechanism, and

$$Q_p = -\left[\frac{df\,(\alpha)}{d\alpha}\right], \tag{4}$$

$$\alpha = \alpha_p \tag{5}$$

A similar method to Kissinger method is Ozawa method that relates the $\ln\beta$ and ($1/T_p$) as follows:

$$\ln\beta = \ln\left(\frac{Q_p AR}{E_a}\right) - \ln F(\alpha) - 5.331 - 1.052\frac{E_a}{RT_p}, \tag{6}$$

$$F(\alpha) = \int_0^\alpha \frac{d\alpha}{f\,(\alpha)}$$

where $F(\alpha)$ is a constant function.

According to the Kissinger and Ozawa method, good linear relationship between the heating rate and the reversal of the exothermic peak temperature can be obtained as shown in Figure 5.13. The value of E_a can also be determined from the slope of the plot. The E_a values of all systems are shown in Table 5.5. It was found that the E_a values obtained from both methods show fairly consistent results indicating that the E_a values significantly decreased with the presence of MWCNTs, especially functionalized MWCNTs. This curing acceleration caused by the reactive functional groups on their surface. The decrease in curing temperature and activation energy of MWCNT/epoxy composites has a positive effect on the underfill manufacturing, i.e., a relatively lower curing temperature or lower energy consumption can be used.

Table 5.5 Activation energy evaluated from Kissinger and Ozawa methods

Sample	Ea ($kJmol^{-1}$)	
	Kissinger	Ozawa
Neat Epoxy	44.21	50.49
U-MWCNT0.3	40.78	47.15
BTC-MWCNT0.3	36.84	43.28
DAB-MWCNT0.3	37.71	44.05

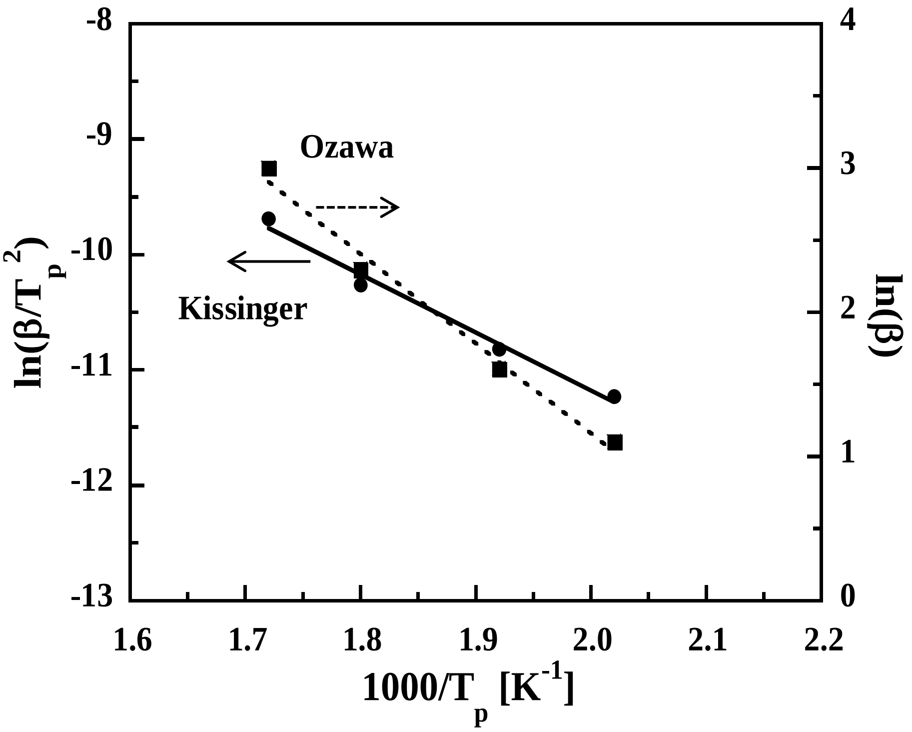

Figure 5.13 Average activation energy determinations by using Kissinger method and Ozawa method plots of epoxy composite filled with 0.3vol% of DAB-MWCNTs

5.2.2 Dynamic mechanical properties of MWCNT/epoxy composites

Dynamic mechanical analysis (DMA) is an effective technique to measure the properties of the viscoelastic materials as a function of temperature and frequency. Usually, the storage modulus (E′) and the loss modulus (E″) are the quantity of stored energy and the energy dissipated as heat through elastic and viscous behavior of polymer, respectively.

The storage moduli of epoxy composites recorded at 1 Hz frequency are illustrated in Figure 5.14(a). The storage modulus at room temperature of neat epoxy resin is approximately 1.56 GPa whereas that of U-MWCNT/epoxy composite is about 2.42 GPa. It is due to the high aspect ratio and outstanding mechanical properties of U-MWCNT. Moreover, the small amounts of oxygen-containing groups on the surface of U-MWCNT possibly react with the epoxy monomer. The effective load transfer was caused by the continuity of U-MWCNT networks in the matrix and better interfacial interaction between U-MWCNT and epoxy matrix, resulting in the enhanced storage modulus. This result is in good agreement with the results of the previous work [80]. Interestingly, the storage moduli at room temperature of epoxy composites incorporated with BTC-MWCNTs and DAB-MWCNTs substantially increased to be in the range of 2.68 GPa and 2.64 GPa, respectively. This behavior suggested that the effect of functionalization provided the restriction of the polymer mobility [81, 82]. The presence of carboxylic and amino groups of the substituted compounds attached onto MWCNT surface are believed to enhance the uniform dispersion in epoxy matrix and to provide moderately strong interfacial interaction between nanotubes and the matrix. Furthermore, the incorporation of unmodified and functionalized MWCNTs into the epoxy matrix can enhance the storage modulus at the room temperature, indicating the increased stiffness as well as good stability in the glassy region of material. The improvement of thermal stability of epoxy composites incorporated with functionalized MWCNTs allows these materials to be used in the wide range of temperature, especially in high thermal applications.

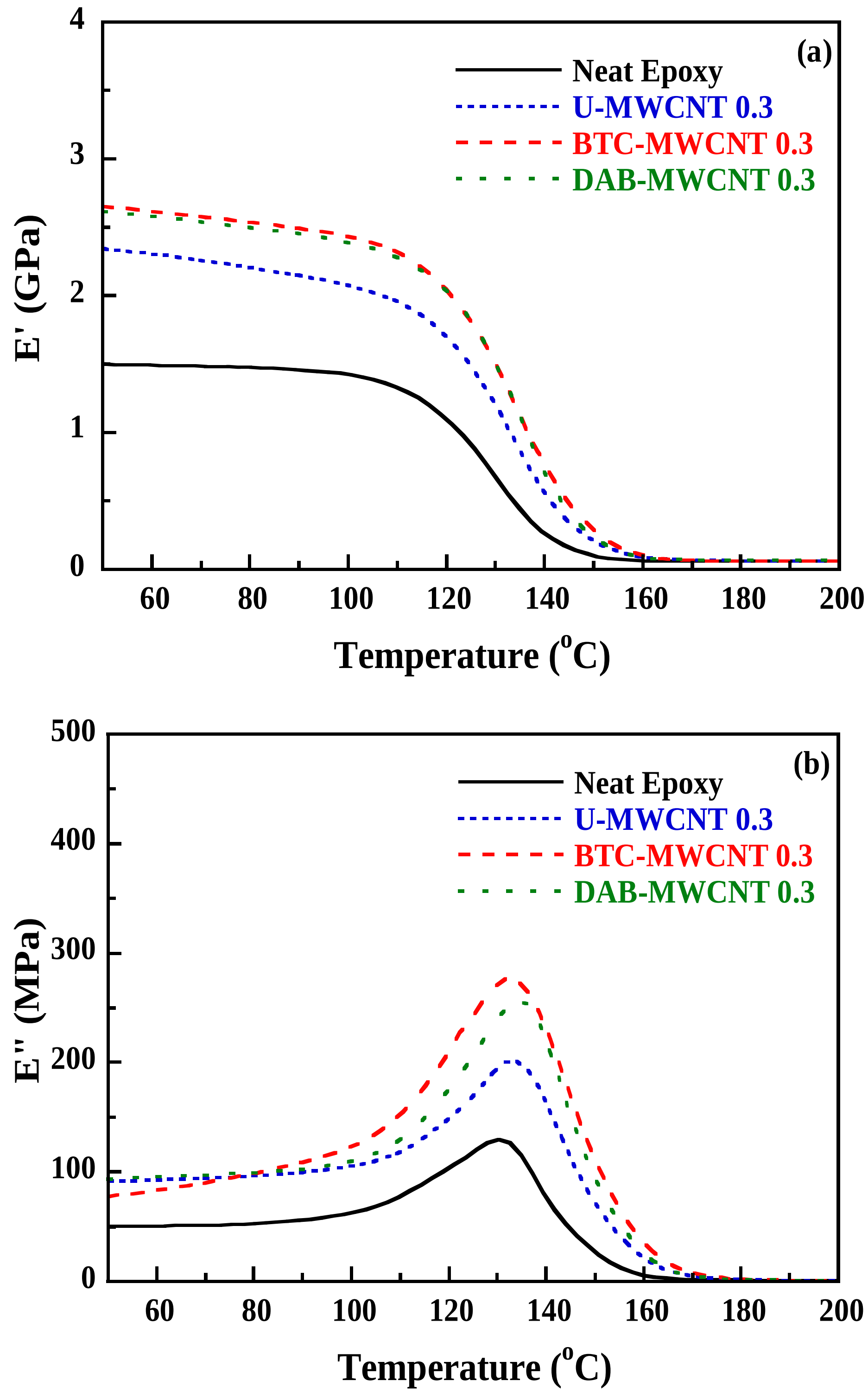

Figure 5.14 (a) Storage moduli and (b) loss moduli of epoxy composites incorporated with unmodified and functionalized of MWCNTs at the filler content of 0.3 vol%

Figure 5.14(b) shows a plot of loss moduli of epoxy composites as a function of temperature at 1 Hz frequency. The glass transition temperature (T_g) can be investigated from the maximum value at the peak of loss modulus curve, corresponding to the initial drop from the glassy state into the rubbery state. The change in the glass transition is attributed to the increase of molecular mobility when the molecular chain obtained adequate energy to overcome configurational rearrangements of polymer chain backbones. The results revealed that the loss modulus peak shifts to higher temperature with the value ranging from 131 ºC in neat epoxy resin to 136 ºC in DAB-MWCNT/epoxy composite as shown in Table 5.6. It is well known that T_g of materials involves the mobility of polymer chain or free volume fraction. The addition of MWCNTs possibly hinders chain mobility of the matrix and reduces free volume fraction, resulting in the enhancement of T_g.

Based on the viscoelastic properties obtained from DMA measurements, the crosslink density is proportional to the storage modulus in the rubbery plateau and can be determined according to the following equation[83, 84]:

$$\lambda = \frac{E'}{3RT} \qquad (7)$$

where λ is the crosslink density, E' is the storage modulus at T_g+50ºC, R is the gas constant (8.314 $J.K^{-1}mol^{-1}$) and T is the absolute temperature at T_g+50ºC .

As shown in Table 5.6, the incorporation of MWCNTs into the epoxy matrix provided higher crosslink density than 5213 mol/m^3 of neat epoxy. This behavior implied that the addition of only 0.3 vol% MWCNTs yielded higher crosslink degree. Especially, carboxyl and amino groups functionalized MWCNTs possibly reacted with the oxirane rings of epoxy resins to obtain more crosslink networks. Furthermore, the crosslink density of thermosetting polymer directly correlated to the T_g. As the crosslink density increases, the T_g tends to increase which corresponds with the mentioned results.

Table 5.6 Glass transition temperature and crosslink density of epoxy composites filled with 0.3 vol% MWCNTs

Sample	T_g (°C)	λ (10^{-3}molm^{-3})
Neat Epoxy	131	5.213
U-MWCNT 0.3	134	5.399
BTC-MWCNT 0.3	134	5.473
DAB-MWCNT 0.3	136	5.807

5.2.3 Thermomechanical properties of MWCNT/epoxy composites

The linear thermal expansion as a function of temperature was investigated using TMA. Generally, the linear thermal expansion of polymer composite gradually increased in a glassy state due to rigidity of crosslink materials. Then, it sharply increased in the rubbery state because polymer chains were more flexible and dilated at temperature higher than T_g. The coefficient of thermal expansion (CTE) was determined from a slope of a plot between linear thermal expansion and temperature. Commonly, the linear expansion of polymer composite rapidly increased when temperature is higher than T_g. Therefore, the CTE of polymer composites are often reported 2 values, i.e., in the glassy state and above T_g. Table 5.7 displays the CTE below T_g of all samples. It is important to point out that the incorporation of MWCNTs into epoxy matrix led to rather low CTE than that of the neat epoxy sample possibly due to the intrinsic low CTE of MWCNTs. Considering epoxy composites filled with functionalized MWCNTs, the carboxylic and amino groups in the structure of BTC and DAB attached on MWCNT surface were available to react with the oxirane rings in epoxy molecules. This point is believed to effectively provide strong interfacial interaction and additional crosslink networks that restrict the mobility of matrix and decrease the free volume fraction. Also, the enhancement of the interfacial interaction has a positive effect on thermal stability of MWCNT/polymer composites due to the achieving of the thermal transfer between MWCNTs and the polymer matrix. Consequently, the CTE of epoxy composites fairly decreased with the presence of functionalized MWCNTs. These materials are good candidates for using in the applications which require low CTE, especially in the underfill applications applying in microelectronic packaging.

Table 5.7 Coefficient of thermal expansion (CTE) of epoxy composites filled with 0.3 vol% MWCNTs

Material	**CTE (ppm°C^{-1})**
Neat Epoxy	72.91
U-MWCNT 0.3	69.02
BTC-MWCNT 0.3	67.36
DAB-MWCNT 0.3	66.31

5.2.4 Free volume characteristic of MWCNT/epoxy composites

The viscoelastic properties of thermosetting polymer, especially T_g, can be explained in terms of free volume theory. This theory starts with a Williams-Landell-Ferry (WLF) equation which is one of well-known equations used to describe the material behavior with respect to temperature [85, 86]. The WLF equation can be modified and written in terms of frequency as follows [87]:

$$\frac{1}{\mathrm{Log}\left(\frac{f}{f_r}\right)} = \frac{C_2}{C_1}\left(\frac{1}{T_g - T_{gr}}\right) + \frac{1}{C_1} \qquad (8)$$

where f_r is the reference frequency at 1 Hz; f is the applied frequencies in DMA analysis. The T_{gr} was T_g obtained at the reference frequency of 1 Hz and the T_g was obtained by the maximum value of the loss modulus peak at each frequency. The WLF parameters, C_1 and C_2, associating with the free volume fraction and the empirical Doolittle expression are defined below:

$$C_1 = \frac{B}{2.303f_g} = \frac{1}{2.303f_g} \quad (9)$$

where f_g is the free volume fraction at T_g and B is a constant parameter close to unity.

$$C_2 = \frac{f_g}{\Delta CTE} \quad (10)$$

where $\Delta CTE = CTE_2 - CTE_1$ is possibly identified with the difference between the CTE above and below T_g, respectively. Consequently, it becomes the calculation of the free volume fraction at T_g [88].

A good linear correlation between 1/Log (f/f_r) and 1/(T_g -T_{gr}) is observed as demonstrated in Figure 5.15. The values of the constants C_1 and C_2, C_2/C_1 and the free volume fraction are summarized in Table 5.8. The constants C_1 and C_2 are commonly dependent on the material characteristic in which the universal values are 17 and 54 at T_g, respectively. According to the obtained values, C_1 increased with the addition of functionalized MWCNTs into epoxy matrix. The value of C_1 obtained from the empirical method is close to the universal value for the epoxy resin [86]. Consequently, the free volume fraction, f_g, at T_g of all systems was calculated following the equation (3). It was found that f_g decreased from 0.0244 in neat epoxy resin to be in the range of 0.0214 - 0.0187 with the presence of MWCNTs. As expected, the f_g significantly decreased in case of functionalized MWCNT/epoxy composites. This phenomenon can be explained in terms of high reactivity of functional groups on the surface of MWCNTs that possessed the strong interfacial interaction between nanotubes and the matrix. The decrease of f_g referred to the lack of chain's mobility due to the introduction of unmodified and functionalized MWCNT into epoxy matrix. This result is consistent with the increase of T_g and the decrease of CTE as mentioned above.

Table 5.8 WLF constants and the free volume fraction for epoxy composites

Material	**C_2/C_1**	**$1/C_1$**	**C_1**	**C_2**	**f_g**
Neat Epoxy	3.1882	0.0563	17.76	56.62	0.0244
U-MWCNT 0.3	0.1372	0.0492	20.33	2.79	0.0214
BTC-MWCNT 0.3	0.1562	0.0470	21.28	3.33	0.0204
DAB-MWCNT 0.3	0.1484	0.0431	23.20	3.44	0.0187

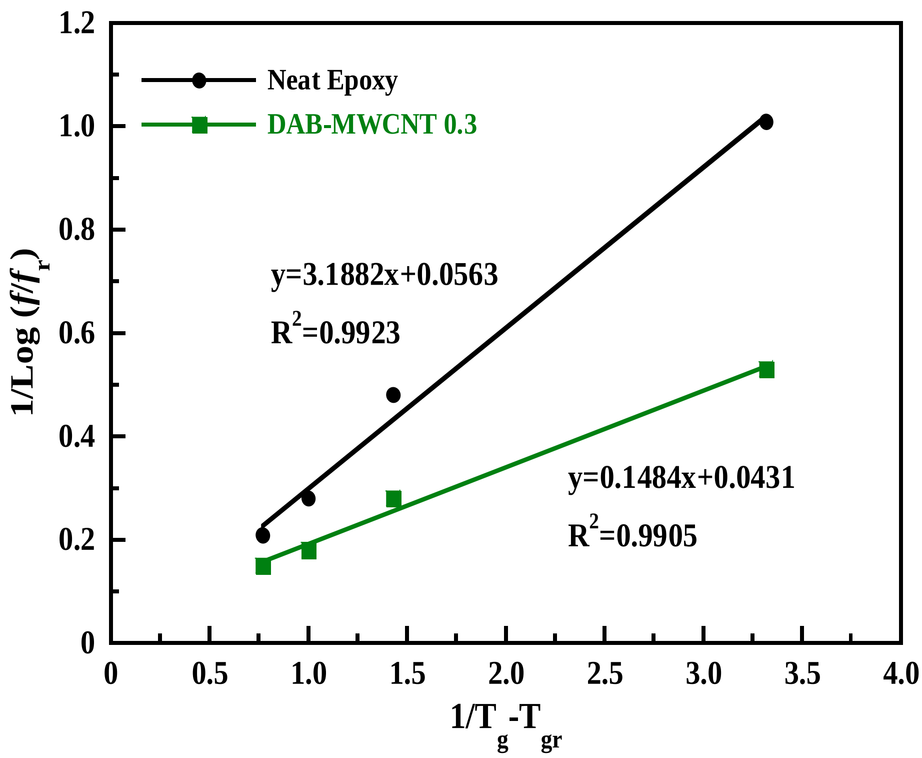

Figure 5.15 The plot of 1/Log(f/f_r) versus 1/(T_g -T_{gr}) for determination of the WLF parameter constants C_1 and C_2 of neat epoxy and epoxy composites

5.2.5 Morphology of MWCNT/epoxy composites

Furthermore, the dispersion of MWCNTs in polymer matrix is one of the most considerable issues for high performance composite fabrication. A homogeneous dispersion of MWCNTs and strong interfacial interaction between polymer matrix and MWCNTs can efficiently enhance the properties of composites. The dispersion of unmodified and functionalized MWCNTs in epoxy matrix at 0.3 vol% was investigated by using SEM as shown in Figure 5.16. The neat epoxy displayed a relatively smooth fracture surface which commonly referred to brittle characteristic of epoxy resin. The composites reinforced with MWCNTs exhibited obviously greater roughness of the fracture surface. It reveals that the addition of MWCNTs into polymer matrix can highly improve the fracture toughness of composites. As seen in Figure 5.16(b), it is clear that the U-MWCNTs were heterogeneously dispersed within epoxy matrix. It is due to that fact that U-MWCNTs were entangled and formed large bundles in epoxy matrix. On the contrary, BTC-MWCNTs and DAB-MWCNTs exhibit well homogeneous dispersion in epoxy resin as shown in Figure 5.16(c) and (d), respectively. This phenomenon might be due to the functional groups introduced onto the surface of MWCNTs which can enhance dispersion and provide better interfacial interaction between functionalized MWCNTs and polymer matrix.

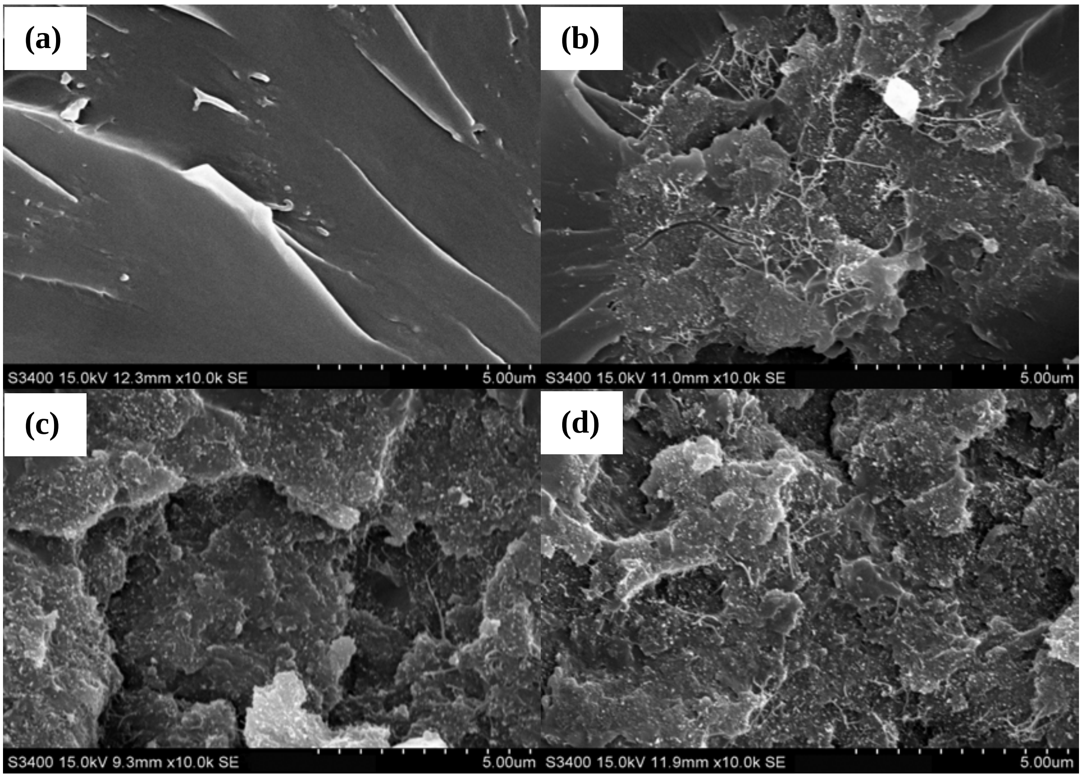

Figure 5.16 Fracture surfaces of (a) neat epoxy and epoxy composites filled with (b) U-MWCNTs, (c) BTC-MWCNTs, and (d) DAB-MWCNTs at filler content of 0.3 vol%

5.2.6 Thermal conductivity of MWCNT/epoxy composites

In order to elucidate the effect of the functionalization of MWCNTs on the thermal conductivity of epoxy composites, the values of thermal conductivity were calculated from the equation

$$K = \alpha \rho C_p \tag{11}$$

where K, α, ρ and C_p are the thermal conductivity of composites, thermal diffusivity, density and heat capacity, respectively.

Figure 5.17 shows the temperature dependence of thermal diffusivity of all composites. It was found that the thermal diffusivity gradually decreased as the temperature increased. However, the thermal diffusivity of composites remarkably increased by adding only 0.3 vol% of fillers. Clearly, the thermal diffusivities of functionalized MWCNT/epoxy composites were higher than that obtained from U-MWCNT/epoxy composites. It is possibly due to the continuity of randomly dispersed MWCNTs and good interfacial interaction between MWCNT and polymer matrix caused by the functionalization.

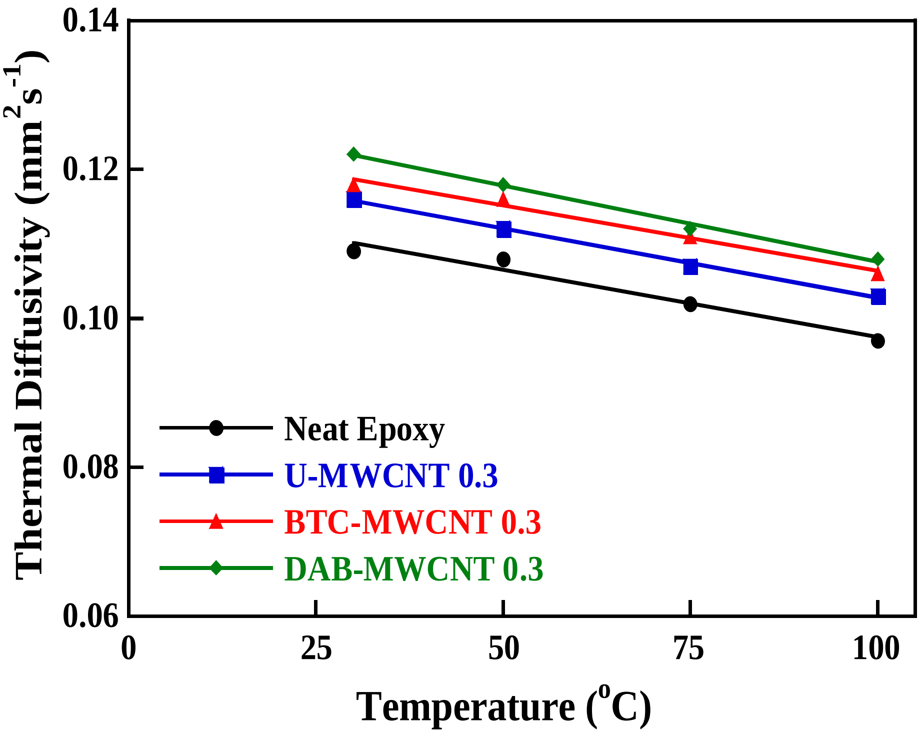

Figure 5.17 Thermal diffusivities of epoxy composites filled with unmodified and functionalized of MWCNTs at the filler content of 0.3 vol%

Thermal conductivity of epoxy composites filled with 0.3 vol% unmodified and functionalized MWCNTs at 50 °C as shown in Table 5.9. Thermal conductivity of epoxy composites was higher than that of neat epoxy. Owing to U-MWCNTs randomly dispersed in polymer matrix, heat conductive pathways were performed in polymer matrix, enhancing heat transfer through the composite. After the functionalization, the dispersion of functionalized MWCNTs within epoxy resin was greatly improved. The functional groups on their surface provided better interfacial interaction between MWCNT and polymer matrix, reducing the interfacial thermal resistance. Beside that the effective heat conductive pathways were provided in the composite because of more continuity of MWCNT networks after the functionalization. Thus, functionalized MWCNTs, especially DAB-MWCNTs, provided high thermal conductivity, comparing with that of neat epoxy.

Table 5.9 Thermal conductivity of epoxy composites filled with 0.3 vol% MWCNTs

Material	**K ($Wm^{-1}K^{-1}$)**	**K_R (%)**
Neat Epoxy	0.157	100.00
U-MWCNT 0.3	0.182	115.92
BTC-MWCNT 0.3	0.189	120.38
DAB-MWCNT 0.3	0.193	122.93

5.3 Variation of MWCNT concentration

According the preliminary results as mentioned above, DAB-MWCNTs exhibit high performance as effective fillers in epoxy composites. Thus, DAB-MWCNTs were used to investigate the effect of filler loading on the properties of epoxy composites in this section. The thermal and mechanical properties of epoxy composites incorporated with DAB-MWCNTs were discussed in further detail below, comparing with U-MWCNT/epoxy composites. The filler contents were varied from 0.3 vol% to 1.0 vol%.

5.3.1 Curing behavior of MWCNT/epoxy composites

In this study, the curing behavior of epoxy composites as a function of filler concentration was evaluated by using DSC. Figure 5.18 shows the plot of T_p versus filler concentration of epoxy composites incorporated with U-MWCNTs and DAB-MWCNTs at heating rate of 10 ºC min^{-1}. Obviously, the T_p of epoxy composites decreased as filler concentration increased. Especially DAB-MWCNT/epoxy composites, T_p of epoxy composites significantly decreased from 281 ºC to 229 ºC. It is attributed highly reactive diaminobenzoyl groups and oxygen-containing groups their surface which can react with the oxirane ring in epoxy structure as curing agent. The addition of high volume fraction of DAB-MWCNTs into the systems contributed high content of curing agents, thereby inducing the curing reaction of epoxy composites occurred at lower temperature. This evidence is intensely consistent with the decrease of E_a values as a function of DAB-MWCNT loading. The E_a values determined according to the Kissinger method as a function of the filler concentration are shows Figure 5.19.

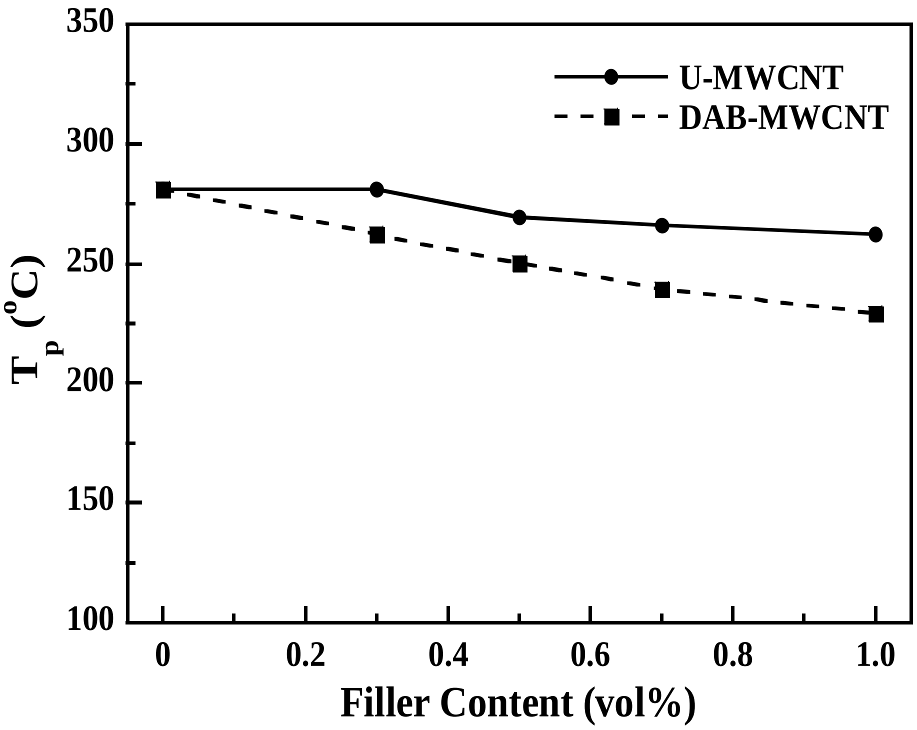

Figure 5.18 Exothermic peak temperature of epoxy composites filled with MWCNTs at various contents

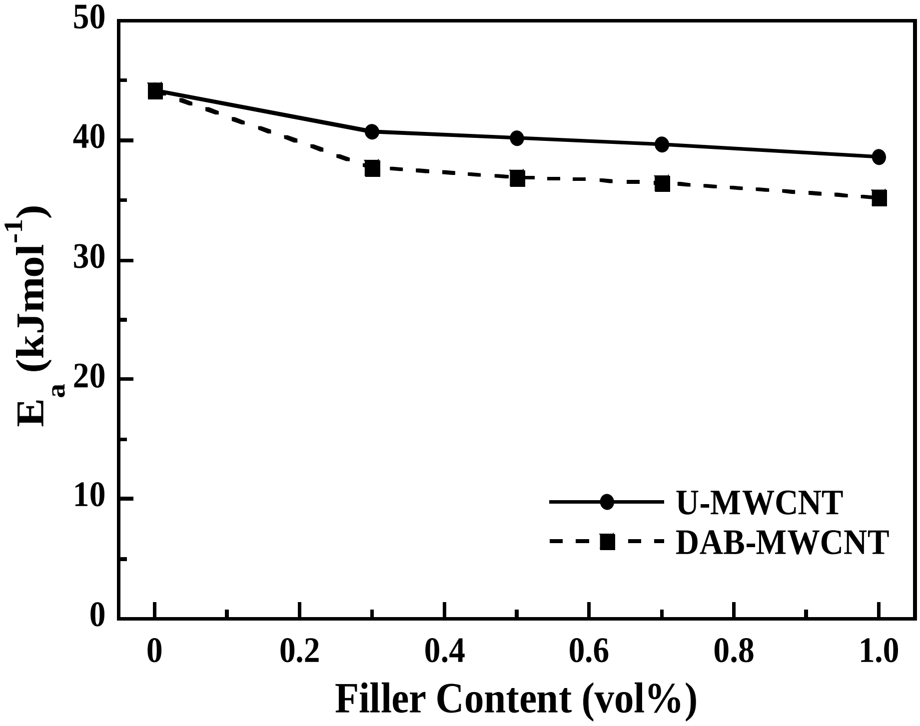

Figure 5.19 Activation Energy of epoxy composites filled with MWCNTs at various contents

5.3.2 Dynamic mechanical analysis of MWCNT/epoxy composites

In this section, the dynamic mechanical properties of epoxy composites reinforced with U-MWCNTs and DAB-MWCNTs at low concentration are discussed. The plots of storage modulus (E′) and loss modulus (E″) as a function of temperature for epoxy composites filled with various loading of U-MWCNTs and DAB-MWCNTs are illustrated in Figure 5.20 and 5.21, respectively. As can be seen in Figure 5.20(a), the storage moduli at room temperature of U-MWCNT/epoxy composites increased with increasing filler concentration because of their high aspect ratio and excellent mechanical properties. However, the decrease of E′ was found at high loading of U-MWCNTs. It is explained by considering the fact that U-MWCNTs were easily entangled and formed large agglomerates in epoxy matrix because of high surface area and high intrinsic van der Waals force between the nanotubes, resulting in a lack of continuity in load transfer. Evidently, E′ of DAB-MWCNT/epoxy composites linearly increased as a function of volume fraction as shown in Figure 5.21(a) and was higher than that of U-MWCNTs at the same filler loading. It can be attributed to well homogeneous dispersion of DAB-MWCNTs in the polymer matrix after the functionalization. It is mainly because the presence of amino groups in DAB structure and oxygen-containing groups on their surface led to the decrease of van der Waals force among the nanotubes. Another possible reason to explain this phenomenon is better interfacial interaction between the nanotube and polymer matrix. The existence of amino groups and small amount of oxygen containing groups on MWCNTs could provide fairly strong interaction with epoxy resin, corresponding to effective load and heat transfer from MWCNTs through epoxy matrix.

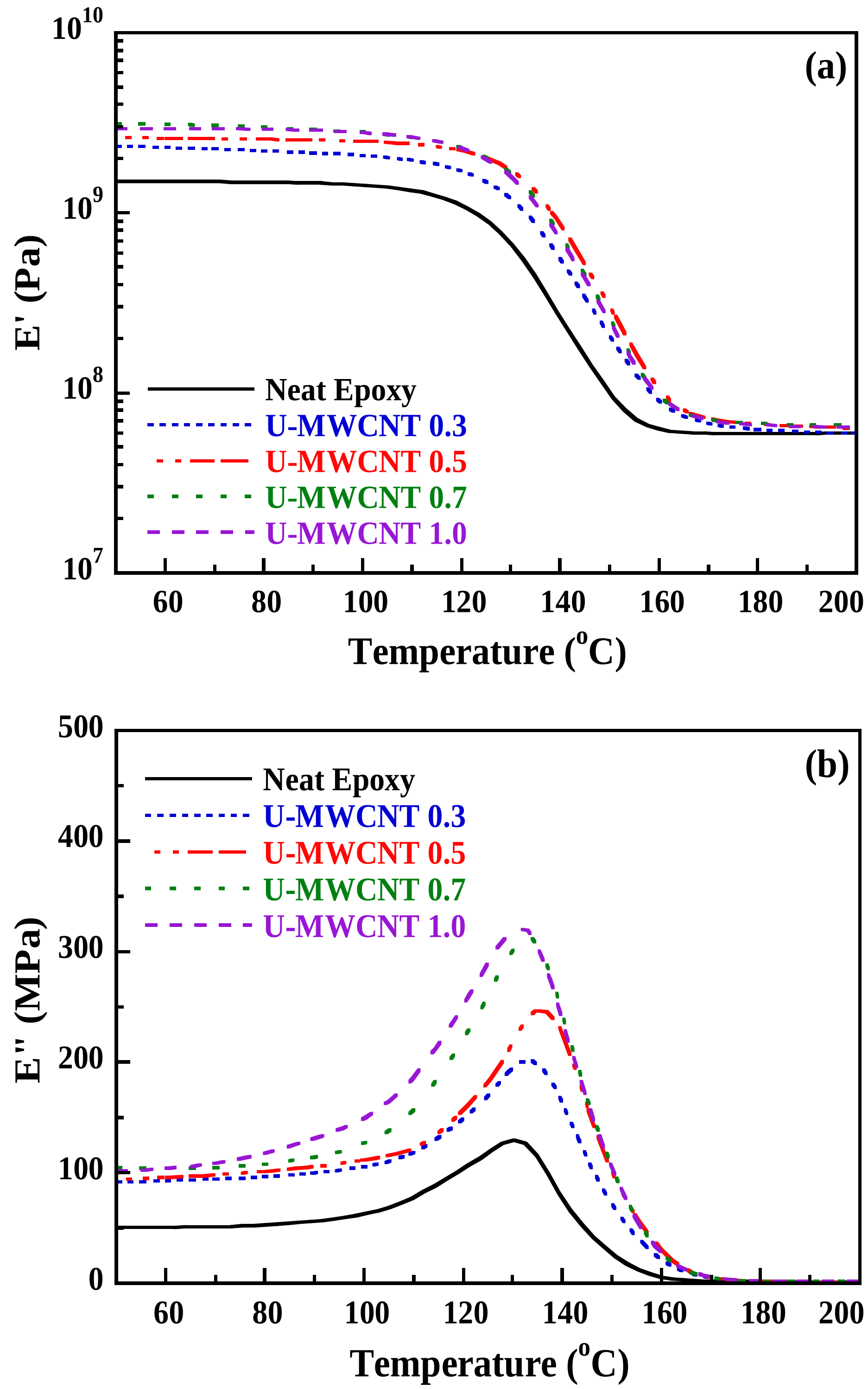

Figure 5.20 Dynamic mechanical properties of epoxy composites reinforced with U-MWCNTs: (a) storage modulus and (b) loss modulus

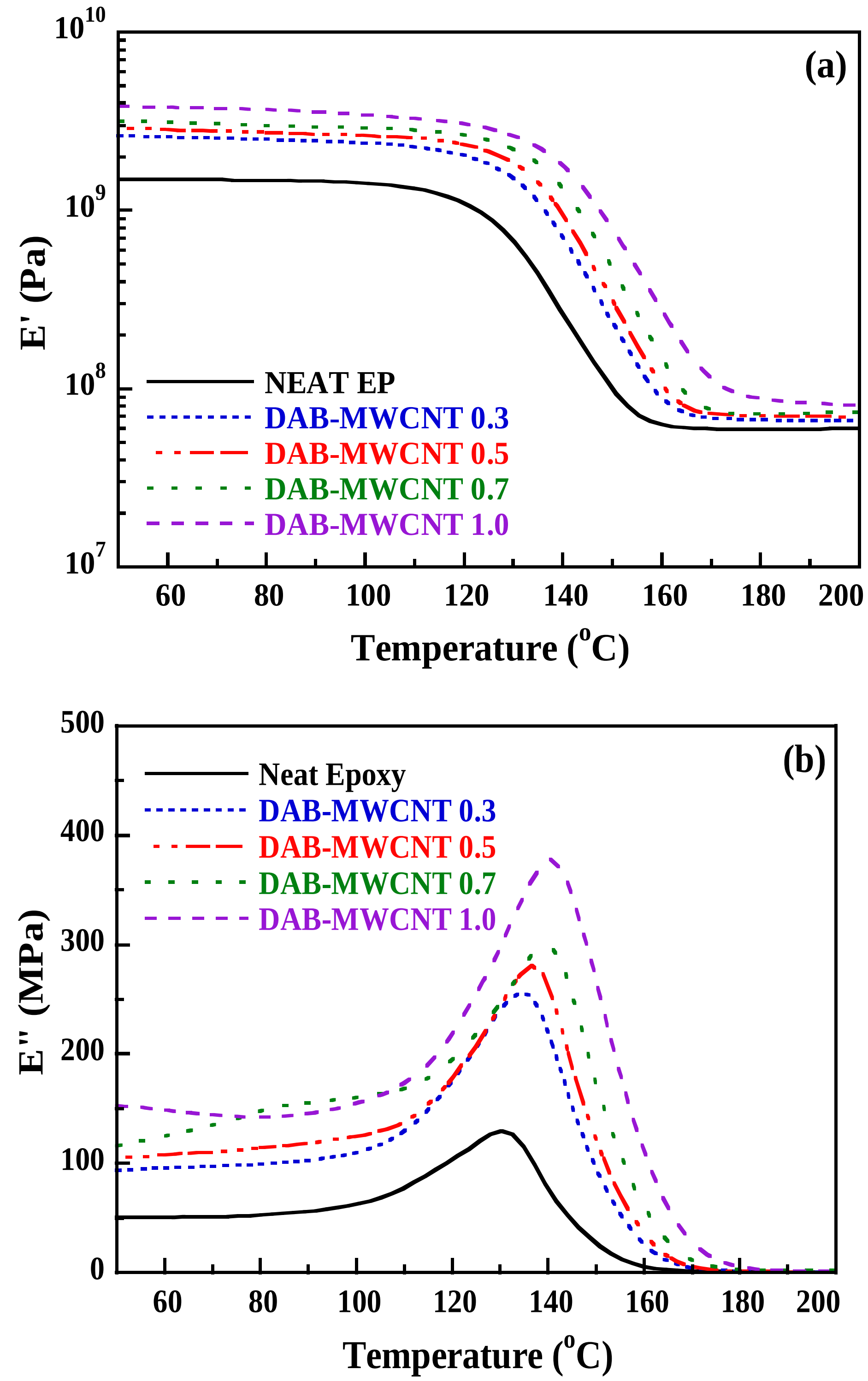

Figure 5.21 Dynamic mechanical properties of epoxy composites reinforced with DAB-MWCNTs: (a) storage modulus and (b) loss modulus

According to the calculation of the crosslink density (λ) as described in previous section, the crosslink density of epoxy composites as a function of filler concentration is shown in Figure 5.22. It is well known that the epoxide group can be attacked by amine or carboxyl acid and then form the crosslinking structure of epoxy resin via nucleophilic addition reaction. With the addition of U-MWCNTs, the crosslink density of composites slightly increased. It is believed that small amounts of oxygen-containing groups embedded on the MWCNT surface probably reacted with the oxirane rings in epoxy monomer, providing more crosslink degree. In case of DAB-MWCNT/epoxy composites, the diamino functional groups of DAB introduced onto the surface of MWCNTs could react with epoxy monomers and formed additional crosslink networks in composites. Thus, the crosslink density of DAB-MWCNT/epoxy composites linearly increased as a function of volume fraction and was higher than that of U-MWCNTs as well.

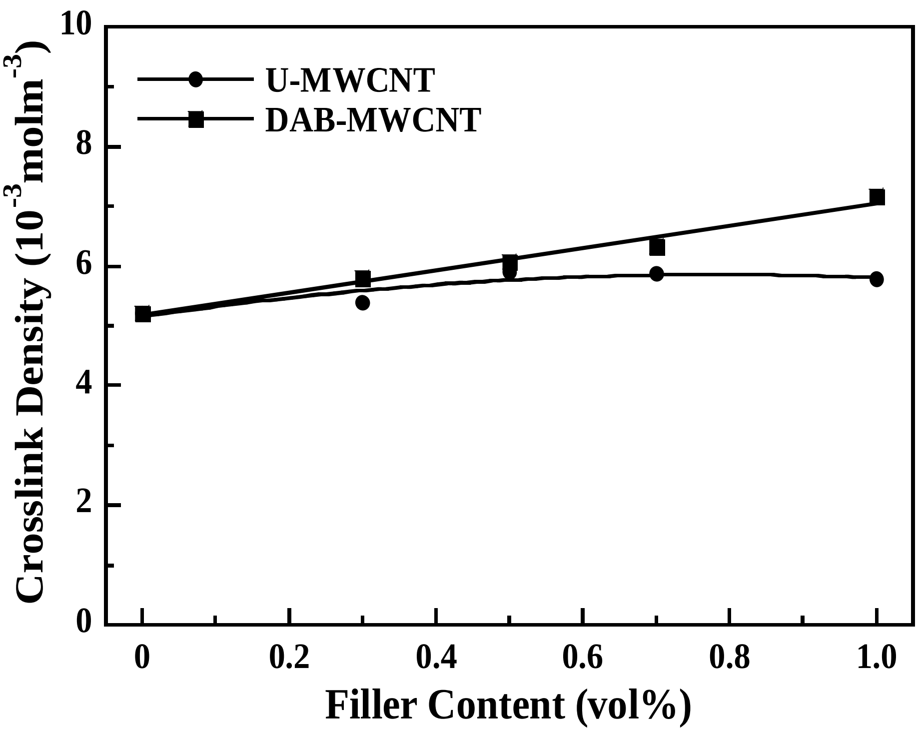

Figure 5.22 Crosslink density of epoxy composites filled with MWCNTs at various contents

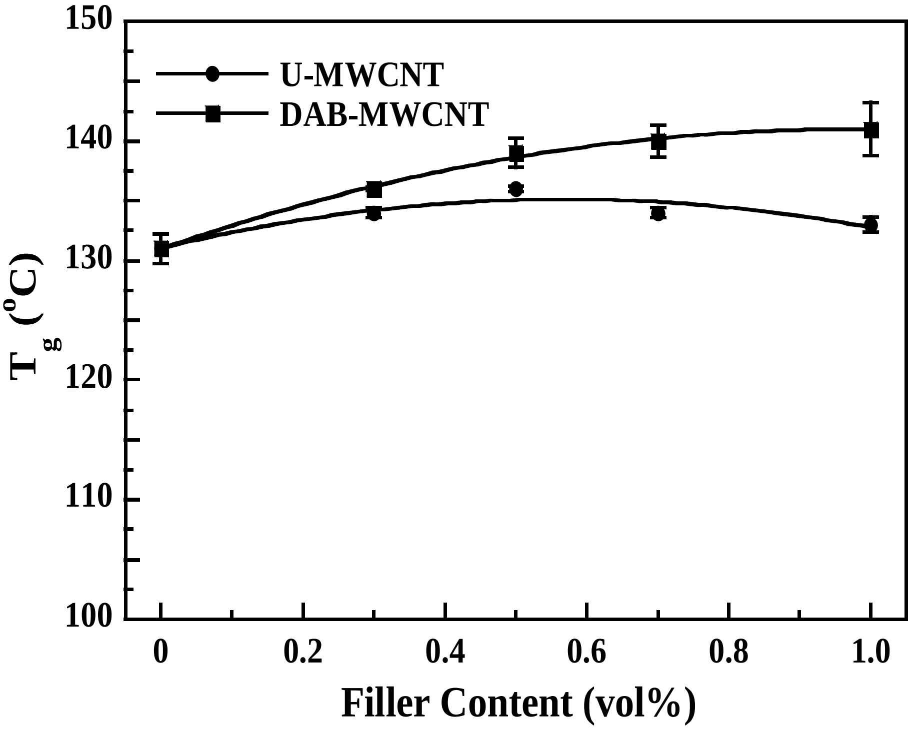

Figure 5.23 Glass transition temperature of epoxy composites filled with MWCNTs at various contents

Figure 5.20(b) and 5.21(b) illustrates the loss moduli of epoxy composites reinforced with U-MWCNTs and DAB-MWCNTs as a function of temperature, respectively. The E″ peaks obviously shifted to higher temperature at very low loading of MWCNTs, indicating the T_g enhancement. This phenomenon is attributed to the existence of randomly dispersed U-MWCNTs in epoxy matrix restricted the mobility of polymer chains. It is known that the T_g of polymer composite substantially related to the mobility of polymer segments or the free volume fraction in polymer. Nonetheless, the T_g of composites slightly decreased with further increase of U-MWCNT contents. It can be definitely considered that large bundles of U-MWCNTs dispersed heterogeneously in polymer matrix possibly interrupted the formation of crosslink networks in the composites. This behavior is consistent with the insignificant change in the crosslink density of U-MWCNT/epoxy composites when the filler loading was higher than 0.5 vol%. In contrast, the T_g of composites noticeably increased with the incorporation of DAB-MWCNTs because of the good dispersion and greatly improved interfacial interaction after the functionalization as discussed previously. Figure 5.23 demonstrates the plot of T_g versus filler volume fraction of composites. Besides, the increase of crosslink density in composites referred to the decrease of free volume fraction could restrict the polymer mobility, leading to high T_g[82, 87, 89].

5.3.3 Thermo mechanical analysis of MWCNT/epoxy composites

As illustrated in Figure 5.24, the CTE decreased as the volume fraction of fillers increased, resulting in decrease of free volume fraction as mentioned above. Especially DAB-MWCNT/epoxy composites, diamino groups on the DAB-MWCNT surface probably formed the chemical bonding with epoxy resin, increasing the crosslink density and reducing the free volume fraction.

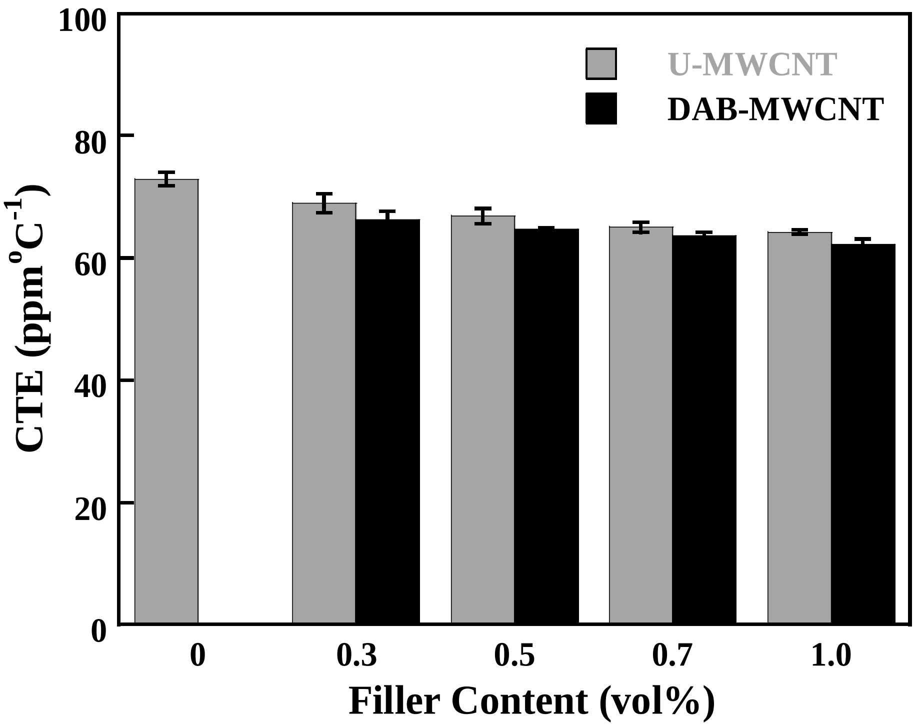

Figure 5.24 Coefficient of thermal expansion of epoxy composites filled with U-MWCNTs and DAB-MWCNTs at various contents

5.3.4 Morphology analysis of MWCNT/epoxy composites

As can be seen in Figure 5.25, the fracture surface of epoxy composites filled with various filler contents was also observed in this work. It can be observed that U-MWCNTs exhibit poor dispersion within polymer matrix in which large bundles of U-MWCNTs can be observed when U-MWCNT loading increase. It is due to their high surface area and high van der Waals force between the nanotubes. After the functionalization, DAB-MWCNTs were dispersed more homogeneously in polymer matrix. The small white dots, representing the broken ends of embedded MWCNTs, were mainly observed in the composite as shown in Figure 5.25(d). This phenomenon might be due to enhanced dispersibility and interfacial interaction caused by diaminobenzoyl functional groups established on the surface of DAB-MWCNTs.

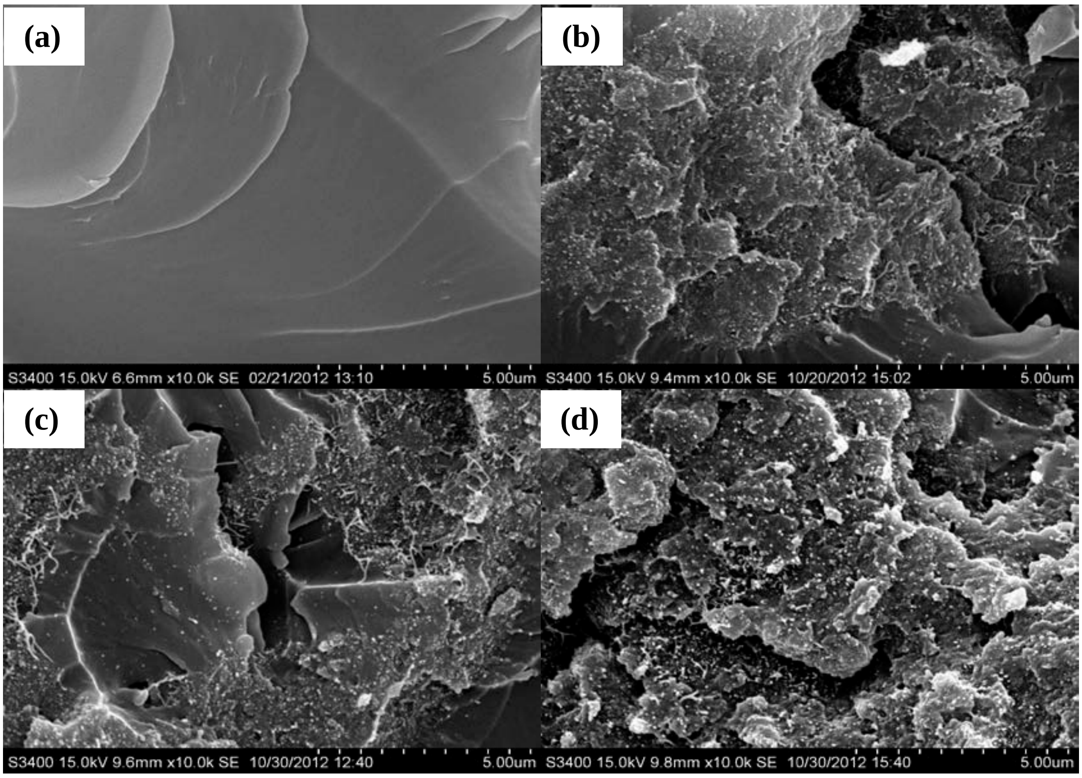

Figure 5.25 Fracture surfaces of (a) neat epoxy and composites filled with (b) U-MWCNT 0.5 vol%, (c) U-MWCNT 1.0 vol% and (d) DAB-MWCNT 1.0 vol%

5.3.5 Thermal conductivity of MWCNT/epoxy composites

In order to elucidate the effect of MWCNT concentration and the functionalization on the thermal conductivity of composite, the values of thermal conductivity were calculated from Eq. (11). The density of MWCNT/epoxy composites was measured by water displacement. The comparison between the measured and theoretical density is illustrated in Figure 5.26. The measured density is very close to the theoretical density. Figure 5.27 shows the temperature dependence of thermal diffusivity of composites incorporated with U-MWCNTs and DAB-MWCNTs. For all samples, the thermal diffusivity gradually decreased as the temperature increased. However, the thermal diffusivity of composites remarkably increased by adding small amounts of fillers. Clearly, the thermal diffusivity of DAB-MWCNT/epoxy composites is higher than that obtained from U-MWCNT/epoxy composites. It is possibly due to good interfacial interaction between DAB-MWCNT and polymer matrix caused by the functionalization.

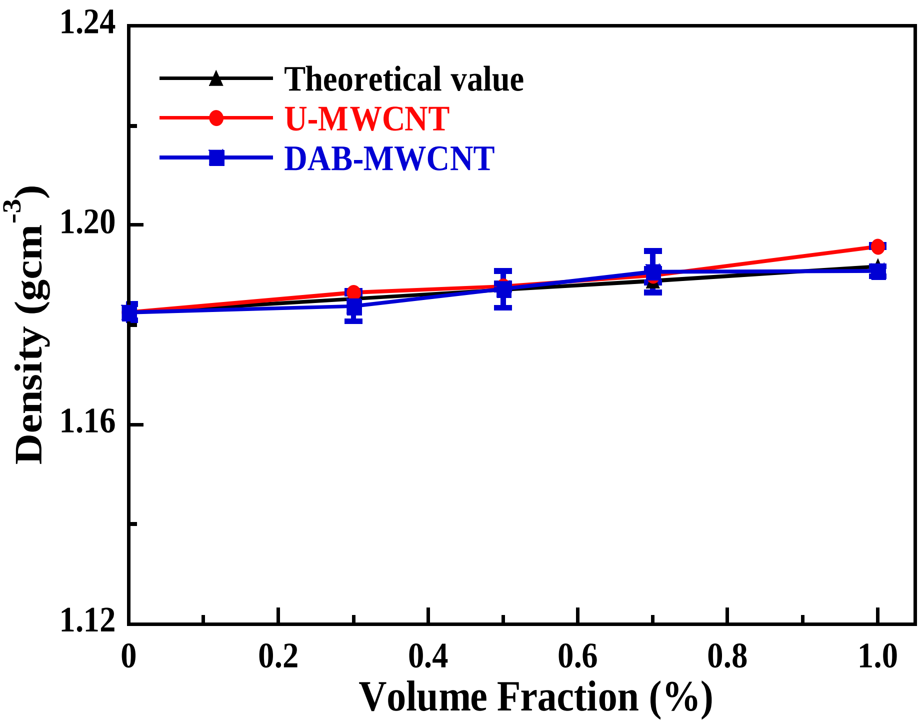

Figure 5.26 Density of epoxy composites as a function of filler loading

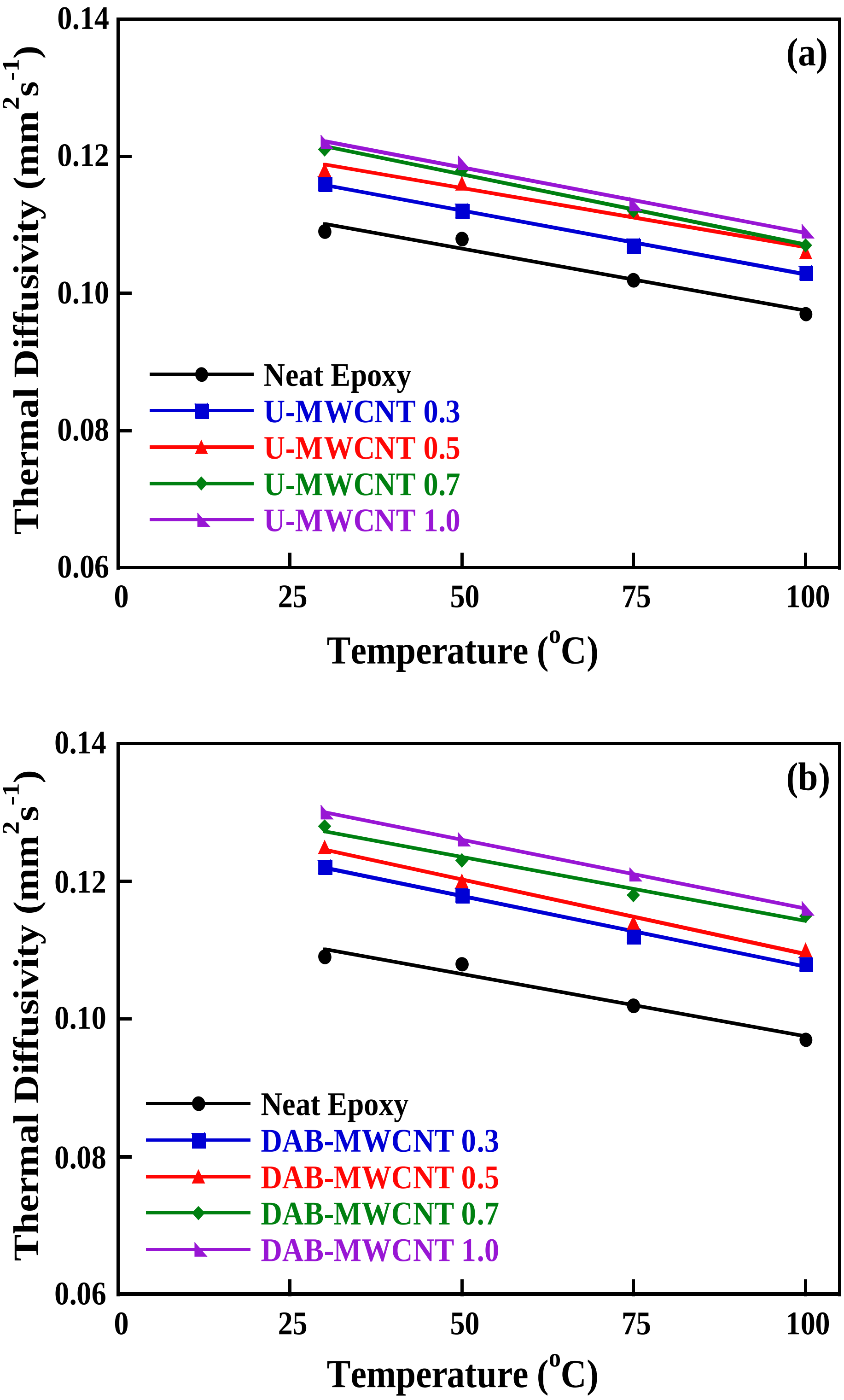

Figure 5.27 Thermal diffusivity of epoxy composites incorporated with (a) U-MWCNT and (b) DAB-MWCNT at various loading

Figure 5.28 shows the thermal conductivity of epoxy composites at 50 °C. At very low concentration, U-MWCNTs were randomly dispersed in polymer matrix and provided heat conductive pathways in the polymer matrix. Thus, thermal conductivity of composites was higher than that of neat epoxy. With further increase of U-MWCNT loading, thermal conductivity scarcely increased. It is attributed to their high surface area, high aspect ratio and high van der Waals force between the nanotubes, causing the heterogeneous dispersion of U-MWCNTs at high volume fraction in polymer matrix as seen in SEM images. This behavior hindered the potential of U-MWCNTs. After the functionalization with DAB, the dispersion of DAB-MWCNTs within epoxy resin was greatly improved. The DAB moieties on their surface provided better interfacial interaction between DAB-MWCNT and polymer matrix, reducing the interfacial thermal resistance. The effective heat conductive pathways were provided in the composite. Therefore, the thermal conductivity of epoxy composites increased as a function of DAB-MWCNT concentration. Also, thermal conductivity of epoxy filled with DAB-MWCNTs was higher than that of U-MWCNTs at the same filler loading.

5.3.6 Prediction of thermal conductivity of MWCNT/epoxy composites

To investigate the effect of the addition of thermally conductive filler on the thermal conductivity of polymer composites, various theoretical and empirical models have been considered [31, 90-92]. The most common equations based on Maxwell-Eucken's and Lewis-Nielsen's models were used in this work to predict the thermal conductivity of epoxy composites.

The Maxwell-Eucken's model can be used to predict the thermal conductivity of composites by

$$K=K_m\frac{[K_f+2K_m+2V_f(K_f-K_m)]}{[K_f+2K_m-V_f(K_f-K_m)]} \tag{12}$$

where K, K_m and K_f are the thermal conductivity of composites, polymer matrix and filler, respectively; V_f is the volume fraction of filler. It was clearly seen that the experimental data were higher than those predicted values which is due to the assumption of this model which indicates that the fillers are spherical particles without mutual interaction dispersed randomly in the polymer matrix [93]. While, MWCNTs used in this work have extremely high aspect ratio and the mutual interaction with each other. Therefore, MWCNTs could provide more heat conductive networks in the composite, resulting in the enhancement of thermal conductivity. It is, especially true for DAB-MWCNTs because the DAB functional groups on their surface could achieve good dispersion and interaction between the polymer matrix and filler as mentioned above.

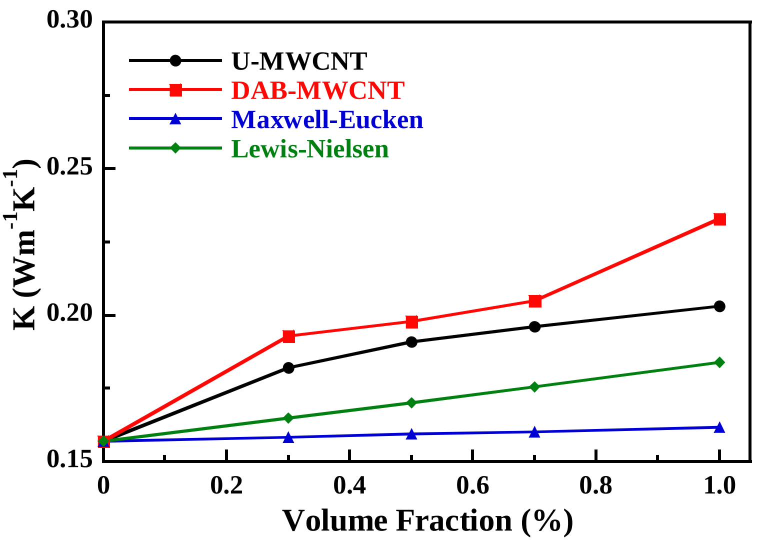

Figure 5.28 The experimental and theoretical thermal conductivity of epoxy composites as a function of filler loading

The Lewis-Nielsen's model was further applied to evaluate the thermal conductivity of composites by taking the geometry and the maximum volume fraction of filler into the consideration [94]. It can be explained by

$$K = K_m \frac{1+ABV_f}{1-B\psi V_f} \tag{13}$$

where

$$A = K_E - 1, \tag{14}$$

$$B = \frac{K_f/K_m - 1}{K_f/K_m + A}, \tag{15}$$

$$\psi=1+\left(\frac{1-V_m}{V_m^{\ 2}}\right)V_f, \tag{16}$$

where K_E is an Einstein constant related to the shape and orientation of the filler; B is a factor depending on the thermal conductivity of each component; V_m is the maximum packing fraction of filler; and ψ is a parameter related to the volume fraction of filler.

Generally, the values of A and V_m are constant for each type of filler. For instance, A = 8.38 and V_m = 0.52 are often used for the polymer composites based on the short fibers with aspect ratio less than 15 randomly dispersed in 3D direction. As shown in Figure 5.28, the experimental values of thermal conductivity of epoxy composites incorporated with U-MWCNTs and DAB-MWCNTs was compared to that obtained from this model. It was found that the experimental values did not fit well with the predicted values. The thermal conductivity based on this model was close to the experimental values rather than those calculated from Maxwell-Eucken's model. It is due to the fact that this model is the most versatile for the particulate/short fiber composites, whereas MWCNTs are much stronger and have higher aspect ratio than the conventional fibers. Besides, the value of A, which strongly affects the prediction, is not suitable for MWCNT/ polymer composites.

As mentioned above, the measured thermal conductivity of MWCNT/epoxy composites was fairly higher than those predicted from the conventional models. Consequently, the effective medium approaches (EMA) have been proposed to evaluate the effective thermal conductivity of polymer composites [95]. The Maxwell-Garnett (MG) typed EMA has been found suitable for predicting the thermal conductivity of polymer composites filled with low concentration of MWCNTs [96]. The MG-EMA was built on the basis of a random orientation of MWCNTs and high aspect ratio (p>1000) [97].

The MG-EMA equation can be expressed as

$$\frac{K_e}{K_m} = \frac{3+2V_f\left[\beta_x(1-L_x)+\beta_z(1-L_z)\right]}{3-V_f(2\beta_x L_x+\beta_z L_z)}, \tag{17}$$

where K_e is the effective thermal conductivity of composite; K_m and K_f are the thermal conductivity of polymer matrix and filler, respectively; and V_f is the volume fraction of filler. β_x and β_z are defined as

$$\beta_x = \frac{K_x-K_m}{K_m+L_x(K_f-K_m)}, \tag{18}$$

$$\beta_z = \frac{K_z-K_m}{K_m+L_z(K_f-K_m)}, \tag{19}$$

where K_x and K_z are the thermal conductivity of MWCNTs along transverse and longitudinal axes, respectively. L_x and L_z are the geometrical factors depending on the aspect ratio (p) of MWCNTs, given by

$$L_x = \frac{p^2}{2(p^2-1)} - \frac{p}{2(p^2-1)^{3/2}}\cosh^{-1}p, \tag{20}$$

$$L_z = 1-2L_x, \tag{21}$$

The high aspect ratio (p>100) of MWCNTs gives $L_x = 0.5$ and $L_z = 0$. If K_x and K_z of MWCNTs are much larger than K_m, then Eq. (17) can be simplified as [96]

$$\frac{K_e}{K_m} = \frac{3+V_f K_f/K_m}{3-2V_f}. \tag{22}$$

Figure 5.29 shows the effective thermal conductivity (K_e) of composite as a function of MWCNT loading. As seen, the simplified equation predicted much higher thermal conductivity than the experimental values. The deviation between the theoretical and experimental values is possibly due to the interfacial thermal resistance (R_k) between the nanotube and the polymer matrix. Therefore, the K_e in Eq. (22) was developed by considering the perfect interface without any interfacial thermal resistance ($R_k = 0$). The modified MG-EMA model was developed by taking the interfacial thermal resistance into the consideration in term of Kapitza radius (a_k) which can be described as a following expression [98, 99]

$$\frac{K_e}{K_m}=1+\frac{V_f p}{3}\frac{K_f/K_m}{p+\frac{2a_k}{d}\frac{K_f}{K_m}} \tag{23}$$

where

$$a_k=R_k K_m \tag{24}$$

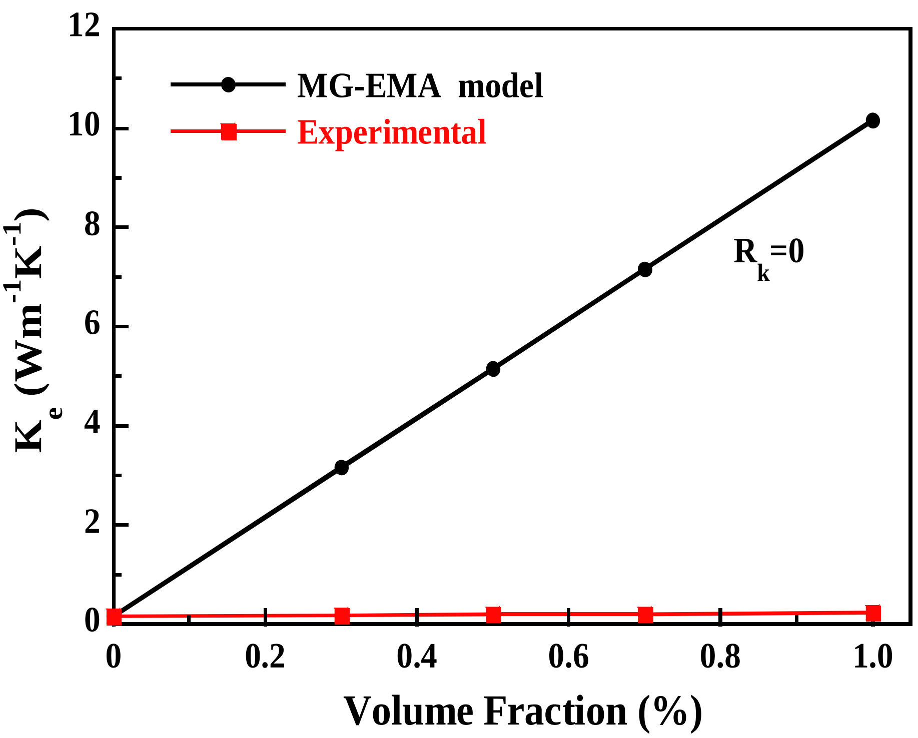

Figure 5.29 Effective thermal conductivity of epoxy composites predicted by using Maxwell-Garnett (MG) typed EMA model with $R_k = 0$

Figure 5.30 shows the predicted K_e/K_m ratio with various R_k values. The enhancement of thermal conductivity was noticeably observed with low R_k. The measured values for U-MWCNT/epoxy composites were close to the predicted values according to Eq. (23) with R_k = 4x10^{-7} m^{2}K/W, whereas the experimental data for DAB-MWCNT/epoxy composites fit quite well with the theoretical values when R_k is about 2x10^{-7} m^{2}K/W. These results indicated that the interfacial thermal resistance slightly decreased after the functionalization. The amino groups in the DAB structure established on the surface of MWCNTs could provide chemical bonding between DAB-MWCNT and epoxy resin, resulting in the decrease of interfacial thermal resistance. Therefore, the thermal conductivity of DAB-MWCNT/epoxy composites greatly enhanced.

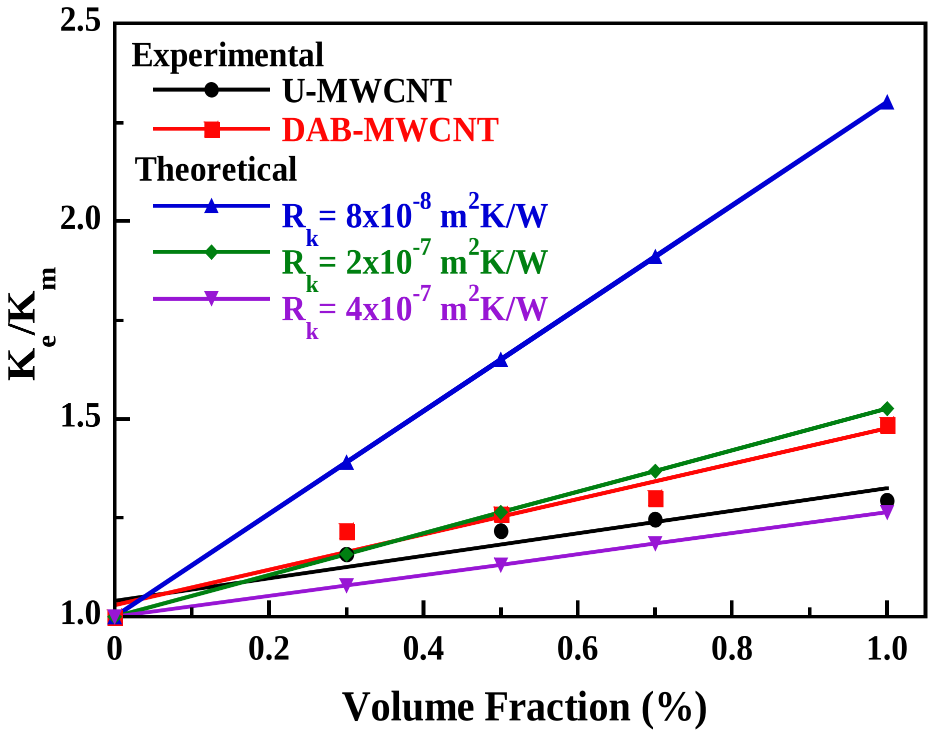

Figure 5.30 K_e/K_m ratio with various R_k values

5.4 Hybrid filler/epoxy composites

To improve the thermal conductivity of epoxy resin for using in microelectronic packaging, the addition of hybrid filler systems into the polymer matrix was focused in this part. However, the insulation properties are still required for underfills. The content of electrically conducting MWCNTs should be kept as low as possible but still high enough for good heat dissipation. Consequently, the combinations of 1.0 vol% MWCNTs and various contents of submicron-sized Si_3N_4 particles were studied as hybrid filler systems.

5.4.1 Dynamic mechanical properties of hybrid filler/epoxy composites

Additionally, the storage moduli and loss moduli of composites containing hybrid fillers are illustrated in Figure 5.31. It can be seen that E′ of epoxy composites filled with hybrid filler were higher than that with single filler. The E′ increased with increasing of Si_3N_4 content. The effective reinforcement of submicron-sized Si3N4 particles may be attributed to their rigidity and intrinsic high modulus. From the results of E″ peak, it reveals that the addition of Si_3N_4 particles into U-MWCNT based epoxy composites slightly enhanced their Tg. It is possibly due to the fact that the increase of filler concentration could reduce the free volume fraction. Considering the hybrid filler system containing 1.0 vol% DAB-MWCNTs and 7.5 vol% Si_3N_4, the composite exhibits high E′ and high Tg. It is believed that these behaviors are attributed to the presence of amino groups that promoted good dispersion of fillers and better interfacial interaction, possibly hindering polymer chain mobility and reducing free volume fraction in the composite. However, the addition of submicron-sized Si_3N_4 fairly obstructed the formation of crosslink structures in composites, decreasing the crosslink density. The Tg and crosslink density of epoxy composites added with hybrid fillers are determined and shown in Table 5.10.

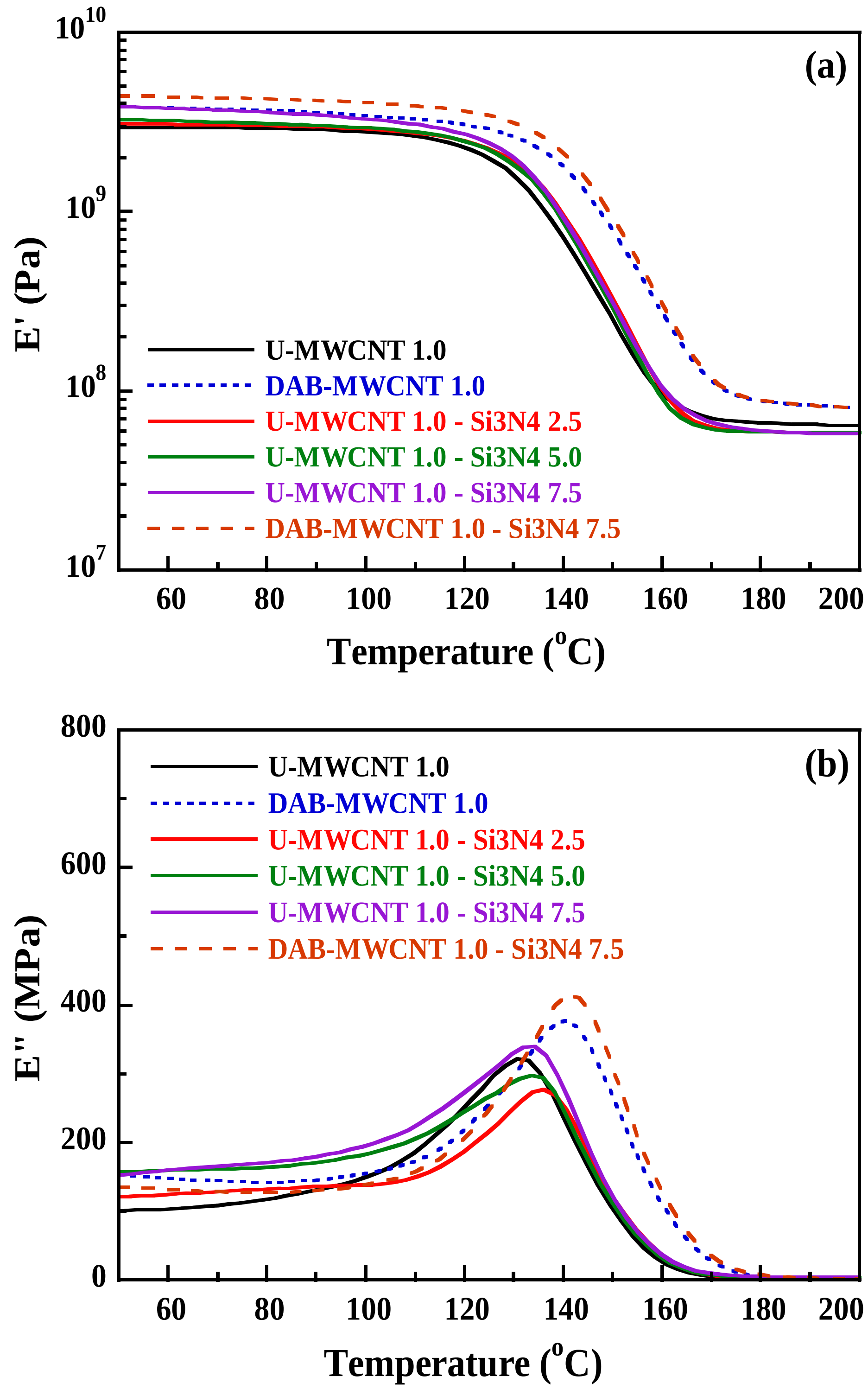

Figure 5.31 Dynamic mechanical properties of epoxy composites reinforced with various hybrid fillers: (a) storage modulus and (b) loss modulus

Table 5.10 Properties of epoxy composites filled with various hybrid fillers

Sample	**T_g (°C)**	**λ (10^{-3}molm^{-3})**
U-MWCNT 1.0	133	5.779
U-MWCNT 1.0 – Si_3N_4 2.5	136	5.132
U-MWCNT 1.0 – Si_3N_4 5.0	136	5.095
U-MWCNT 1.0 – Si_3N_4 7.5	134	5.094
DAB-MWCNT 1.0	141	7.173
DAB-MWCNT 1.0 – Si_3N_4 7.5	142	6.898

5.4.2 Thermomechanical properties of hybrid filler/epoxy composites

As shown in Figure 5.32, the addition of hybrid fillers as MWCNTs and Si_3N_4 particles into polymer matrix provided rather low CTE because of low intrinsic CTE of fillers. Especially, the CTE of composite remarkably reduced by the incorporation of hybrid fillers based on DAB-MWCNTs into epoxy matrix. It is possibly due to optimal packing density of DAB-MWCNTs and Si_3N_4 particles, caused by amino functional groups of DAB-MWCNTs that effectively formed filler-filler interaction. It has a positive effect on thermal stability of composites, thus the CTE of epoxy composites remarkably decreased.

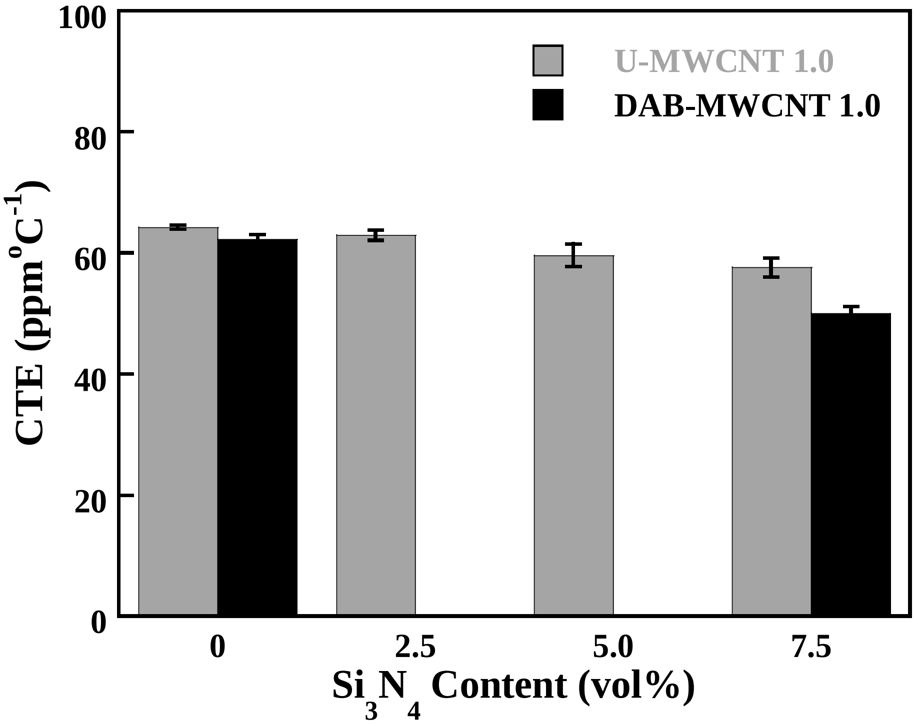

Figure 5.32 Coefficient of thermal expansion of epoxy composites filled with hybrid fillers

5.4.3 Morphology of hybrid filler/epoxy composites

The dispersion of hybrid fillers containing MWCNTs and Si_3N_4 particles in the polymer matrix was evaluated as shown in Figure 5.33. The fracture surface of the composite reinforced with U-MWCNTs and Si_3N_4 fillers is quite smooth. It might be due to the heterogeneous distribution of fillers in epoxy matrix and weak interfacial interaction between fillers and polymer matrix. On the other hand, the addition of hybrid filler based on DAB-MWCNTs into polymer matrix provided more roughness of the fractured surface. It is due to the fact that amino groups of DAB moieties on their surface improved the dispersion of fillers in the matrix and also enhanced interfacial interaction between fillers and the polymer matrix.

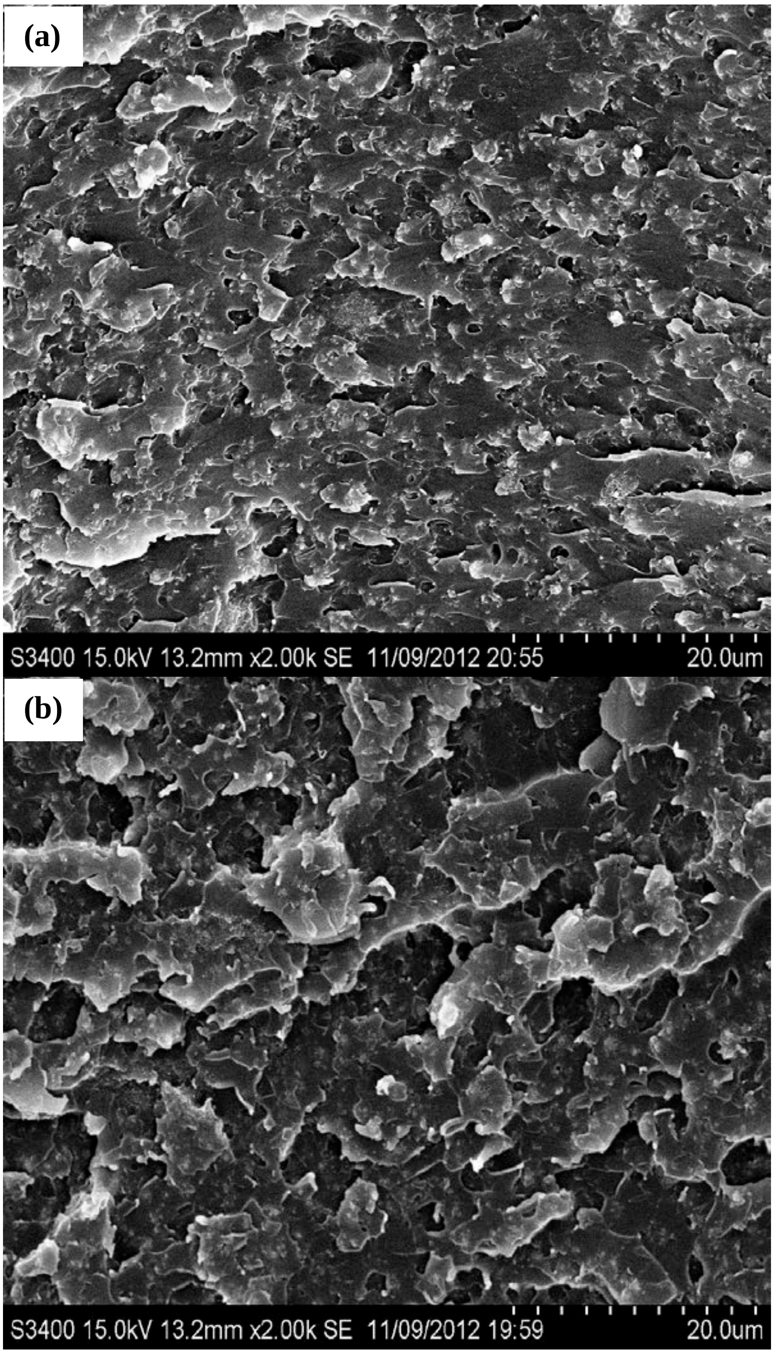

Figure 5.33 Fracture surfaces of (a) U-MWCNT 1.0 vol%-Si_3N_4 7.5 vol% and (b) DAB-MWCNT 1.0 vol%-Si_3N_4 7.5vol%

5.4.4 Thermal conductivity of hybrid filler/epoxy composites

To obtain higher thermal conductivity of composites, MWCNTs were partially replaced with submicron-sized fillers. The effects of hybrid filler systems on the thermal conductivity were investigated and summarized in Table 5.11. The 1.0 vol% U-MWCNTs filled epoxy composites were incorporated with various contents of Si_3N_4 particles. It was found that thermal conductivity increased with increasing Si_3N_4 content. The addition of submicron-sized fillers in the composites promoted more heat conductive pathways and high packing density, enhancing the heat dissipation of materials. In case of epoxy resin filled with 1.0 vol% DAB-MWCNTs and 7.5 vol% Si_3N_4, the heat conductive networks were effectively formed with optimal packing density, thereby increasing thermal conductivity more than 134% compared with that of neat epoxy. This result confirms that the hybrid fillers can be used as effective filler to improve the thermal conductivity of composites.

Table 5.11 Properties of epoxy composites filled with various hybrid fillers

Sample	ρ (gcm^{-3})	α (mm^2s^{-1})	K ($Wm^{-1}K^{-1}$)	K_R (%)
U-MWCNT 1.0	1.1958	0.119	0.203	129.30
U-MWCNT 1.0 – Si_3N_4 2.5	1.2584	0.145	0.255	162.42
U-MWCNT 1.0 – Si_3N_4 5.0	1.3202	0.166	0.304	193.63
U-MWCNT 1.0 – Si_3N_4 7.5	1.3865	0.170	0.324	206.37
DAB-MWCNT 1.0	1.1908	0.126	0.233	148.41
DAB-MWCNT 1.0 – Si_3N_4 7.5	1.3818	0.175	0.367	233.76

CHAPTER VI
CONCLUSIONS AND RECOMMENDATIONS

6.1 Conclusions

Directly functionalized multiwalled carbon nanotubes (MWCNTs) with benzene-1,3,5-tricarboxylic acid (BTC) and 3,5-diaminobenzoic acid (DAB) were successfully accomplished with less structural damage as confirmed by XPS, FT-IR and FT-Raman results. The functionalization of MWCNTs with BTC and DAB enhanced the dispersibility and interfacial interaction between the nanotubes and the polymer matrix. From DSC results, the reactive functional groups introduced onto MWCNT surfaces can accelerate the curing reaction of epoxy composites remarkable inducing low exothermic peak temperature and exothermic heat of reaction. The activation energy values obtained from Kissinger and Ozawa methods show fairly consistent results in which the activation energy values obviously decrease with the introduction of MWCNTs, especially DAB-MWCNTs. The incorporation of only 0.3 vol% of unmodified and functionalized MWCNTs remarkably enhanced the dynamic mechanical properties of epoxy composites, especially T_g. The storage moduli of epoxy composites were substantially increased with the addition of functionalized MWCNTs. High crosslink density of composites resulted in the decrease of free volume fraction which was calculated from the WLF equation. The thermal stability was improved as observed in the decrease of CTE.

The composites reinforced with DAB-MWCNTs remarkably exhibit high E′, high Tg and low CTE rather than those of U-MWCNTs at the same filler content. Amino groups of diaminobenzoyl compound promoted strong interfacial interaction between DAB-MWCNT and polymer matrix that can reduce the interfacial thermal resistance, resulting in an increase of thermal conductivity. The modified MG-EMA model by taking the interfacial thermal resistance into the consideration is appropriate for predicting the thermal conductivity of epoxy composites filled with low concentration of MWCNTs. The study on the properties of epoxy composites reinforced with hybrid filler systems was also performed. According to the results, the hybrid filler systems were effective filler to enhance dynamic mechanical properties and thermal properties of composites. Especially, the hybrid filler containing 1.0 vol% DAB-MWCNTs and 7.5 vol% Si_3N_4 promoted effective heat conductive pathways and optimal packing density in polymer matrix, thereby achieving 134% higher thermal conductivity than that of neat epoxy resin.

6.2 Recommendations for further study

1. Transmission electron micrograph should be taken to characterize size and structure of MWCNTs in epoxy composites.
2. The viscosity and flow behavior of MWCNT/epoxy composites should be investigated.
3. The effect of MWCNTs on the pot life of underfill should be explored.
4. Thermal stability of epoxy composites, decomposition temperature (T_d), should be investigated.
5. The dielectric constant of epoxy composites should be studied.

REFERENCES

[1] Sun Lee, W., and Yu, J. Comparative study of thermally conductive fillers in underfill for the electronic components. Diamond and Related Materials 14 (2005): 1647-1653.

[2] Wong, C.P., and Bollampally, R.S. Comparative study of thermally conductive fillers for use in liquid encapsulants for electronic packaging. Ieee Transactions on Advanced Packaging 22 (1999): 54-59.

[3] Wong, C.P., and Bollampally, R.S. Thermal conductivity, elastic modulus, and coefficient of thermal expansion of polymer composites filled with ceramic particles for electronic packaging. Journal of Applied Polymer Science 74 (1999): 3396-3403.

[4] Li, H.Y., Jacob, K.I., and Wong, C.P. An improvement of thermal conductivity of underfill materials for flip-chip packages. Ieee Transactions on Advanced Packaging 26 (2003): 25-32.

[5] Zhou, T., Wang, X., Mingyuan, G.U., and Liu, X. Study of the thermal conduction mechanism of nano-SiC/DGEBA/EMI-2,4 composites. Polymer 49 (2008): 4666-4672.

[6] Gu, J.W., Zhang, Q.Y., Dang, J., and Xie, C. Thermal conductivity epoxy resin composites filled with boron nitride. Polymers for Advanced Technologies 23 (2012): 1025-1028.

[7] Zhu, B.L., Ma, J., Wu, J., Yung, K.C., and Xie, C.S. Study on the Properties of the Epoxy-Matrix Composites Filled with Thermally Conductive AlN and BN Ceramic Particles. Journal of Applied Polymer Science 118 (2010): 2754-2764.

[8] Ohashi, M., Kawakami, S., Yokogawa, Y., and Lai, G.-C. Spherical Aluminum Nitride Fillers for Heat-Conducting Plastic Packages. Journal of the American Ceramic Society 88 (2005): 2615-2618.

[9] Yung, K.C., and Liem, H. Enhanced thermal conductivity of boron nitride epoxy-matrix composite through multi-modal particle size mixing. Journal of Applied Polymer Science 106 (2007): 3587-3591.

[10] Hill, R.F., and Supancic, P.H. Thermal Conductivity of Platelet-Filled Polymer Composites. Journal of the American Ceramic Society 85 (2002): 851-857.

[11] Lee, W.S., Han, I.Y., Yu, J., Kim, S.J., and Byun, K.Y. Thermal characterization of thermally conductive underfill for a flip-chip package using novel temperature sensing technique. Thermochimica Acta 455 (2007): 148-155.

[12] Xu, Y., Chung, D.D.L., and Mroz, C. Thermally conducting aluminum nitride polymer-matrix composites. Composites Part A: Applied Science and Manufacturing 32 (2001): 1749-1757.

[13] Zeng, J., et al. Numerical Simulation of Thermal Conductivity of Particle Filled Epoxy Composites. Journal of Electronic Packaging 131 (2009): 041006-041007.

[14] Yu, H., et al. Thermal and insulating properties of epoxy/aluminum nitride composites used for thermal interface material. Journal of Applied Polymer Science 124 (2012): 669-677.

[15] Li, S.S., Qi, S.H., Liu, N.L., and Cao, P. Study on thermal conductive BN/novolac resin composites. Thermochimica Acta 523 (2011): 111-115.

[16] Esawi, A.M.K., and Farag, M.M. Carbon nanotube reinforced composites: Potential and current challenges. Materials & Design 28 (2007): 2394-2401.

[17] Ma, P.-C., Siddiqui, N.A., Marom, G., and Kim, J.-K. Dispersion and functionalization of carbon nanotubes for polymer-based nanocomposites: A review. Composites Part A: Applied Science and Manufacturing 41 1345-1367.

[18] Rosca, I.D., Watari, F., Uo, M., and Akasaka, T. Oxidation of multiwalled carbon nanotubes by nitric acid. Carbon 43 (2005): 3124-3131.

[19] Datsyuk, V., et al. Chemical oxidation of multiwalled carbon nanotubes. Carbon 46 (2008): 833-840.

[20] Auad, M.L., Mosiewicki, M.A., Uzunpinar, C., and Williams, R.J.J. Single-wall carbon nanotubes/epoxy elastomers exhibiting high damping capacity in an extended temperature range. Composites Science and Technology 69 (2009): 1088-1092.

[21] Song, Y.S. Effect of surface treatment for carbon nanotubes on morphological and rheological properties of poly(ethylene oxide) nanocomposites. Polymer Engineering & Science 46 (2006): 1350-1357.

[22] Yang, K., and Gu, M. The effects of triethylenetetramine grafting of multi-walled carbon nanotubes on its dispersion, filler-matrix interfacial interaction and the thermal properties of epoxy nanocomposites. Polymer Engineering & Science 49 (2009): 2158-2167.

[23] Han, S.W., Oh, S.J., Tan, L.S., and Baek, J.B. One-pot purification and functionalization of single-walled carbon nanotubes in less-corrosive poly(phosphoric acid). Carbon 46 (2008): 1841-1849.

[24] Lee, H.-J., Han, S.-W., Kwon, Y.-D., Tan, L.-S., and Baek, J.-B. Functionalization of multi-walled carbon nanotubes with various 4-substituted benzoic acids in mild polyphosphoric acid/phosphorous pentoxide. Carbon 46 (2008): 1850-1859.

[25] Yang, S.-Y., et al. Effect of functionalized carbon nanotubes on the thermal conductivity of epoxy composites. Carbon 48 (2010): 592-603.

[26] Teng, C.-C., Ma, C.-C.M., Chiou, K.-C., Lee, T.-M., and Shih, Y.-F. Synergetic effect of hybrid boron nitride and multi-walled carbon nanotubes on the thermal conductivity of epoxy composites. Materials Chemistry and Physics 126 (2011): 722-728.

[27] Teng, C.-C., Ma, C.-C.M., Chiou, K.-C., and Lee, T.-M. Synergetic effect of thermal conductive properties of epoxy composites containing functionalized multi-walled carbon nanotubes and aluminum nitride. Composites Part B: Engineering 43 (2012): 265-271.

[28] Yang, K., and Gu, M. Enhanced thermal conductivity of epoxy nanocomposites filled with hybrid filler system of

triethylenetetramine-functionalized multi-walled carbon nanotube/silane-modified nano-sized silicon carbide. Composites Part A: Applied Science and Manufacturing 41 (2010): 215-221.

[29] Zhou, T., Wang, X., Liu, X., and Xiong, D. Improved thermal conductivity of epoxy composites using a hybrid multi-walled carbon nanotube/micro-SiC filler. Carbon 48 (2010): 1171-1176.

[30] He, H., Fu, R., Shen, Y., Han, Y.C., and Song, X.F. Preparation and properties Of Si3N4/PS composites used for electronic packaging. Composites Science and Technology 67 (2007): 2493-2499.

[31] An, Q., Qi, S., and Zhou, W. Thermal, electrical, and mechanical properties of Si3N4 filled LLDPE composite. Polymer Composites 30 (2009): 866-871.

[32] Zhou, W., et al. A novel fiber-reinforced polyethylene composite with added silicon nitride particles for enhanced thermal conductivity. Composites Part A: Applied Science and Manufacturing 40 (2009): 830-836.

[33] Shi, Z., Fu, R., Agathopoulos, S., Gu, X., and Zhao, W. Thermal conductivity and fire resistance of epoxy molding compounds filled with Si3N4 and Al(OH)3. Materials & Design 34 (2012): 820-824.

[34] Sun, Y.Y., Zhang, Z.Q., and Wong, C.P. Study and characterization on the nanocomposite underfill for flip chip applications. Ieee Transactions on Components and Packaging Technologies 29 (2006): 190-197.

[35] Wong, C.P., Vincent, M.B., and Shi, S. Fast-flow underfill encapsulant: Flow rate and coefficient of thermal expansion. Ieee Transactions on Components Packaging and Manufacturing Technology Part A 21 (1998): 360-364.

[36] Zhang, Z., and Wong, C., Flip-Chip Underfill. In *Smart Materials*, CRC Press: 2008; Vol. null.

[37] Fan, L., Zhang, Z., and Wong, C.P. Effect of Filler Settling of Underfill Encapsulant on Reliability Performance. International Symposium on Advanced Packaging Materials (2001): 219-223.

[38] James J. Licari, D.W.S. Adhesives Technology for Electronic Applications: Materials, Processes, Reliability. William Andrew Publishing, 2005.

[39] Zhang, Z.Q., and Wong, C.P. Recent advances in flip-chip underfill: Materials, process, and reliability. Ieee Transactions on Advanced Packaging 27 (2004): 515-524.

[40] Lu, D., and Wong, C.P. Materials for Advanced Packaging. Springer, 2008.

[41] Zhang, Z.Q., Beatty, E., and Wong, C.P. Study on the curing process and the gelation of epoxy/anhydride system for no-flow underfill for flip-chip applications. Macromolecular Materials and Engineering 288 (2003): 365-371.

[42] Zhang, Z.Q., Shi, S.H., and Wong, C.P. Development of no-flow underfill materials for lead-free solder bumped flip-chip applications. Ieee Transactions on Components and Packaging Technologies 24 (2001): 59-66.

[43] Zhang, Z.Q., and Wong, C.P. Study on metal chelates as catalysts of epoxy and anhydride cure reactions for no-flow underfill applications. In Lin, Q.; Pearson, R. A.; Hedrick, J. C., (eds.) pp. 264-278, 2004.

[44] Zhang, Z.Q., and Wong, C.P. Modeling of the curing kinetics of no-flow underfill in flip-chip applications. Ieee Transactions on Components and Packaging Technologies 27 (2004): 383-390.

[45] Goulding, T., Epoxy Resin Adhesives. In *Handbook of Adhesive Technology, Revised and Expanded*, CRC Press: 2003.

[46] Petrie, E.M. Epoxy Adhesive Formulations. McGRAW-HILL, 2006.

[47] Ma, P.C., Siddiqui, N.A., Marom, G., and Kim, J.K. Dispersion and functionalization of carbon nanotubes for polymer-based nanocomposites: A review. Composites Part a-Applied Science and Manufacturing 41 1345-1367.

[48] Shanmugharaj, A.M., et al. Physical and chemical characteristics of multiwalled carbon nanotubes functionalized with aminosilane and its influence on the properties of natural rubber composites. Composites Science and Technology 67 (2007): 1813-1822.

[49] Yang, S.-Y., et al. Effect of functionalized carbon nanotubes on the thermal conductivity of epoxy composites. Carbon 48 592-603.

[50] Spitalsky, Z., Tasis, D., Papagelis, K., and Galiotis, C. Carbon nanotube-polymer composites: Chemistry, processing, mechanical and electrical properties. Progress in Polymer Science 35 357-401.

[51] Miyagawa, H., Rich, M.J., and Drzal, L.T. Thermo-physical properties of epoxy nanocomposites reinforced by carbon nanotubes and vapor grown carbon fibers. Thermochimica Acta 442 (2006): 67-73.

[52] Shen, J.F., Huang, W.S., Wu, L.P., Hu, Y.Z., and Ye, M.X. Thermo-physical properties of epoxy nanocomposites reinforced with amino-functionalized multi-walled carbon nanotubes. Composites Part a-Applied Science and Manufacturing 38 (2007): 1331-1336.

[53] Gojny, F.H., et al. Evaluation and identification of electrical and thermal conduction mechanisms in carbon nanotube/epoxy composites. Polymer 47 (2006): 2036-2045.

[54] Sun, L., et al. Mechanical properties of surface-functionalized SWCNT/epoxy composites. Carbon 46 (2008): 320-328.

[55] Liao, S.-H., et al. Preparation and properties of functionalized multiwalled carbon nanotubes/polypropylene nanocomposite bipolar plates for polymer electrolyte membrane fuel cells. Journal of Power Sources 195 263-270.

[56] Xie, N., Jiao, Q.J., Zang, C.G., Wang, C.L., and Liu, Y.Y. Study on dispersion and electrical property of multi-walled carbon nanotubes/low-density polyethylene nanocomposites. Materials & Design 31 1676-1683.

[57] Mirershadi, S., Mortazavi, S.Z., Reyhani, A., Moniri, N., and Novinrooz, A.J. Effective Condition for Purification of Multi-walled Carbon Nanotubes by Nitric Acid. Synthesis and Reactivity in Inorganic Metal-Organic and Nano-Metal Chemistry 39 (2009): 312-316.

[58] Jiang, L.Q., and Gao, L. Effect of chemical treatment on the dispersion properties of carbon nanotubes. Journal of Inorganic Materials 18 (2003): 1135-1138.

[59] Huang, Y.L., et al. Morphological, electrical, electromagnetic interference (EMI) shielding, and tribological properties of functionalized multi-walled carbon nanotube/poly methyl methacrylate (PMMA)

composites. Composites Science and Technology 69 (2009): 1991-1996.

[60] Kathi, J., and Rhee, K. Surface modification of multi-walled carbon nanotubes using 3-aminopropyltriethoxysilane. Journal of Materials Science 43 (2008): 33-37.

[61] Yang, K., Gu, M., Guo, Y., Pan, X., and Mu, G. Effects of carbon nanotube functionalization on the mechanical and thermal properties of epoxy composites. Carbon 47 (2009): 1723-1737.

[62] Aviles, F., Cauich-Rodriguez, J.V., Moo-Tah, L., May-Pat, A., and Vargas-Coronado, R. Evaluation of mild acid oxidation treatments for MWCNT functionalization. Carbon 47 (2009): 2970-2975.

[63] Baek, J.B., Lyons, C.B., and Tan, L.S. Covalent modification of vapour-grown carbon nanofibers via direct Friedel-Crafts acylation in polyphosphoric acid. Journal of Materials Chemistry 14 (2004): 2052-2056.

[64] Lee, H.-J., et al. In Situ Synthesis of Poly(ethylene terephthalate) (PET) in Ethylene Glycol Containing Terephthalic Acid and Functionalized Multiwalled Carbon Nanotubes (MWNTs) as an Approach to MWNT/PET Nanocomposites. Chemistry of Materials 17 (2005): 5057-5064.

[65] Yesil, S., and Bayram, G. Poly(ethylene terephthalate)/carbon nanotube composites prepared with chemically treated carbon nanotubes. Polymer Engineering & Science 51 1286-1300.

[66] Zhang, L., Ni, Q.-Q., Shiga, A., Natsuki, T., and Fu, Y. Preparation of polybenzimidazole/functionalized carbon nanotube nanocomposite films for use as protective coatings. Polymer Engineering & Science 51 1525-1532.

[67] Wang, J., Liang, G., Yan, H., and He, S. Mechanical and thermal properties of functionalized multiwalled carbon nanotubes/cyanate ester composite. Polymer Engineering & Science 49 (2009): 680-684.

[68] Wang, J., Fang, Z., and Gu, A. Effect of multi-walled carbon nanotubes dispersity on the light transmittancy of multi-walled carbon

nanotubes/epoxy composites. Polymer Engineering & Science 46 (2006): 635-642.

[69] Chen, W., Qian, X.-M., He, X.-Q., Liu, Z.-Y., and Liu, J.-P. Surface modification of Kevlar by grafting carbon nanotubes. Journal of Applied Polymer Science 123 (2012): 1983-1990.

[70] Kundu, S., Wang, Y., Xia, W., and Muhler, M. Thermal Stability and Reducibility of Oxygen-Containing Functional Groups on Multiwalled Carbon Nanotube Surfaces: A Quantitative High-Resolution XPS and TPD/TPR Study. The Journal of Physical Chemistry C 112 (2008): 16869-16878.

[71] Okpalugo, T.I.T., Papakonstantinou, P., Murphy, H., McLaughlin, J., and Brown, N.M.D. High resolution XPS characterization of chemical functionalised MWCNTs and SWCNTs. Carbon 43 (2005): 153-161.

[72] Koysuren, O., Karaman, M., and Ozyurt, D. Effect of noncovalent chemical modification on the electrical conductivity and tensile properties of poly(methyl methacrylate)/carbon nanotube composites. Journal of Applied Polymer Science 127 (2013): 4557-4563.

[73] Cooper, C.A., Young, R.J., and Halsall, M. Investigation into the deformation of carbon nanotubes and their composites through the use of Raman spectroscopy. Composites Part a-Applied Science and Manufacturing 32 (2001): 401-411.

[74] Rong, H., Han, K., Li, S., Tian, Y., and Muhuoyu A novel method to graft carbon nanotube onto carbon fiber by the use of a binder. Journal of Applied Polymer Science 127 (2013): 2033-2037.

[75] Chapartegui, M., et al. Curing of epoxy/carbon nanotubes physical networks. Polymer Engineering & Science 52 663-670.

[76] Allaoui, A., and El Bounia, N. How carbon nanotubes affect the cure kinetics and glass transition temperature of their epoxy composites? - A review. Express Polymer Letters 3 (2009): 588-594.

[77] Zhou, T., Wang, X., Liu, X.H., and Lai, J.Z. Effect of silane treatment of carboxylic-functionalized multi-walled carbon nanotubes on the

thermal properties of epoxy nanocomposites. Express Polymer Letters 4 217-226.

[78] Kasemsiri, P., Hiziroglu, S., and Rimdusit, S. Properties of wood polymer composites from eastern redcedar particles reinforced with benzoxazine resin/cashew nut shell liquid copolymer. Composites Part a-Applied Science and Manufacturing 42 1454-1462.

[79] Wang, F., Li, S.Q., Wang, J.W., and Xiao, J. Effect of functionalized multi-walled carbon nanotubes on the curing behavior and thermal stability of epoxy resin. High Performance Polymers 24 97-104.

[80] Montazeri, A., and Montazeri, N. Viscoelastic and mechanical properties of multi walled carbon nanotube/epoxy composites with different nanotube content. Materials & Design 32 2301-2307.

[81] Abdalla, M., et al. The effect of interfacial chemistry on molecular mobility and morphology of multiwalled carbon nanotubes epoxy nanocomposite. Polymer 48 (2007): 5662-5670.

[82] Samthong, C., Laine, R.M., and Somwangthanaroj, A. Synthesis and characterization of organic/inorganic epoxy nanocomposites from poly(aminopropyl/phenyl)silsesquioxanes. Journal of Applied Polymer Science (2012).

[83] Liu, W.S., Wang, Z.G., Chen, Z., Li, J.F., and Zhao, L.N. Synthesis and properties of two novel silicon-containing cycloaliphatic epoxy resins for electronic packaging application. Polymers for Advanced Technologies 23 (2012): 367-374.

[84] Miyagawa, H., Misra, M., Drzal, L.T., and Mohanty, A.K. Fracture toughness and impact strength of anhydride-cured biobased epoxy. Polymer Engineering and Science 45 (2005): 487-495.

[85] He, Y. Thermomechanical and viscoelastic behavior of a no-flow underfill material for flip-chip applications. Thermochimica Acta 439 (2005): 127-134.

[86] Falat, T., Wymyslowski, A., Kolbe, J., Jansen, K.M.B., and Ernst, L. Influence of matrix viscoelastic properties on thermal conductivity of TCA -

Numerical approach. Microelectronics Reliability 47 (2007): 1989-1996.

[87] Montazeri, A., Pourshamsian, K., and Riazian, M. Viscoelastic properties and determination of free volume fraction of multi-walled carbon nanotube/epoxy composite using dynamic mechanical thermal analysis. Materials & Design 36 (2012): 408-414.

[88] Leroy, E., Dupuy, J., Maazouz, A., and Seytre, G. Evolution of the coefficient of thermal expansion of a thermosetting polymer during cure reaction. Polymer 46 (2005): 9919-9927.

[89] Pongsa, U., Samthong, C., and Somwangthanaroj, A. Direct functionalization with 3,5-substituted benzoic acids of multiwalled carbon nanotube/epoxy composites. Polymer Engineering & Science (2013): n/a-n/a.

[90] Shen, M.-x., Cui, Y.-x., He, J., and Zhang, Y.-m. Thermal conductivity model of filled polymer composites. International Journal of Minerals, Metallurgy, and Materials 18 (2011): 623-631.

[91] Weber, E.H., Clingerman, M.L., and King, J.A. Thermally conductive nylon 6,6 and polycarbonate based resins. II. Modeling. Journal of Applied Polymer Science 88 (2003): 123-130.

[92] Li, S.S., Qi, S.H., Liu, N.L., Cao, P., and Zhang, Y. Preparation and thermal conductivity of novolac/Ni/graphite nanosheet composites. Journal of Applied Polymer Science 124 (2012): 4403-4408.

[93] Tu, H., and Ye, L. Preparation and characterization of thermally conductive polystyrene/carbon nanotubes composites. Journal of Applied Polymer Science 116 (2010): 2336-2342.

[94] Gaxiola, D.L., Keith, J.M., King, J.A., and Johnson, B.A. Nielsen thermal conductivity model for single filler carbon/polypropylene composites. Journal of Applied Polymer Science 114 (2009): 3261-3267.

[95] Clancy, T.C., Frankland, S.J.V., Hinkley, J.A., and Gates, T.S. Multiscale modeling of thermal conductivity of polymer/carbon nanocomposites. International Journal of Thermal Sciences 49 (2010): 1555-1560.

[96] Nan, C.W., Shi, Z., and Lin, Y. A simple model for thermal conductivity of carbon nanotube-based composites. Chemical Physics Letters 375 (2003): 666-669.

[97] Nan, C.-W., Liu, G., Lin, Y., and Li, M. Interface effect on thermal conductivity of carbon nanotube composites. Applied Physics Letters 85 (2004): 3549-3551.

[98] Im, H., and Kim, J. Thermal conductivity of a graphene oxide–carbon nanotube hybrid/epoxy composite. Carbon 50 (2012): 5429-5440.

[99] Clancy, T.C., and Gates, T.S. Modeling of interfacial modification effects on thermal conductivity of carbon nanotube composites. Polymer 47 (2006): 5990-5996.

APPENDICES

APPENDIX A

Calculation of acivation energy for epoxy composites

In this work, the curing exotherms of epoxy composites were investigated at various heating rates to calculate the activation energy (E_a). The determination of E_a according Kissinger and Ozawa methods was demonstrated here.

Kissinger method:

$$\ln \frac{\beta}{T_p^2} = \ln\left(\frac{Q_p AR}{E_a}\right) - \frac{E_a}{RT_p}$$

Ozawa method:

$$\ln\beta = \ln\left(\frac{Q_p AR}{E_a}\right) - \ln F(\alpha) - 5.331 - 1.052\frac{E_a}{RT_p}$$

The details of E_a determination for neat epoxy resin and epoxy composites filled with BTC-MWCNT at filler content of 0.3 vol% were shown as follows:

Example A-1: Neat epoxy resin

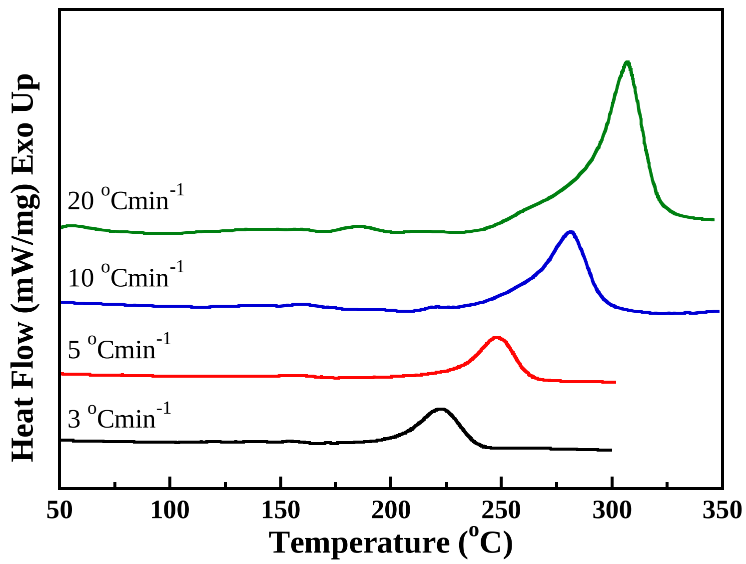

Figure A.1 DSC thermograms of neat epoxy resin at various heating rates

Table A.1 Curing exothermic temperatures and kinetic parameters of neat epoxy resin evaluated from Kissinger and Ozawa methods

β (°C/min)	**T_p**		**Kissinger**		**Ozawa**	
	(°C)	**(K)**	**1000/Tp**	**$\ln(\beta/T_p^2)$**	**1000Tp**	**lnβ**
3	222.55	495.70	2.02	-11.31	2.02	1.10
5	248.38	521.53	1.92	-10.90	1.92	1.61
10	281.15	554.30	1.80	-10.33	1.80	2.30
20	306.93	580.08	1.72	-9.73	1.72	3.00
Ea ($kJmol^{-1}$)			**44.21**		**50.49**	

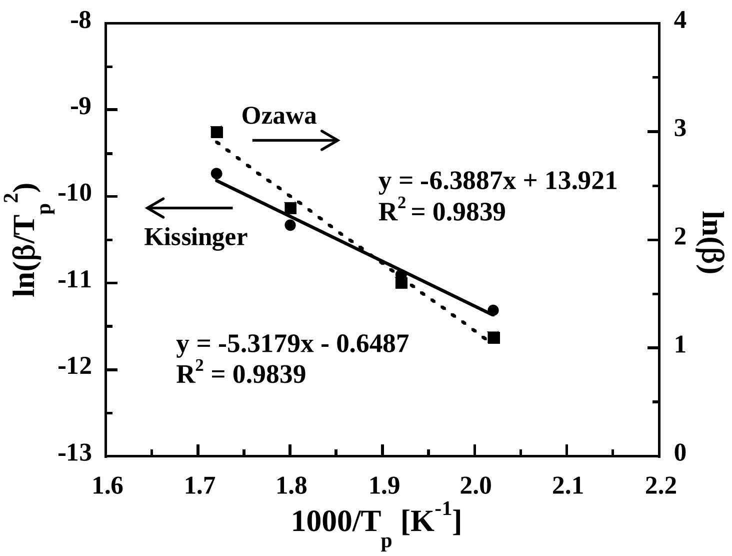

Figure A.2 Averaged activation energy determinations by using Kissinger method and Ozawa method plots of neat epoxy resin

Example A-2: 0.3vol% BTC-MWCNT/epoxy composite

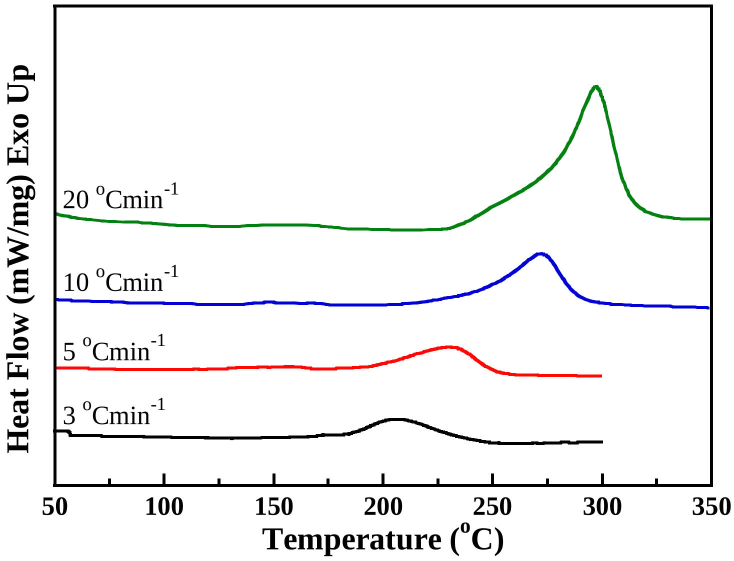

Figure A.3 DSC thermograms of epoxy composites filled with 0.3vol% BTC-MWCNTs at various heating rates

Table A.2 Curing exothermic temperatures and kinetic parameters of epoxy composites filled with 0.3vol% BTC-MWCNTs evaluated from Kissinger and Ozawa methods

β (°C/min)	**T_p**		**Kissinger**		**Ozawa**	
	(°C)	**(K)**	**1000/Tp**	**$\ln(\beta/T_p^2)$**	**1000Tp**	**lnβ**
3	206.68	479.83	2.08	-11.25	2.08	1.10
5	229.21	502.36	1.99	-10.83	1.99	1.61
10	272.22	545.37	1.83	-10.30	1.83	2.30
20	297.32	570.47	1.75	-9.70	1.75	3.00
Ea ($kJmol^{-1}$)			**36.84**		**43.28**	

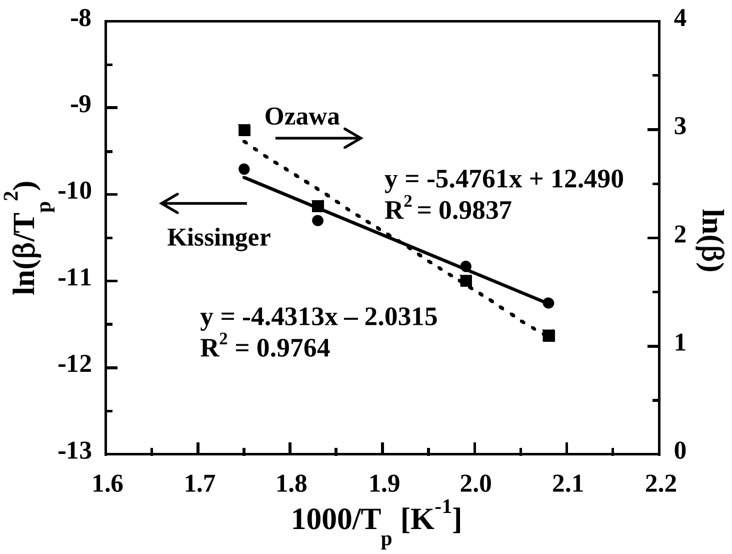

Figure A.4. Averaged activation energy determinations by using Kissinger method and Ozawa method plots of epoxy composite filled with 0.3vol% of BTC-MWCNTs

Also, these values was done for our data and listed in Table A.3.

Table A.3 Exothermic peak temperatures and activation energy of epoxy composites

Sample	β ($^{o}Cmin^{-1}$)	T_p (^{o}C)	T_p (K)	E_a Kissinger	E_a Ozawa
U-MWCNT 0.3	3	216.33	489.48	40.78	47.15
	5	248.38	521.53		
	10	281.09	554.24		
	20	304.62	577.77		
U-MWCNT 0.5	3	213.85	487.00	40.24	46.59
	5	231.05	504.20		
	10	269.57	542.72		
	20	300.88	574.03		
U-MWCNT 0.7	3	207.85	481.00	39.67	45.96
	5	228.75	501.90		
	10	265.90	539.05		
	20	294.95	568.10		
U-MWCNT 1.0	3	205.63	478.78	38.60	44.88
	5	219.24	492.39		
	10	262.38	535.53		
	20	289.78	562.93		
DAB-MWCNT 0.3	3	203.49	476.64	37.71	44.05
	5	226.63	499.78		
	10	262.34	535.49		
	20	294.72	567.87		
DAB-MWCNT 0.5	3	193.76	466.91	36.92	41.59
	5	219.37	492.52		
	10	250.25	523.40		
	20	285.03	558.18		
DAB-MWCNT 0.7	3	180.61	453.76	36.46	42.53
	5	204.05	477.20		
	10	239.16	512.31		
	20	265.14	538.29		
DAB-MWCNT 1.0	3	174.53	447.68	35.27	41.77
	5	198.81	471.96		
	10	229.26	502.41		
	20	262.05	535.20		

APPENDIX B

Calculation of free volume fraction for epoxy composites

According Williams-Landell-Ferry (WLF) equation, the free volume fraction of epoxy composites can determine by using with following equations.

$$\frac{1}{\mathrm{Log}\,(\frac{f}{f_r})} = \frac{C_2}{C_1}\left(\frac{1}{T_g\text{-}T_{gr}}\right) + \frac{1}{C_1}$$

where

$$C_1 = \frac{B}{2.303 f_g} = \frac{1}{2.303 f_g} \text{ and } C_2 = \frac{f_g}{\Delta CTE}.$$

Based on DMA analysis, the loss moduli of epoxy composites as a function of temperature at various frequencies were investigated as illustrated below.

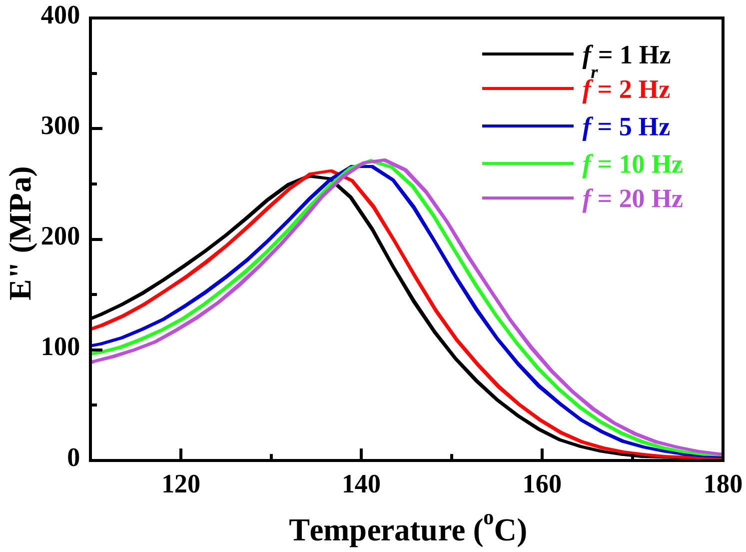

Figure B.1 Loss moduli as a function of temperature of neat epoxy resin at various frequencies

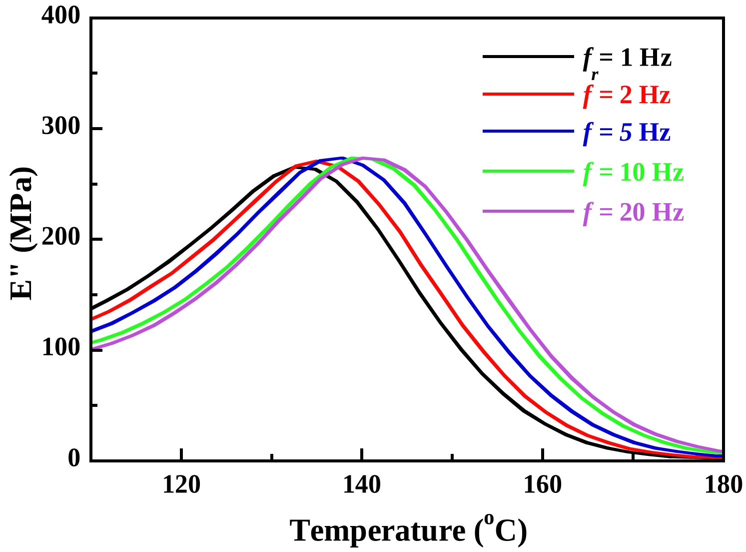

Figure B.2 Loss moduli as a function of temperature of 0.3vol% U-MWCNT/epoxy composite at various frequencies

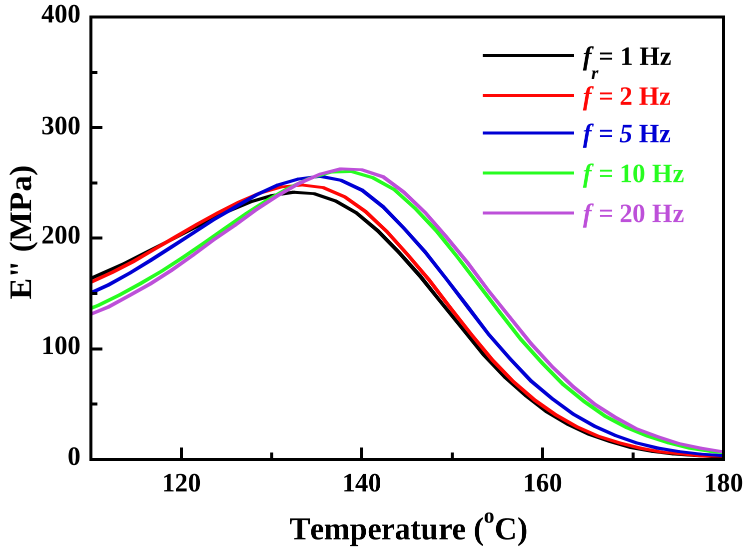

Figure B.3 Loss moduli as a function of temperature of 0.3vol% BTC-MWCNT/epoxy composite at various frequencies

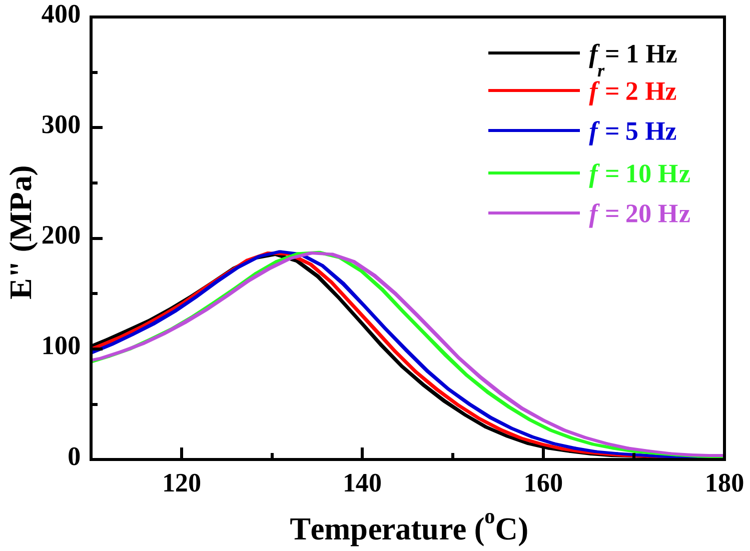

Figure B.4 Loss moduli as a function of temperature of 0.3vol% DAB-MWCNT/epoxy composite at various frequencies

Table B.1 Tg obtained from the maximum value of loss modulus peak of epoxy composites reinforced with various fillers at content of 0.3 vol%

Sample		***f* (Hz)**				
		1	**2**	**5**	**10**	**20**
Neat epoxy	ºC	131	131.99	133.09	134.57	135.84
	K	404.14	405.13	406.23	407.71	408.98
U-MWCNT 0.3	ºC	134.01	135.98	138.46	139.04	140.32
	K	407.15	409.12	411.6	412.18	413.46
BTC-MWCNT 0.3	ºC	134.41	136.17	138.17	139.1	140.6
	K	407.55	409.31	411.31	412.24	413.74
DAB-MWCNT 0.3	ºC	136.33	138.22	139.9	141.77	143.2
	K	409.47	411.36	413.04	414.91	416.34

Table B.2 The values of T_g-T_{gr} and 1/(T_g-T_{gr}) of epoxy composites when T_{gr} is the T_g of epoxy composite at the reference frequency of 1 Hz

Sample		*f* (Hz)				
		1	**2**	**5**	**10**	**20**
Neat epoxy	**T_g-T_{gr}**	0	0.99	2.09	3.57	4.84
	1/(T_g-T_{gr})	-	1.01	0.48	0.28	0.21
U-MWCNT 0.3	**T_g-T_{gr}**	0	1.96	4.45	5.03	6.31
	1/(T_g-T_{gr})	-	0.51	0.22	0.2	0.16
BTC-MWCNT 0.3	**T_g-T_{gr}**	0	1.77	3.76	4.69	6.19
	1/(T_g-T_{gr})	-	0.57	0.27	0.21	0.16
DAB-MWCNT 0.3	**T_g-T_{gr}**	0	1.89	3.57	5.44	6.87
	1/(T_g-T_{gr})	-	0.53	0.28	0.18	0.15

Table B.3 The values of f/f_r, Log(f/f_r) and 1/Log(f/f_r) when f_r is the reference frequency of 1 Hz

f **(Hz)**	f/f_r	**Log(f/f_r)**	**1/Log(f/f_r)**
1	1.00	0.0000	-
2	2.00	0.3010	3.32
5	5.00	0.6990	1.43
10	10.00	1.0000	1.00
20	20.00	1.3010	0.77

Then, the plot of 1/Log(f/f_r) versus 1/(T_g -T_{gr}) for each sample was performed as demonstrated in Figure B.5.

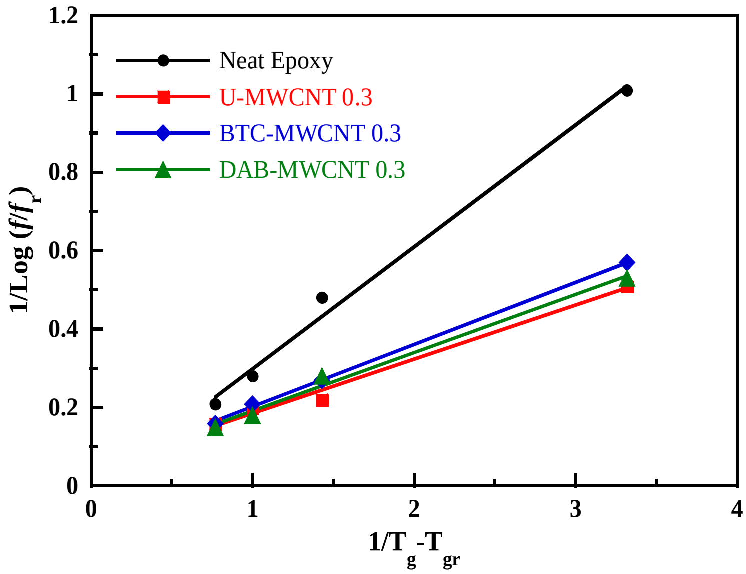

Figure B.5 The plot of 1/Log(f/f_r) versus 1/(T_g -T_{gr}) for determination of the WLF parameter constants C_1 and C_2

The WLF parameter constants, C_1 and C_2, of neat epoxy resin and epoxy composites were calculated from the intercept and the slope of the plot which are summarized in Table B.4.

Table B.4 WLF constants for epoxy composites

Sample	Equation	C_2/C_1	$1/C_1$	C_1	C_2
Neat Epoxy	y = 3.1882X + 0.0563	3.1882	0.0563	17.76	56.62
U-MWCNT 0.3	y = 0.1372X + 0.0492	0.1372	0.0492	20.33	2.79
BTC-MWCNT 0.3	y = 0.1563X + 0.0470	0.1562	0.0470	21.28	3.33
DAB-MWCNT 0.3	y = 0.1484X + 0.0431	0.1484	0.0431	23.20	3.44

Table B.5 Free volume fraction for epoxy composites

Sample	f_g
Neat Epoxy	0.0244
U-MWCNT 0.3	0.0214
BTC-MWCNT 0.3	0.0204
DAB-MWCNT 0.3	0.0187

APPENDIX C

Calculation of density of epoxy composites

The theoretical density of epoxy composites was calculated by using a following equation

$$\rho = \rho_m(1 - \sum_{i=1}^{n} V_i) + \sum_{i=1}^{n} \rho_i V_i$$

where

ρ = the density of composite

ρ_m = the density of polymer matrix

ρ_i = the density of each filler

V_i = the volume fraction of each filler

Then, the theoretical density of epoxy composites filled with MWCNTs at difference volume contents are listed in Table C.1.

Table C.1 Theoretical density of MWCNT/epoxy composites

Filler content (vol%)	V_i	ρ_m (g/ml)	ρ_{MWCNT} (g/ml)	ρ (g/ml)
0	0	1.16	2.10	1.1825
0.3	0.003	1.16	2.10	1.1852
0.5	0.005	1.16	2.10	1.1871
0.7	0.007	1.16	2.10	1.1889
1.0	0.010	1.16	2.10	1.1917
1.2	0.012	1.16	2.10	1.1935

Also, the theoretical density of epoxy composites incorporated with hybrid fillers between MWCNTs and submicron-sized Si_3N_4 was determined as listed in Table C.2.

Table C.2 Theoretical density of epoxy composites filled with hybrid fillers

Filler content (vol%)		V_i		ρ_m (g/ml)	ρ_{MWCNT} (g/ml)	ρ_{Si3N4} (g/ml)	ρ (g/ml)
MWCNT	Si_3N_4	MWCNT	Si_3N_4				
1.0	2.5	0.010	0.025	1.16	2.10	3.34	1.2481
1.0	5.0	0.010	0.050	1.16	2.10	3.34	1.3045
1.0	7.5	0.010	0.075	1.16	2.10	3.34	1.3610

The density of epoxy composites was measured by water displacement which can be given by

$$\rho = \frac{W_{dry}}{W_{dry} - W_{wet}} \rho_{water}(T) \tag{1}$$

where

ρ = the density of epoxy composite;

W_{dry} = the weight of sample in air

W_{wet} = the weight of sample in water

$\rho_{water}(T)$ = the density of water at measured temperature.

The measured density of epoxy composites filled with unmodified and functionalized MWCNTs are listed in Table C.3 and C.4, respectively.

Table C.3 Measured density of U-MWCNT/epoxy composites

Sample	No.	Wdry (g)	Wwet (g)	T (ºC)	ρ_{water} (g/ml)	ρ (g/ml)
Neat epoxy	1	2.7561	0.436	26.5	0.99668	1.1840
	2	2.5511	0.4012	26.5	0.99668	1.1827
	3	2.4097	0.3758	26.5	0.99668	1.1808
	AVG					**1.1825**
	SD					0.0016
U-MWCNT 0.3	1	2.7304	0.4373	26.7	0.99662	1.1867
	2	2.6552	0.4254	26.7	0.99662	1.1868
	3	2.6931	0.4306	26.7	0.99662	1.1863
	AVG					**1.1866**
	SD					0.0002
U-MWCNT 0.5	1	2.5656	0.4132	26.5	0.99668	1.1880
	2	2.6822	0.4301	26.5	0.99668	1.1870
	3	2.7657	0.4455	26.5	0.99668	1.1881
	AVG					**1.1877**
	SD					0.0006
U-MWCNT 0.7	1	2.6385	0.4263	27.1	0.99651	1.1885
	2	2.9240	0.4753	27.1	0.99651	1.1899
	3	2.6790	0.4377	27.1	0.99651	1.1911
	AVG					**1.1899**
	SD					0.0013
U-MWCNT 1.0	1	1.5968	0.2659	26.0	0.99681	1.1960
	2	2.7067	0.45	26.1	0.99678	1.1955
	AVG					**1.1958**
	SD					0.0003

Table C.4 Measured density of functionalized MWCNT/epoxy composites

Sample	No.	Wdry (g)	Wwet (g)	T (ºC)	ρ_{water} (g/ml)	ρ (g/ml)
BTC-MWCNT 0.3	1	0.3356	0.0529	26.5	0.99668	1.1832
	2	0.3833	0.0609	26.5	0.99668	1.1849
	3	0.3996	0.0648	26.5	0.99668	1.1896
	4	0.1539	0.0247	26.5	0.99668	1.1872
	AVG					**1.1862**
	SD					0.0028
DAB-MWCNT 0.3	1	0.3427	0.0536	28.9	0.996	1.1807
	2	0.3145	0.0498	28.5	0.99612	1.1835
	3	0.2925	0.0472	28.5	0.99612	1.1878
	4	0.3089	0.0488	28.4	0.99614	1.1830
	AVG					**1.1838**
	SD					0.0030
DAB-MWCNT 0.5	1	0.3536	0.057	28	0.99626	1.1877
	2	0.3336	0.0532	28	0.99626	1.1853
	3	0.1686	0.0267	27.9	0.99629	1.1838
	4	0.3682	0.0605	27.9	0.99629	1.1922
	AVG					**1.1872**
	SD					0.0037
DAB-MWCNT 0.7	1	0.3122	0.0498	26.6	0.99665	1.1858
	2	0.2920	0.0481	26.6	0.99665	1.1932
	3	0.2827	0.0457	26.5	0.99668	1.1889
	4	0.2641	0.0438	26.5	0.99668	1.1948
	AVG					**1.1907**
	SD					0.0041
DAB-MWCNT 1.0	1	2.2312	0.3631	25.4	0.99697	1.1907
	2	2.7191	0.4425	25.3	0.99699	1.1908
	AVG					**1.1908**
	SD					0.0010

The measured density of epoxy composites filled with hybrid fillers is listed in Table C.5.

Table C.5 Measured density of epoxy composites filled with hybrid fillers

Sample		No.	Wdry (g)	Wwet (g)	T (ºC)	ρ_{water} (g/ml)	ρ (g/ml)
U-MWCNT 1.0	Si_3N_4 2.5	1	2.2064	0.4588	26.6	0.99665	1.2583
		2	3.0166	0.6276	26.5	0.99668	1.2585
		AVG					**1.2584**
		SD					0.0001
U-MWCNT 1.0	Si_3N_4 5.0	1	2.8491	0.6975	26.3	0.99673	1.3198
		2	2.9784	0.7304	26.3	0.99673	1.3206
		AVG					**1.3202**
		SD					0.0005
U-MWCNT 1.0	Si_3N_4 7.5	1	3.0300	0.8456	26.1	0.99678	1.3826
		2	2.9521	0.8296	26.1	0.99678	1.3864
		AVG					**1.3845**
		SD					0.0026
DAB-MWCNT 1.0	Si_3N_4 7.5	1	3.3246	0.9244	25.6	0.99691	1.3809
		2	1.5735	0.439	25.6	0.99691	1.3827
		AVG					**1.3818**
		SD					0.0013

APPENDIX D

Calculation of thermal conductivity of epoxy composites

Table D.1 Thermal conductivity of U-MWCNT/epoxy composites

Sample	T (ºC)	α (mm^2s^{-1})	ρ (gcm^{-3})	C_p ($Jg^{-1}{}^{o}C^{-1}$)	K (W/mK)
Neat epoxy	30	0.109	1.1825	0	0.000
	50	0.108		1.229	0.157
	75	0.102		1.316	0.159
	100	0.097		1.387	0.159
	125	0.094		1.431	0.159
	150	0.089		1.592	0.168
U-MWCNT 0.3	30	0.116	1.1866	0.000	0.000
	50	0.112		1.369	0.182
	75	0.107		1.755	0.223
	100	0.103		2.148	0.263
	125	0.098		2.646	0.308
	150	0.094		3.188	0.356
U-MWCNT 0.5	30	0.118	1.1877	0.000	0.000
	50	0.116		1.388	0.191
	75	0.112		1.856	0.247
	100	0.106		2.342	0.295
	125	0.101		2.961	0.355
	150	0.097		3.610	0.416
U-MWCNT 0.7	30	0.121	1.1899	0.000	0.000
	50	0.118		1.394	0.196
	75	0.112		2.105	0.281
	100	0.107		2.688	0.342
	125	0.102		3.350	0.407
	150	0.098		3.877	0.452
U-MWCNT 1.0	30	0.122	1.1958	0.000	0.000
	50	0.119		1.428	0.203
	75	0.113		2.103	0.284
	100	0.109		2.754	0.359
	125	0.105		3.456	0.434
	150	0.100		3.891	0.465

Table D.2 Thermal conductivity of functionalized MWCNT/epoxy composites

Sample	T (ºC)	α (mm^2s^{-1})	ρ (gcm^{-3})	C_p ($Jg^{-1}{}^{o}C^{-1}$)	K (W/mK)
BTC-MWCNT 0.3	30	0.118	1.1862	0.000	0.000
	50	0.116		1.371	0.189
	75	0.112		1.802	0.239
	100	0.106		2.258	0.284
	125	0.101		2.863	0.343
	150	0.097		3.365	0.387
DAB-MWCNT 0.3	30	0.122	1.1838	0.000	0.000
	50	0.118		1.381	0.193
	75	0.112		1.867	0.248
	100	0.108		2.302	0.294
	125	0.103		3.169	0.386
	150	0.098		3.496	0.406
DAB-MWCNT 0.5	30	0.125	1.1872	0.000	0.000
	50	0.120		1.391	0.198
	75	0.114		1.874	0.254
	100	0.110		2.402	0.314
	125	0.105		3.169	0.395
	150	0.098		3.961	0.461
DAB-MWCNT 0.7	30	0.128	1.1907	0.000	0.000
	50	0.123		1.401	0.205
	75	0.118		2.441	0.343
	100	0.115		3.198	0.438
	125	0.105		4.047	0.506
	150	0.098		4.538	0.530
DAB-MWCNT 1.0	30	0.130	1.1901	0.000	0.000
	50	0.126		1.554	0.233
	75	0.121		2.530	0.364
	100	0.116		3.232	0.446
	125	0.111		4.117	0.544
	150	0.103		4.827	0.592

Table D.3 Thermal conductivity of epoxy composites filled with hybrid fillers

Sample		T (°C)	α (mm^2s^{-1})	ρ (gcm^{-3})	C_p ($Jg^{-1o}C^{-1}$)	K (W/mK)
U-MWCNT 1.0	Si_3N_4 2.5	30	0.151	1.2584	0.000	0.000
		50	0.145		1.396	0.255
		75	0.141		1.617	0.287
		100	0.136		1.763	0.302
U-MWCNT 1.0	Si_3N_4 5.0	30	0.176	1.3202	0.000	0.000
		50	0.166		1.387	0.290
		75	0.160		1.393	0.280
		100	0.154		1.767	0.342
U-MWCNT 1.0	Si_3N_4 7.5	30	0.178	1.3845	0.000	0.000
		50	0.170		1.375	0.294
		75	0.161		2.200	0.446
		100	0.151		2.930	0.557
DAB-MWCNT 1.0	Si_3N_4 7.5	30	0.181	1.3818	0.000	0.000
		50	0.175		1.518	0.334
		75	0.167		2.520	0.530
		100	0.160		3.217	0.648

APPENDIX E
List of publications

1. Pongsa, U.; Samthong, C.; and Somwangthanaroj, A. Direct Functionalization with 3,5-Substituted Benzoic Acids of Multiwalled Carbon Nanotube/Epoxy Composites. Polymer Engineering and Science (2013): DOI: 10.1002/pen.23472.

2. Pongsa, U.; and Somwangthanaroj, A. Effective Thermal Conductivity of 3,5-Diaminobenzoyl-functionalized Multiwalled Carbon Nanotubes /Epoxy Composites. Journal of Applied Polymer Science (2013).

3. Pongsa, U.; and Somwangthanaroj, A. Thermally conductive epoxy composites filled with multiwalled carbon nanotubes and silicon nitride for underfill application. Proceeding of Pure and Applied Chemistry International Conference (PACCON2013), January 23-25, 2013, Chon Buri, Thailand (Poster Presentation).

4. Pongsa, U.; and Somwangthanaroj, A. Effect of Hybrid Carbon Nanotube-Inorganic filler systems on Properties of Thermal Conductive Underfill Materials. The 2nd Joint Symposium Chulalongkorn University-Nagaoka University of Technology (CU-NUT), October 11-12, 2012, Bangkok, Thailand (Poster Presentation).

5. Somwangthanaroj, A.; and Pongsa, U. Curing Behavior and Characterization of Various Functional Groups on Single-Walled Carbon Nanotube/Epoxy Composites. Proceeding of Asian International Conference on Materials, Minerals and Polymer (MAMIP2012), March 23–24, 2012, Penang, Malaysia, p.154-162 (Oral presentation).

6. Pongsa, U.; and Somwangthanaroj, A. Surface Characterization of Single-walled and Multi-walled Carbon Nanotubes Functionalized via Friedel-Crafts Acylation. Proceedings of the 4th AUN-SEED Net Regional Conference on Materials, December 8-9, 2011, Hanoi, Vietnam.

7. Pongsa, U.; Samthong, C.; and Somwangthanaroj, A. Thermomechanical and thermal properties of functionalized multiwalled carbon nanotube/epoxy composites. The 3rd International Symposium: Frontiers in Polymer Science, May 21-23, 2013, Melia Sitges, Spain.

VITAE

Miss Uraiwan Pongsa was born on June 30, 1985 in Prachuap Khiri Khan, Thailand. She completed high school at Benjama Thep Utit school, Phetchaburi. She received the Bachelor's Degree from the Department of Chemical Engineering, Faculty of Engineering and Industrial Technology, Silpakorn University in 2008. After graduation, she immediately pursued her graduate study for a Doctoral Degree in Chemical Engineering at the Department of Chemical Engineering, Faculty of Engineering, Chulalongkorn University.

9